# NAVAL POSTGRADUATE SCHOOL

**MONTEREY, CALIFORNIA**

# THESIS

**DESIGN, FABRICATION AND TESTING OF A SCALABLE SERIES AUGMENTED RAILGUN RESEARCH PLATFORM**

by

Brian C. Black

March 2006

Thesis Advisor: William B. Maier II
Co-Advisor: Terry R. McNelley

THIS PAGE INTENTIONALLY LEFT BLANK

| REPORT DOCUMENTATION PAGE | | | *Form Approved OMB No. 0704-0188* |
|---|---|---|---|
| Public reporting burden for this collection of information is estimated to average 1 hour per response, including the time for reviewing instruction, searching existing data sources, gathering and maintaining the data needed, and completing and reviewing the collection of information. Send comments regarding this burden estimate or any other aspect of this collection of information, including suggestions for reducing this burden, to Washington headquarters Services, Directorate for Information Operations and Reports, 1215 Jefferson Davis Highway, Suite 1204, Arlington, VA 22202-4302, and to the Office of Management and Budget, Paperwork Reduction Project (0704-0188) Washington DC 20503. | | | |
| **1. AGENCY USE ONLY *(Leave blank)*** | **2. REPORT DATE** March 2006 | **3. REPORT TYPE AND DATES COVERED** Master's Thesis | |
| **4. TITLE AND SUBTITLE**: Design, Fabrication, and Testing of a Scalable Series Augmented Railgun Research Platform | | | **5. FUNDING NUMBERS** |
| **6. AUTHOR(S) Brian C. Black** | | | |
| **7. PERFORMING ORGANIZATION NAME(S) AND ADDRESS(ES)** Naval Postgraduate School Monterey, CA 93943-5000 | | | **8. PERFORMING ORGANIZATION REPORT NUMBER** |
| **9. SPONSORING /MONITORING AGENCY NAME(S) AND ADDRESS(ES)** N/A | | | **10. SPONSORING/MONITORING AGENCY REPORT NUMBER** |
| **11. SUPPLEMENTARY NOTES** The views expressed in this thesis are those of the author and do not reflect the official policy or position of the Department of Defense or the U.S. Government. | | | |
| **12a. DISTRIBUTION / AVAILABILITY STATEMENT** Approved for public release; distribution is unlimited | | | **12b. DISTRIBUTION CODE** |

**13. ABSTRACT (maximum 200 words)**

The design and material properties of rails and projectiles are critical to the success of the Navy railgun. This thesis addresses the design, fabrication, and testing of a scalable square bore electromagnetic railgun. This railgun is designed to permit series augmented operation, and incorporates disposable rail liners to facilitate investigating the suitability of various rail materials. A series of shots has demonstrated performance consistent with theoretical modeling, including significant performance enhancement as a result of both slotted rail geometry and augmentation over solid rail and un-augmented configurations. A capacitor based stored energy supply input of 35 kJ resulted in a measured velocity of 294 m/s for an 11.4 gram projectile. Suggestions are provided for future power supply configurations, rail materials and surface treatments, and a variety of armature geometries.

| **14. SUBJECT TERMS** | | | **15. NUMBER OF PAGES** |
|---|---|---|---|
| Railgun, Rail-gun, Augmentation, Electromagnetic launch, Armature, Pulsed Power, Hypervelocity launch, Hypervelocity Projectile, Ion beam surface treatment, IBEST, Laser peening, Electromagnetic Weapon | | | 135 |
| | | | **16. PRICE CODE** |
| **17. SECURITY CLASSIFICATION OF REPORT** | **18. SECURITY CLASSIFICATION OF THIS PAGE** | **19. SECURITY CLASSIFICATION OF ABSTRACT** | **20. LIMITATION OF ABSTRACT** |
| Unclassified | Unclassified | Unclassified | UL |

NSN 7540-01-280-5500

Standard Form 298 (Rev. 2-89)
Prescribed by ANSI Std. 239-18

THIS PAGE INTENTIONALLY LEFT BLANK

**Approved for public release; distribution is unlimited**

# DESIGN, FABRICATION AND TESTING OF A SCALABLE SERIES AUGMENTED RAILGUN RESEARCH PLATFORM

Brian C. Black
Lieutenant, United Stated Navy
B.A., Political Science, Dickinson College, 1991
B.S., Mechanical Engineering, University of Pittsburgh, 1998

Submitted in partial fulfillment of the
requirements for the degree of

**MASTER OF SCIENCE IN MECHANICAL ENGINEERING**

from the

**NAVAL POSTGRADUATE SCHOOL**
**March 2006**

Author: Brian C. Black

Approved by: William B. Maier II
Thesis Advisor
Department of Physics

Terry R. McNelley
Co-Advisor
Department of Mechanical and
Astronautical Engineering

Anthony J. Healey
Chairman, Department of Mechanical and
Astronautical Engineering

THIS PAGE INTENTIONALLY LEFT BLANK

# ABSTRACT

The design and material properties of rails and projectiles are critical to the success of the Navy railgun. This thesis addresses the design, fabrication, and testing of a scalable square bore electromagnetic railgun. This railgun is designed to permit series augmented operation, and incorporates disposable rail liners to facilitate investigating the suitability of various rail materials. A series of shots has demonstrated performance consistent with theoretical modeling, including significant performance enhancement as a result of both the slotted rail geometry and augmentation over solid rail configurations. A capacitor based stored energy supply input of 35 kJ resulted in a measured velocity of 294 m/s for an 11.4 gram projectile. Suggestions are provided for future power supply configurations, rail materials and surface treatments, and a variety of armature geometries.

THIS PAGE INTENTIONALLY LEFT BLANK

# TABLE OF CONTENTS

THIS PAGE INTENTIONALLY LEFT BLANK

# LIST OF FIGURES

# LIST OF TABLES

THIS PAGE INTENTIONALLY LEFT BLANK

# ACKNOWLEDGEMENTS

Thank you Professor Bill Maier for your confidence and support throughout this project, and for facilitating exposure to resources beyond the Naval Postgraduate School. Thank you to Professor Terry McNelley and both the Physics and Mechanical Engineering Departments for facilitating a mixed curriculum tailored to this research. Thank you Don Snyder, George Jaksha, and Frank Franzen for your professional expertise and personal commitments which turned theory into practice in the fabrication and testing of this railgun prototype. Thank you Tania Zaleski and Tim Renk for your professional courtesy in supporting the materials processing collaboration between the National Laboratories and the Navy Postgraduate School. Thank you to all of the professional engineers at the Institute for Advanced Technology and the Center for Electromechanics at the University of Texas at Austin for direct contributions to the materials, design, and modeling methods used throughout this thesis. Thank you Fred Beach, Donald Gillich, Michael Lockwood, Michael Graham, and Juan Ubiera for building the NPS Railgun Laboratory infrastructure and establishing a standard of excellence. Finally, thank you Romina, Sophia, and Carmen for making success important.

THIS PAGE INTENTIONALLY LEFT BLANK

# I. INTRODUCTION

## A. BACKGROUND

The military potential of the U.S. Navy's notional electromagnetic railgun for Naval surface-fire support missions is well defined. The focused investment and research of both Army and Navy sponsored programs through the Office of Naval Research and U.S. Army ARDEC has identified the remaining engineering obstacles to be overcome prior to fielding a practical system. The Naval Postgraduate School (NPS) is uniquely positioned to leverage such investments in order to investigate alternatives. The Center for Electromechanics (CEM) and the Institute for Advanced Technology (IAT) from the University of Texas at Austin have pushed the envelope in terms of materials, pulsed power, and systems engineering approaches to applied railgun technology. In January 2005, IAT engineers published an IEEE article entitled "Development of a Naval Railgun" summarizing the status of Naval railgun development and detailing areas where further research is warranted [1]. The railgun specific issues are directly related to extending bore life to as high as 10,000 shots. Although progress has been made toward identifying the destructive mechanisms of transitioning contacts and hyper-velocity gouging, no design parameters, material combination, or processing treatment have resolved their impact on bore life.

Simultaneously achieving the full scale notional parameters listed in Table 1 while achieving shot frequencies of 6-12 rounds per minute is presently beyond the capacity of even large scale laboratory facilities.

Therefore, economy of simulation and scalable applied research is critical to the success of the railgun program.

| Parameter | Value |
| --- | --- |
| Flight Mass (kg) | 16.0 |
| Launch mass (kg) | 21.0 |
| Peak acceleration (gees) | 30,000 |
| Muzzle velocity, $V_m$ (m/s) | 2,000 |
| Rail height and separation (mm) | 127.0 |
| Muzzle energy, $E_m$ (MJ) | 42.0 |
| Total gun length, $L_{gun}$ (m) | 12.0 |
| Acceleration time, $t_e$ (ms) | 11.5 |
| Maximum current, $I_{max}$ (MA) | 5.0 |
| Recoil momentum (N-s) | 42,000 |

Table 1. Nominal EM Gun Parameters, [From Ref. 1]

Over the past decade, NPS railgun research has produced several iterations of small scale demonstrator weapons to facilitate applied research. During the 2005 fiscal year, the NPS Railgun program has made a substantial investment in laboratory infrastructure including the purchase of ten 11 kV 830 μ–Farad capacitors from General Atomics and advanced high current switches, supplementing the existing pulsed power energy storage capacity by an order of magnitude. By leveraging the collaborative direct input of CEM, IAT, material modifications research support from Lawrence Livermore and Sandia National Laboratories, as well as multi-curriculum contributions from within the campus, NPS railgun research is now more than ever positioned to confront railgun technological deficiencies through applied engineering.

## B. OBJECTIVE

The objective of this thesis is the design, fabrication, and testing of a scalable, reconfigurable bore, conventional railgun capable of achieving launch package velocities in excess of 1500 m/s. The initial 3/4" (19mm) square bore configuration supports comparisons between single rail and series augmentation, solid and slotted rail geometries. Shot repetition and materials performance comparisons are accomplished with disposable rail liners at the rail to armature interface to protect the permanent main conductor rail structure. The railgun test platform incorporates a manual loading apparatus to facilitate consistent initial conditions including armature firing position and an interference armature fit which does not require full disassembly between consecutive shots. Alternative armature geometries and proposals for power conditioning are provided to inform follow-on testing. Unreliable performance of the TVS-40 switches caused spontaneous triggering above 7,000 volts, requiring a practical capacitor charge limit of 6500 volts and a corresponding total stored energy limit of 35 kJ.

Chapter II examines weapon design including decisions regarding materials, geometry, and firing configurations. Chapter III discusses the design and limits of the existing pulsed power supply, as well as a proposed multi-module system. Chapter IV provides design verification analysis including ideal railgun parameter modeling, containment static deflection considerations, and an applied conservation of energy model. Chapter V discusses experimental results. Chapter VI concludes with recommendations for future testing, alternative armature geometries, and processing methods for rail liner materials.

# II. RAILGUN TEST PLATFORM DESIGN

## A. GENERAL

The exploded assembly of Figure 1 below depicts the main structural elements of the railgun design without the loading apparatus. SolidWorks CAD software was used extensively for 3D modeling and for creating the technical drawings required for fabrication. Appendix B includes a comprehensive collection of individual parts and assemblies.

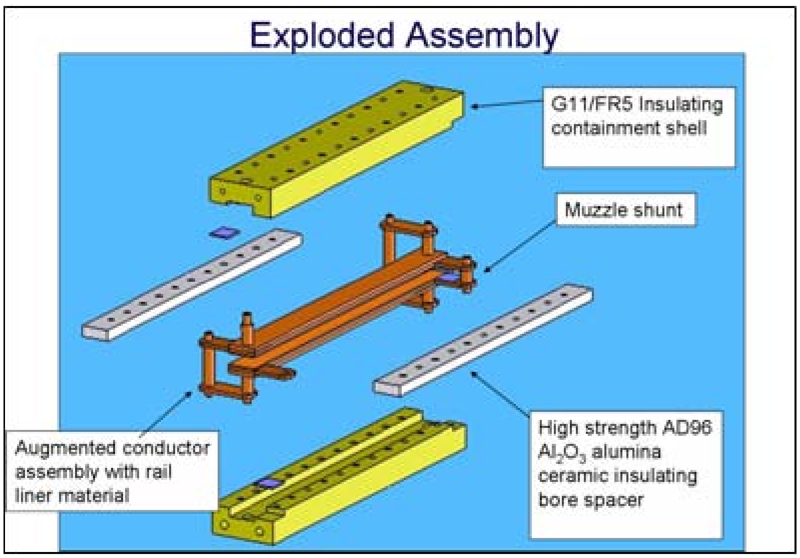


Figure 1. Exploded Railgun Assembly

## B. MATERIAL PROPERTIES

Materials selections were based on an analysis of the property tables included in Appendix A. These values were either obtained directly from the vendor or from the MATWEB online material database. None of the material selections are entirely new to railgun applications.

The thickness and placement of the two insulating bars fixes the bore dimensions given the clamshell containment design. Due to superior compressive dimensional stability, adequate dielectric constant, and ease of refurbishment over glass reinforced epoxy phenolics such as G-10, CoorsTek Alumina ($Al_2O_3$) AD-96 ceramic was chosen. No subsequent fabrication was required as these parts were fired to specification including +/-1% positional tolerances of through holes for the containment bolts and outer surface dimensions finished to +/-0.005 inch tolerance. Surface dimension tolerances were verified by micrometer measurements for both insulators.

The main conductor and a range of rail liner materials were selected after a lengthy process that began with a much larger list extracted directly from materials handbooks based strictly on parameters of conductivity and hardness. This list was subsequently limited after a literature review of previously proven railgun materials, and by the final process of locating vendors with an inventory of 1/8" thick bar or plate stock suitable for the liner geometry. Table 2 below summarizes the properties of interest. The stainless alloy properties are included as a point of comparison.

| Untreated Material Properties | | | | |
|---|---|---|---|---|
| Material | Hardness Rockwell B | Conductivity %IACS ** | Resisitivity (ohm-cm) @ 20ºC | density (g/cm³) |
| oxygen free copper | 50 | 101 | 1.71E-06 | 8.94 |
| **chromium copper** | **79** | **80** | **2.16E-06** | **8.89** |
| phosphor bronze | 93 | 20 | 8.70E-06 | 8.86 |
| copper tungsten | 98 | 45 | 3.83E-06 | 14.84 |
| aluminum 7075 | 87 | 33 | 5.15E-06 | 2.81 |
| Stainless alloy 410 | * 110 | 3 | 5.70E-05 | 7.8 |
| * linear extrapolation from Rockwell C | | ** based on %IACS = (172.41e-6 / Resistivity) | | |

Table 2. Summary of Rail Properties [After Ref. 2]

At the time of completion of this thesis, testing has been restricted to the chromium copper rail liners in order to preserve processed samples for higher velocity regimes.

Several alternative armature geometries were fabricated by using three variants of aluminum including Al-6063, Al-6061, and Al-1100. All testing has been conducted using standard u-shaped Al-6063 armatures shown in Figure 25 of Appendix B.

The main containment clamshell pieces were fabricated from 2” thick blocks of G-11 FR-5 glass reinforced epoxy laminate. This common small-bore railgun containment material has high resistance, high strength, and excellent machinability. Containment hardware includes twenty-two 3/8” Grade 2 stainless steel hex cap nuts, bolts, and washers.

### C. IMPROVED INDUCTANCE GRADIENT WITH SERIES AUGMENTATION

One of the critical railgun design parameters is the inductance gradient, or inductance per unit length (L’). This parameter is a function of the rail and bore geometry. The most fundamental method for determining this parameter is based on modeling the rails as two infinite wires with a fixed radius, separated by a fixed distance representing the bore width between the rails. Although this is a fair approximation, extensive empirical research has produced more accurate results applicable to the case of the rectangular rail and square bore configuration, commonly referred to as Kerrisk’s Method [3]. Appendix C includes the spreadsheets used to evaluate the inductance gradient for the rail geometries selected for this design.

The energy efficiency of a small scale railgun driven through a pulse forming network is significantly limited even under ideal modeling conditions neglecting dissipative losses such as electrical resistance and friction. This ideal efficiency can be expressed by the following equation [4].

$$\eta = \frac{L'x}{\left(L + L'x\right)}$$

*L'* is the inductance gradient, *L* is the total system inductance, and *x* is the rail length. Applying the actual values of *L*= 5.5 micro-Henries and *L'* = 0.683 micro-Henries/meter for this specific design to a 10 meter gun length predicts an ideal energy efficiency approaching 50%. Using the actual effective railgun length of 50 cm, based on these same values of *L* and *L'*, the maximum ideal efficiency is only 5.8%. This entering argument for performance emphasizes the need for maximizing *L'* while minimizing the total system inductance of the pulse forming network.

There are several methods for enhancing the *L'* parameter by enhancing the magnetic field in the bore above that created by a single rail pair. My design permits the use of series augmentation by incorporating a second pair of rails and connecting conductors to create the circuit path illustrated in Figure 2 below.

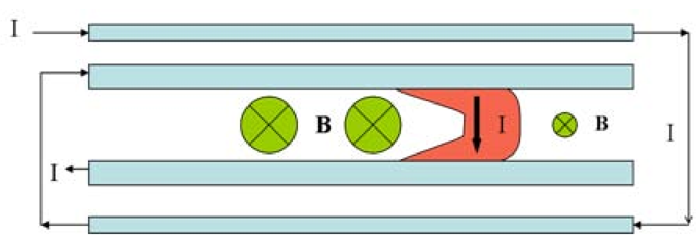


Figure 2. Series Augmented Current Path

The result is an enhanced magnetic field in the bore region due to contributions from the same current pulse flowing through both rail pairs. Current through the outer rail pair establishes a field in the bore region ahead of the advancing armature as indicated in Figure 2. A review of literature regarding series augmentation indicates that for large scale high velocity applications, based on a fixed Lorentz force, the benefits of lower current requirements due to stronger magnetic fields in the bore region are offset by the resistive losses [5]. However, for my design, given the short rail length, no requirement to recover energy for high frequency repetitive shots, and considering the constraint of a limited stored energy supply, series augmentation is a practical method to improve projectile velocity.

Whereas Kerrisk's method for evaluating the inductance gradient is well defined for the simple railgun, a method for determining the new inductance gradient as a result of the augmenting rail contribution has not been empirically developed. The augmented $L'$ can be approximated by modeling each rail as a long thin current carrying wire and integrating the magnetic field contribution to the bore region contributed by each wire. Based on 1/4" outer rail width, and 3/8" width for the combined inner rail plus rail liner thickness, and making the assumption that current flows down the rail centerlines, the augmented geometry can be expressed in terms of the half-thickness of the inner rail, R as depicted in Figure 3. The factors used in Figure 3 are based on the actual augmented railgun geometry with bore spacing of 3/4", a 1/32″ insulation gap of mylar film and adhesive laminating sheets separating the rail surfaces, and R = 3/16″.

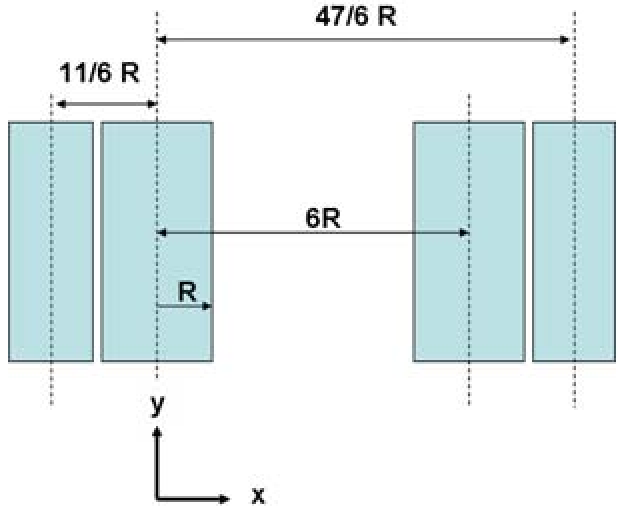


Figure 3. Augmented Railgun Geometry where R = 3/16″

The magnitude of the Lorentz force ($F$) for the geometry depicted in Figure 3 is approximated by the following equation where $\mu_0$ is the permeability constant and I is current.

$$F = \frac{\mu_0 \mathrm{I}^2}{4\pi} \int_R^{5R} \left[ \left(\frac{1}{x}\right) + \left(\frac{1}{6R - x}\right) + \left(\frac{1}{\frac{11}{6} + x}\right) + \left(\frac{1}{\frac{47}{6} - x}\right) \right] dx$$

After integrating and reducing,

$$F = \frac{\mu_0 \mathrm{I}^2}{4\pi} \left[ \ln\left(\frac{5R}{R}\right) + \ln\left(\frac{5R}{R}\right) + \ln\left(\frac{\frac{41}{6}R}{\frac{17}{6}R}\right) + \ln\left(\frac{\frac{41}{6}R}{\frac{17}{6}R}\right) \right] = \frac{\mu_0 \mathrm{I}^2}{4\pi} \left[ 2\ln(5) + 2\ln\left(\frac{41}{17}\right) \right]$$

The equation can be written in terms of the components of the total $L'$.

$$F = \frac{\mu_0 \mathrm{I}^2}{4\pi}\left[3.22+1.76\right] = \frac{1}{2}\left[\frac{\mu_0}{2\pi}\left(3.22+1.76\right)\right]\mathrm{I}^2 = \frac{1}{2}\left[L'_{\mathrm{pri}} + L'_{\mathrm{aug}}\right]\mathrm{I}^2$$

It is convenient to express the augmented inductance gradient as a gain factor that can be applied to the Kerrisk's method *L'* calculated for the non-augmented configuration.

$$\frac{L'_{\mathrm{pri}} + L'_{\mathrm{aug}}}{L'_{\mathrm{pri}}} = \frac{6.44 \bullet 10^{-7} + 3.52 \bullet 10^{-7}}{6.44 \bullet 10^{-7}} = 1.55$$

This gain factor of 1.55 is used for all subsequent discussions of the augmented inductance gradient for both slotted and solid rail configurations as demonstrated in the calculations of Appendix C. Appendix D applies COMSOL Multiphysics finite element software to model the relative improvement of the magnetic field and flux density across the center of the bore region and across the inner rail surface. COMSOL modeling neglects the geometry of the rail liner for all configurations. Electrical separation between inner and outer rail surfaces is accomplished by wrapping the outer rail in two full layers of 1.0 mil Mylar film. Although even a single layer of this film is rated to hold off the magnitude of breech voltage experienced across the rails, a slightly more robust physical interface was necessary to prevent defects in the rail surface finish from compromising the film integrity and short-circuiting the augmenting rails. Three layers of 3.0 mil adhesive laminating film supplementing the 2 layers of mylar film between the adjoining rail faces prevented the short-circuits seen in initial efforts to fire augmented.

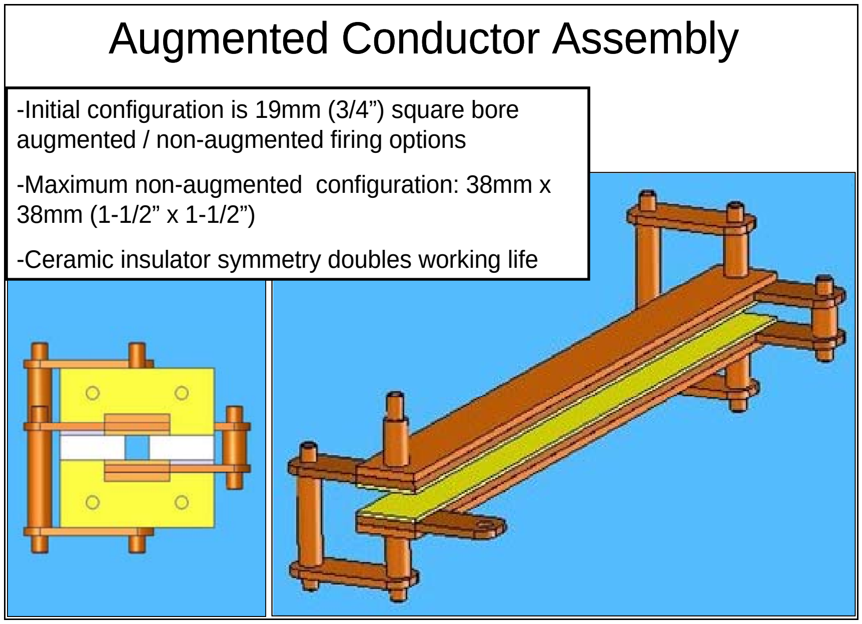


Figure 4. Augmented Conductor Assembly

Figure 4 demonstrates the augmented conductor assembly and bore geometry. By removing the external copper conducting rods the gun can be fired in the non-augmented configuration. For initial non-augmented testing, both the external conductor rods and the augmented rails were removed and a pair of G-11 FR-5 phenolic insulators was substituted to avoid eddy current losses in a disconnected rail pair.

The inner rail pair is configured to support the use of a muzzle shunt. A copper conductor bar was used to short the muzzle shunt connection during initial testing prior to using actual armatures. The limited energy and short duration current pulse available for initial testing produced a minor muzzle flash. Follow-on work will be required to optimize muzzle shunt circuit elements for operating the gun at high power in order to prevent damage to the conductors as the armature breaks contact with the muzzle. At higher energies, an effective muzzle shunt may become critical to preventing muzzle flash interference with the velocity measuring breaks-screens because of the confined operating range of the laboratory environment.

## D. IMPROVED INDUCTANCE GRADIENT WITH SLOTTED RAIL GEOMETRY

Another technique to boost the *L'* is to alter the rail geometry by a series of slots cut in to either side of the rails. The slotted geometry still provides the common rail height necessary for mechanical mounting of the rails within the containment structure, but confines current flow to a narrower center channel. This technique results in a more concentrated magnetic field within the bore region. To predict the gain provided by slotted geometry, the narrowed rail height dimension of 1” was the input parameter into the Kerrisk’s method calculation rather than the full exterior height, resulting in an expected gain factor of 1.45. Verifying an improvement in final armature velocity for a fixed input energy is significant because it has potential applications for both thermal management and rail containment designs for more advanced railgun systems.

Figure 5 demonstrates the slotted rail geometry. A detailed drawing is included in Appendix B, Figure 17. Appendix D demonstrates COMSOL Multiphysics finite element software modeling of the relative magnitude of improvement of the magnetic field (H) and magnetic flux density ($B=\mu_o H$) for slotted and non-slotted rail configurations. Figure 30 demonstrates how the altered slotted rail geometry affects the input parameters used to calculate the inductive gradient.

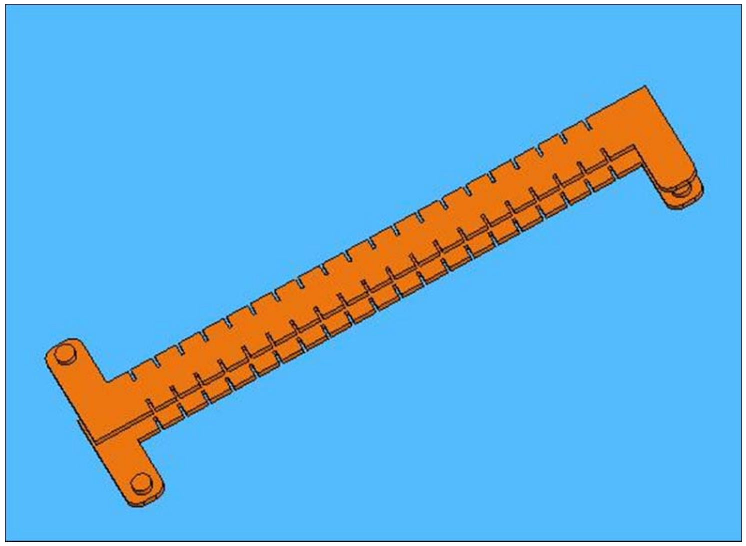

Figure 5. Slotted Rail Geometry

## E. ADDITIONAL COMPONENTS

High tolerance structural design is required to limit rail deflection and maintain a consistent bore profile. Maintaining stiffness and straightness in a short, small bore railgun is significantly easier than for a large bore 10 m gun. In order to achieve a tight rail to rail interference fit when loading the armature, the gun incorporates a manual screw auger which advances a breech block and protruding 3″ ram contoured to the back of the armature. The 3″ ram provides a consistent longitudinal starting point for testing and places the armature in a region where magnetic fields are well established. The effective railgun length beyond the loaded armature position is 50 cm. The loading apparatus is mounted at four points to the containment shells via 3/8″ stainless steel threaded rods and helicoil inserts. This apparatus is currently under-utilized because the lack of sufficient power to overcome static friction mandates a loose armature fit. Although a slight interference fit was used for the preliminary testing discussed herein, the armatures fabricated to actual design bore geometry required some volume reduction via polishing in order to prevent binding. During testing, prior to installing the loading apparatus, a bore ram is used to force the polished armature through the entire length of the gun to identify excessive regions of binding. Figure 6 shows a side and overhead view of the assembled loading apparatus.

Figure 6. Railgun Loading Apparatus

The railgun design also includes a muzzle block mounted with four 1/4" stainless steel bolts into helicoil inserts set in the containment shells. The current muzzle block has a 1-1/4” diameter hole through which the armature exits. Although this design is adequate for testing at 35 kJ, it must be improved prior to upgrading the power supply. A square muzzle port properly sized to the bore dimension may assist in confining the deleterious effects of the muzzle flash to the rail liner rather than to the underlying main conductor rail. The photograph of the muzzle block in Appendix F Figure 59, was taken immediately following a shot, and hints at the potential for arcing damage at the muzzle exit at higher energies.

A series inductor was constructed by tie-wrapping 4/0 welding cable around a PVC shape. Although a much larger inductor was initially fabricated, optimized to maximize the pulse length, its effect of diminishing peak current resulted in the inability to overcome static friction when firing with a stored energy of 35 kJ. A final compromise between peak current and pulse length was accomplished by using the three turn inductor pictured among other components in Figure 7.

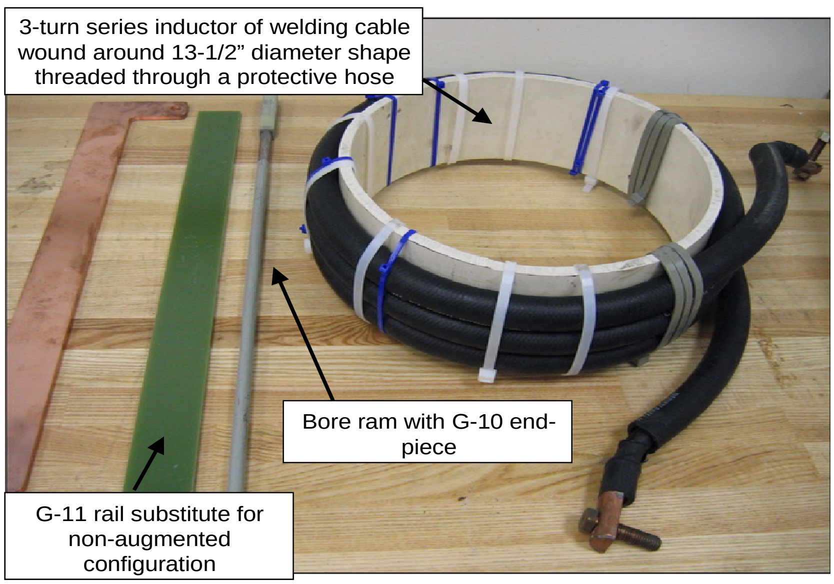


Figure 7. 3.0-μH Series Inductor and Components

In preparation for shooting at high velocities, a target chamber was custom designed and fabricated by MGM Targets. It consists of a three foot long, 10" diameter steel tube with a 6" entry portal. The tube is filled with ground rubber contained by solid rubber sheets at the entry point and along the top, where a bolted access panel allows projectile recovery. The target chamber is pictured in Figure 8.

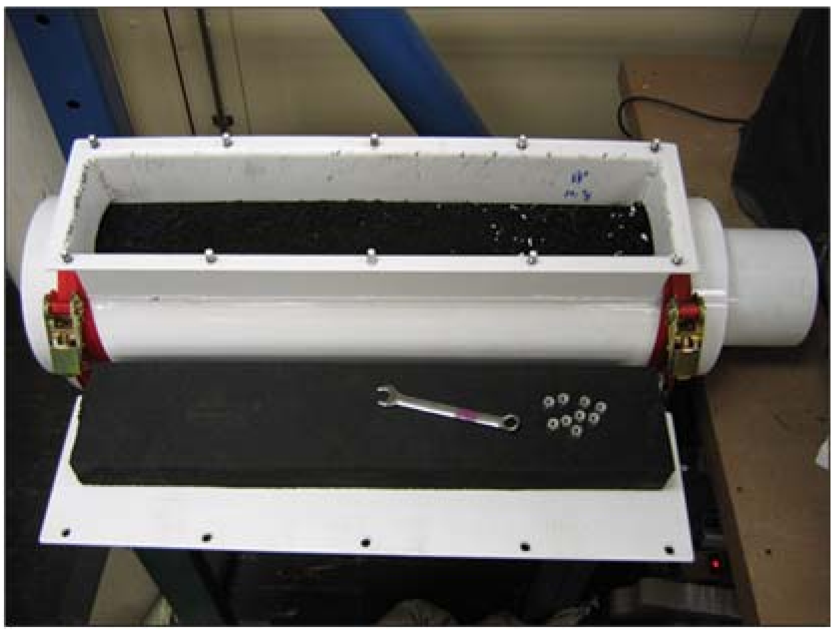

Figure 8. Target Chamber

THIS PAGE INTENTIONALLY LEFT BLANK

# III. PULSED POWER SUPPLY

## A. PRESENT SYSTEM

The stored energy supply consists of two 830 μF, 11 kV rated Maxwell Model 32327 capacitors switched by two parallel Maxwell TVS-40 vacuum switches. These capacitors discharge through dedicated pairs of high power rectifier diodes connected to a common ground which crowbar the current waveform at peak value to prevent oscillation. The diodes are model 5SDD 50N5500, manufactured by ABB Switzerland Ltd. Semiconductors. Each diode pair is constrained by an ABB diode clamp model 5SAC 18V9001, rated at 90 kN. Downstream of the diode strings, current output from each individual capacitor is monitored with two Pearson Model 1330 wide band current monitors. The outputs from the parallel TVS-40 switches are connected by a single bus bar and currents up to 500 kA are monitored by a Pearson model 1423 current monitor. Output and return leads extend through the side of a steel framed, plexiglass covered enclosure, allowing connection to the railgun leads with 4/0 Flex-a-Prene heavy duty welding cable rated for 600 Volts. The input side welding cable is wound around a 13-1/2” PVC shape to serve as a series inductor as pictured in Figure 7. In order to protect the inductor cable run from extreme compressive forces experienced during discharges, the 3/4" cable is threaded through a 7/8” inner diameter rubber hose. Figure 9 shows an overhead view of the power supply cabinet.

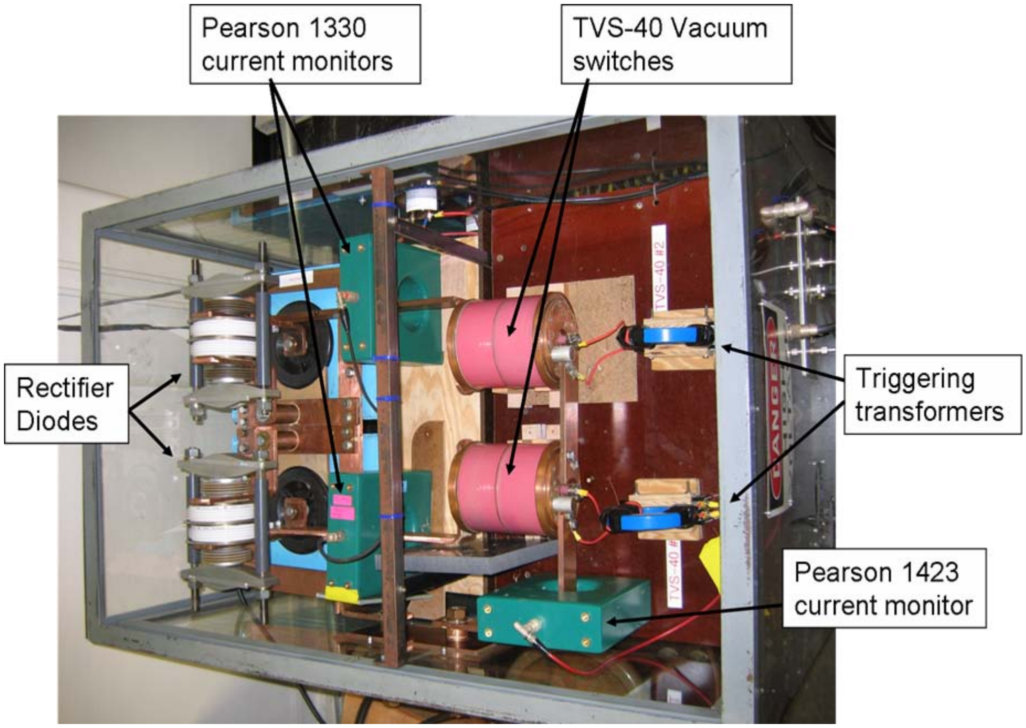


Figure 9. Power Supply Cabinet

The Pearson 1330 produces an initial 5 m-Volt/Amp output, and is further conditioned through a 10:1 attenuator before being processed for display using an Agilent Infinium S4852 oscilloscope. The Pearson 1423 produces a 1 m-Volt/Amp output, and is sent through both a 10:1 attenuator and 2:1 divider for display. Oscilloscope screen captures for each shooting configuration are included in Appendix E. Peak currents registered by the combined Pearson 1423 output ranged from 88-98 k-Amps for all four rail configurations when discharged from an initial capacitor voltage of 6500 volts. PSpice circuit modeling is included in Appendix D for the 6500 Volt initial charge and other experimentally determined values for the railgun test platform including, inductance, resistance and railgun resistance as specified in Figure 45. The railgun resistance value of 0.3 m-Ohm was initially calculated based on the material properties and cross-sectional areas of the entire railgun conductor apparatus from input to output leads.

The main capacitor pair is charged with a Bertan Associates Series 105 1kW High Voltage Power Supply through a separate circuit of diodes and resistor bars. Each capacitor is monitored by a dedicated voltmeter display panel.

Simultaneous triggering of the TVS-40 switches is done with a Glassman High Voltage Inc. Series LX High Voltage Power Supply via two 100 μF General Atomics capacitors catalog #315DM410. On a single firing signal, each 100 μF capacitor discharge is stepped up to 5kV using homemade transformers. Figure 10 demonstrates the power supply cabinet interfaces for charging, triggering, and supply and return to the railgun test platform.

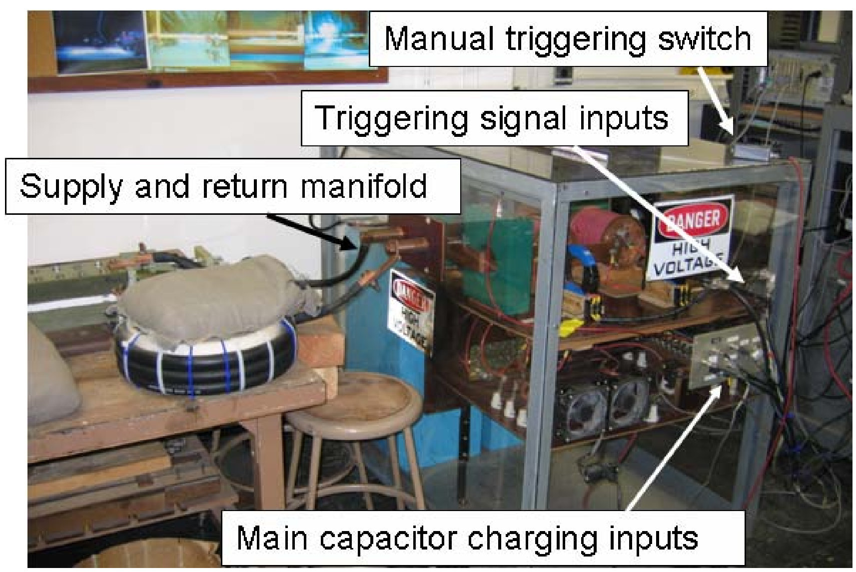


Figure 10. Power Supply Cabinet Interfaces

Throughout various stages of testing, elements within the pulsed power circuit delayed progress due to arcing, failed diodes, non-triggering switches, and ruptured transmission cable leads. Although the initial goal was to operate the capacitors at 9 kV, which would have supplied a total stored energy of 67.2 kJ, erratic switch output and spontaneous triggering above 7 kV demanded that final data collection be conducted at 6.5 kV, which limited total stored energy to 35 kJ. As the TVS-40 switches are rated beyond these limits, a documented trigger rejuvenation procedure may restore them to improved functionality [6]. The oscilloscope current traces in Appendix E clearly identify both uneven current peaking and pulse decay rates from the two capacitors attributed to uneven coupling across the TVS-40 switches.

## B. REDESIGNED POWER SUPPLY

The Naval Postgraduate School Physics Department has invested in ten new General Atomics capacitors with the same catalog number and ratings as the Maxwell Laboratories pair used for testing. Where testing for this research was limited to 35 kJ, incorporating the present and new capacitors into a multiple module system will provide a maximum stored energy capacity of 600 kJ. The older capacitors have been cycled at high voltages since at least June of 1999 and might be contributing to uneven power sharing through the TVS-40 switches. In addition to investigating switch refurbishment, a comparison of output current profiles using a pair of the new capacitors within the existing power supply would indicate whether the irregular discharge can be solely attributed to the TVS-40 switches.

In addition to the new capacitors, two new high current Titan ST-300A high action spark gap switches and associated triggering apparatus have been purchased. The Titan switches are rated for 600 kA peak current and 55 kV peak voltage and will permit a single switch to control the output of a module pair of capacitors.

Figures 47 and 48 of Appendix D demonstrate a practical four module ripple fired circuit designed to maintain an average 280 kA current pulse for 0.67 ms, which should accelerate an 11.4 gram armature to 1500 m/s over the 50 cm rail length for the slotted, augmented configuration (See Table 19). The model circuit incorporates a 1 m-Ohm muzzle shunt resistor for a first look at the dynamics which occur as the armature breaks electrical contact with the muzzle. This model requires that each module be charged to near capacity at 10 kV, and incorporates optimized delay times and series inductors. Achieving the effective rise time and peak current required to overcome the static friction of a tight interference fit requires firing the first two modules simultaneously. Such a fit is critical to maintaining the solid armature to rail interface necessary to delay transition to arcing and to prevent rail damage from intermittent armature caroming within the bore.

THIS PAGE INTENTIONALLY LEFT BLANK

# IV. DESIGN VERIFICATION

## A. PARAMETER MODEL

On May 6, 2004, Dr. Mark Crawford, Pulsed Power and Electromagnetic Launch Team Leader from IAT, presented a colloquium lecture to the Naval Postgraduate School Physics Department [7]. The dissertation outlined a top level parameter-based approach to designing a basic railgun system. The applicable thumb-rules are based on simplifying assumptions such as a symmetric acceleration profile which allows identifying both average and peak accelerations for conservative modeling of velocity performance, rail geometry, electrical action, and rail containment. Appendix C applies this parameter-based approach to the four physical configurations, solid non-augmented, slotted non-augmented, solid augmented, and slotted augmented, and to a range of energy inputs as a basis of comparison to other modeling techniques in order to validate containment bolt sizing, and to correlate average current to final velocity.

P-Spice circuit model predictions in Appendix D for the average current required to reach 1500 m/s over the 50 cm effective railgun length are based on the average required current calculated from the parameter-based model. The experimental results from the solid augmented and slotted augmented experimental shots are also inputted into the parameter model (Tables 21 and 21) for comparison. The parameter model predicts that a final armature velocity of 1500 m/s requires a peak current of nearly 500 kA for the solid, non-augmented configuration as detailed in Table 16. Therefore, 500 kA is used to assess containment deflection, and bolt diameter and spacing in Section C below. A final application of the parameter model uses bolt diameter and yield strength to predict the maximum current of 355 kA, and maximum final velocity of 1085 m/s which can be achieved on the railgun test platform with Grade 2 stainless 3/8” bolts, per Table 21.

## B. CONSERVATION OF ENERGY CIRCUIT MODEL

In order to evaluate experimental results and estimate velocity performance for an effective rail length of 50 cm, a simplified circuit model was developed for a single module capacitive stored energy power supply. Appendix C details the process which applies conservation of energy principles to Kirchhoff’s Voltage law, coupling inductive energy transfer to projectile kinetic energy via Lorentz force parameters. In the following equation, $F$ is the Lorentz force accelerating the armature, $m$ is the armature mass, $dv/dt$ is armature acceleration, $L'$ is the inductive gradient of the rails, and $I$ is the time dependant value of current.

$$F = m\frac{dv}{dt} = \frac{1}{2}L'I^2$$

The model neglects frictional losses and relies on several simplifying assumptions including assuming that the total system inductance $L$ is much larger than the product of $L'$ and rail length x. The model also assumes that the total effective system resistance R is much larger than the resistance R’x, where R’ is the rail resistance per unit length. In both cases, $L$ and R are verified experimentally to be an order of magnitude larger then $L'$x and R’x for the

60 cm test platform. $L$ is calculated based on the rise time to peak current in a discharge cycle, measured by oscilloscope at 150 μs. The following equation for the period of oscillation $T$ demonstrates how inductance can be solved based on the known capacitance C of 1.66 mF.

$$T = 4\Delta t_{rise} = 2\pi\sqrt{LC}$$

In order to simplify the model to a purely inductive energy transfer between the total system inductance and the railgun, the capacitive stored energy is eliminated from the final expression by neglecting the initial 150 μs of current ramping up to its peak value. The increase in armature velocity during the rise time is small. The time dependent expression for current is an exponentially decaying waveform:

$$I(t) = I_o \exp^{\left(\frac{-Rt}{L}\right)},$$

where the peak current $I_o$ is determined by:

$$I_0 = \left(\frac{C}{L}\right)^{\frac{1}{2}} V_o\,.$$

$V_o$ is the initial state of capacitor voltage which for my experimental data runs was 6500 Volts. The resulting expression provides for a separable differential equation for rail length as a function of velocity [4].

$$v\frac{dv}{dx} + \frac{2Rv}{L} + \frac{L'v^2}{L} = \frac{L'I_o^2}{2m}$$

An integral table gives the expression including the integration constant $D$.

$$\int dx = \frac{1}{2a}\ln\left(av^2 + bv + c\right) - \frac{b}{2a}\left[\frac{1}{\sqrt{b^2 - 4ac}}\ln\left(\frac{2av + b - \sqrt{b^2 - 4ac}}{2av + b + \sqrt{b^2 - 4ac}}\right)\right] + D$$

The circuit parameters which comprise factors $a$ , $b$ , and $c$ , are defined below.

$$a = \frac{-L'}{L} \qquad b = \frac{-2R}{L} \qquad c = \frac{\left[L'\left(\frac{1}{2}CV_o^2\right)\right]}{(mL)}$$

The integration constant $D$ scales the solution such that zero velocity corresponds to a zero length railgun. The actual values used for each variable are included in Tables 22-26 of Appendix C.

Table 25 gives the integration for parameters associated with the slotted augmented rail configuration, and predicts a final velocity of 293 m/s corresponding to the 50 cm effective rail length, and total stored energy of 35 kJ. I have neglected the minimal projectile velocity which exists when $I = I_o$, as well as losses due to friction between the rails and armature, the effects of which compensate for each other to some extent.

## C. STRUCTURAL DESIGN

The 24″ railgun containment halves are clamped by a total of 22 Grade 2 stainless hex-head steel bolts of 3/8″ diameter, rated by the vendor at 57 ksi in accordance with the SAE J420 1985 abstract [8]. The bolts are longitudinally spaced at 2″ intervals down the length of the containment beginning 1″ from either end.

Conservative static modeling assumptions were applied to assess the overall containment design in terms of rail deflection, bolt spacing and diameter. From the solid non-augmented configuration and the 500 kA peak current predicted in Table 16 of Appendix C, rail repulsion force per unit length, $p$, is calculated by using the following equation.

$$p = \frac{F}{x} = \frac{\mu_o I^2}{2\pi d} = \frac{\left(4\pi \bullet 10^{-7}\right)\left(500kA\right)^2}{\left(2\pi \bullet 0.0286\right)} \approx 1.75\frac{MN}{m} \approx 9983\frac{lb_f}{in}$$

In the previous equation, $F$ is the rail repulsion force, $x$ is the total rail length, $\mu_o$ is the permeability constant, $I$ is peak current, and $d$ is the length in meters between rail centerlines considering the rail liner and primary rail as a single solid conductor.

Two specific structural design objectives are investigated.

Maximum rail deflection must be limited to less than 0.0001 inches,

Under worst case loading, the containment bolts must not exceed their static yield strength.

A 2-D model of the distributed longitudinal rail repulsion force between any two consecutive bolt pairs is represented by the fixed-end beam model in Figure 11.

$$y_{\max} = y\left(\frac{L}{2}\right) = \frac{pL^4}{384EI}$$

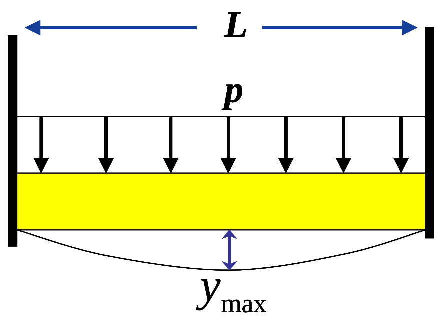


Figure 11. Fixed End Distributed Load Beam Model [After Ref. 9]

Maximum deflection, $y_{\max}$, occurs at the midpoint between bolts spaced at a distance L, of 2″. $E$ is the modulus of elasticity, and $I$ is the moment of inertia based on the beam cross-section. Appendix C, Section C, demonstrates the method used to simplify the composite materials and geometry into a single representative, homogenous beam in order to determine maximum deflection. For 9983 lbf/in loading, the calculated deflection is less than 0.00002 inches, confirming adequate containment stiffness.

The validity of the previous deflection calculation depends on achieving the fixed boundary conditions of no slope and no deflection based on bolt loading conditions. Here I consider the total rail length, x = 24″, and the total of 22 bolts of 3/8″ diameter to determine the maximum load per unit length ($p_{\max}$) achievable at the bolt Yield Strength (YS) threshold of 57 ksi.

$$p_{\max} = \frac{\#bolts \bullet A_{bolt} \bullet YS}{x} = \frac{\left(22 * 0.1104 in^2 \bullet 57{,}000 \frac{lbf}{in^2}\right)}{24 in} \approx 5770 \frac{lbf}{in} < 9983 \frac{lbf}{in}$$

The maximum sustainable load of 5770 lbf/in is less than that which results from the 500 kA peak current condition corresponding to a 1500 m/s exist velocity for the solid non-augmented configuration. As such, $p_{\max}$ is used to determine the actual peak current capacity to inform follow on testing. Converting 5770 *lbf/in* to metric units yields approximately 1.01 *MN/m*.

$$I_{\max} = \sqrt{\frac{2\pi d \bullet p_{\max}}{\mu_o}} \approx \sqrt{\frac{2\pi \bullet 0.0286 m \bullet 1.01 \frac{MN}{m}}{4\pi \bullet 10^{-7} \frac{N}{A^2}}} \approx 380 kA$$

The resulting calculation shows that the present containment design is capable of maintaining bolt loading below yield strength up to a maximum current of 380 kA. Based on parameter modeling in Table 22, this peak load capacity correlates with the alternative method of rail repulsion force and bore height to calculate the force per unit length. Table 22 indicates that the Grade 2 bolt yield strength threshold is achieved at 355 kA, correlating to a final velocity of about 1085 m/s. Therefore, in order to achieve the no-yield requirement at 500 kA, the grade 2 stainless bolts must be upgraded to grade 8. The ACF Components vendor quotes grade 8 hex head bolts at a yield strength of 130,000 ksi [8].

$$p_{\max} = \frac{\#bolts \bullet A_{bolt} \bullet YS}{x} = \frac{\left(22 * 0.1104 in^2 \bullet 130 \frac{kip}{in^2}\right)}{24 in} \approx 13{,}156 \frac{lbf}{in} > 9983 \frac{lbf}{in}$$

The grade 2 hardware currently in use will suffice until considerable additional stored energy is integrated into the pulsed power supply. All containment modeling is based on conservative static loading rather than the actual dynamic loading which occurs during firing. The previous design verification methods demonstrate an adequate containment such that future efforts to improve bore tolerance should concentrate on deficiencies in the rail liner surface finish rather than the overall structural design.

# V. RESULTS

## A. SHOT DIAGNOSTICS

Table 3 lists the experimental results.

| Shot | Configuration | L' | System | Voltage | Initial | Final | Input Energy | $I_{peak}$ | Velocity | KE | Efficiency |
|---|---|---|---|---|---|---|---|---|---|---|---|
| | | (uH/m) | L (μH) | (V) | Mass(g) | Mass(g) | (KJ) | (k-Amps) | (m/s) | (J) | |
| 1 | solid, non-aug | 0.3037 | 5 | 8000 | 11 | 10.2 | 53 | N/A | 246 | 332.8 | 0.63% |
| 2 | solid, non-aug | 0.3037 | 2.5 | 6500 | 11.4 | 10.6 | 35 | 110 | 168 | 160.9 | 0.46% |
| 3 | solid, non-aug | 0.3037 | 5.5 | 6500 | 11.4 | 11 | 35 | 97.8 | 105 | 62.8 | 0.18% |
| 4 | slot, non-aug | 0.4405 | 5.5 | 6500 | 11.4 | 10.9 | 35 | 88.0 | 117 | 78.0 | 0.22% |
| 5 | solid, aug | 0.4707 | 5.5 | 6500 | 11.2 | 10.6 | 35 | 95.0 | 265 | 393.3 | 1.12% |
| 6 | slotted, aug | 0.6828 | 5.5 | 6500 | 11.4 | 11.2 | 35 | 91.4 | 294 | 492.7 | 1.41% |
| 7 | slotted, aug | 0.6828 | 5.5 | 6500 | 11.4 | 11.1 | 35 | 88.9 | 286 | 466.2 | 1.33% |

Table 3. Experimental Data Results

Shots 3-7 were all conducted with the same series inductor and initial capacitor charge of 6.5 kV in order to compare each configuration. Shot 1 was taken with a capacitor charge of 8 kV and a 5 μH total system inductance. This 8 kV shot produced two in a longer series of testing delays caused by the failure of components within the pulsed power supply. On this shot in particular, the series inductor solid copper cable lead separated from the cable run. Also, the forces squeezing the series inductor coils together axially ruptured the rubber insulating sheath and rendered the line unusable. The peak current value for the 8 kV shot was unreadable due to over-ranging the oscilloscope settings. After the 8 kV shot, the TVS-40 switches began to spontaneously trigger when charged up to 7 kV, ultimately demanding that the data runs be limited to 6.5 kV. Prior to re-introducing a new series inductor, a new sheathed cable run was threaded through a 7/8” inner diameter rubber hose to prevent a similar rupture, and new cable leads were fabricated.

The 2.5 μH inductance listed for shot 2 represents the total system inductance with no additional series inductor. Although the resultant velocity of 168 m/s surpassed all other subsequent non-augmented shots which did incorporate a series inductor, the higher current peaking resulted in one TVS-40 switch failing completely. Upon obtaining a replacement switch, a 3 μH series inductor was used for all further testing in order to avoid over-stressing the system while permitting consistent test parameters for all shooting configurations.

The remaining experimental firings, shots 3-7 of Table 3, were conducted at 6.5 kV with a total system inductance of 5.5 μH. Although statistically insignificant for the single point sampling, the resultant velocities demonstrate a trend consistent with each improvement in the inductance gradient, ranging from 105 m/s for the solid non-augmented configuration to an average of 290 m/s for the two slotted augmented shots.

The respective gain factors for slotted geometry, series augmentation, and their combined totals as predicted by the L′ and magnetic field models detailed in Appendix C are compared to the experimental gain in Table 4. The experimental gain factors are determined by the following ratios.

$$\frac{m_{slotted} v_{slotted}^2}{m_{solid} v_{solid}^2} = Gain_{geometry} \qquad \frac{m_{aug} v_{aug}^2}{m_{non-aug} v_{non-aug}^2} = Gain_{aug}$$

For all cases other than solid augmented, the initial mass is 11.4 grams and cancels leaving a ratio of the square of the final velocities. The augmented gain factor is an average of the gains calculated for both the slotted and solid rail geometries. The lower than expected velocities for the non-augmented configurations in shots 3 and 4, suggest that given only 35 kJ of stored energy and diminished magnetic fields without augmentation, the accelerating force is near the threshold of overcoming static friction. Shot 2 for the solid non-augmented configuration with no series inductor produced a final velocity closer to the value expected by the conservation of energy model in Table 23. Although data for a slotted non-augmented shot without a series inductor is not available at this time, the experimentally determined gain factors in Table 4 marked with an asterisk (*) use the 168 m/s velocity result of shot 2.

| Gain Factors | L' Geometry Modeling | Magnetic Field Modeling | Experimental Results ($mv^2$) |
|---|---|---|---|
| **Series Augmentation** | 1.55 | 1.66 | 6.26 ( * 2.49 ) |
| **Slotted Geometry** | 1.45 | 1.5 | 1.22 |
| **Total Gain** | 2.25 | 2.49 | 7.63 ( * 2.98 ) |

Table 4. Predicted vs. Experimental Gain Factors

There is close agreement between gain factors produced by the two respective modeling techniques. Due to the limited data runs, the experimental gain factors are unreliable and deviate from the models. In all cases, both the augmentation and the slotted geometry resulted in improvements in final velocity.

Additional shots which were performed prior to operational velocity diagnostics suggest that the lower velocity results from shots 3 and 4 may have been the result of insufficient power to overcome static friction. During two early shots at the 35 kJ level, using a 22.5 μH series inductor intended to match the current pulse length to the total rail length, the armature in one case did not break static friction at all, and in another traveled only 3 inches down the barrel.

Significant enhancement of the stored energy supply is necessary to generate valid experimental results for comparison to the idealized models which neglect frictional losses. Furthermore, the moderately loose interference fit between the armature and bore used in these tests is entirely inadequate for maintaining effective electrical contact at higher velocity regimes. When the pulsed power supply is adequately hardened to permit extracting stored energy near the capacity of individual modules, and when multiple modules contribute to building an adequate current waveform, the loader mechanism can be used to provide an appropriately tight interference fit. The consistency of this fit along the bore length as indicated by the torque required to manually advance a test round, and the use of a torque wrench on the loading mechanism may be critical to establishing conditions necessary to validate gain factors experimentally.

The parameter based modeling in Appendix C predicts no violations of generally accepted thresholds such as rail heating and linear current density for all configurations when the muzzle velocity is 1500 m/s. The peak current, parameter based calculations for the minimum adequate bolt diameter are in close agreement with the calculations performed using classic beam bending analysis. Both methods indicate that the Grade 2 bolt will reach their yield strength threshold between 335 and 380 kA, with the resulting exit velocity ranging from 1085-1150 m/s.

The conservation of energy model prediction of 293 m/s velocity for the slotted augmented configuration with 35 kJ of stored energy compares with the average experimental velocity of 290 m/s. The conservation of energy model was also evaluated to predict the maximum velocity which could be achieved by a single module of two capacitors charged to 10 kV, which corresponds to 83 kJ of stored energy. The resultant velocity for the 50 cm effective rail length is 495 m/s.

The current traces in Appendix E from the experimental shots indicate that the magnitude of current ($I$) is small as the projectile exits the gun. A total system resistance of 3.3 m-Ohm has been used for all simulations. The power supply resistance was measured to be 3 m-Ohm and the rail resistance was calculated to be 0.3 m-Ohm from the resistivity and geometry of the copper conductors within the railgun assembly from input to output leads. R/L′ is calculated for each shot in Table 5. The R/L′ ratio is calculated by the following equation where each of the terms is defined in Table 5.

$$\frac{R}{L'} = \frac{1}{2mv}\left(W_{o\_} - KE\right)$$

Shots 1-2, and 5-7 support the model parameter of 3.3 m-Ohms of total system resistance. The two low velocity non-augmented results for shots 3 and 4 are outliers at 4.44 and 5.78 m-Ohms respectively, suggesting additional frictional losses.

| Shot | Configuration | L' | Armature | Input Energy | Velocity | Kinetic Energy | R/L' | R |
|---|---|---|---|---|---|---|---|---|
| | | (uH/m) | Mass(g) | $W_o$ (KJ) | (m/s) | KE (J) | (Ohm-m/H ) | (m-Ohm) |
| 1 | solid, non-aug | 0.3037 | 11 | 53 | 246 | 332.8 | 9793 | 2.97 |
| 2 | solid, non-aug | 0.3037 | 11.4 | 35 | 168 | 160.9 | 9137 | 2.77 |
| 3 | solid, non-aug | 0.3037 | 11.4 | 35 | 105 | 62.8 | 14620 | 4.44 |
| 4 | slot, non-aug | 0.4405 | 11.4 | 35 | 117 | 78.0 | 13120 | 5.78 |
| 5 | solid, aug | 0.4707 | 11.2 | 35 | 265 | 393.3 | 5896 | 2.78 |
| 6 | slotted, aug | 0.6828 | 11.4 | 35 | 294 | 492.7 | 5221 | 3.57 |
| 7 | slotted, aug | 0.6828 | 11.4 | 35 | 286 | 466.2 | 5367 | 3.66 |

Table 5. Total System Resistance and R/L′ Results

Appendix F includes photographs of typical rail, insulator, and armature wear. Every shot resulted in a thin coating of melted aluminum deposited along the rail length. Gaps in the presence of the coating correlated to the localized damage in the chromium copper rail material suggesting specific locations where arcing developed between the armature and rail. Micrometer measurements of the as-fabricated 3/4" square Aluminum 6063 armatures measure at 0.748″ where the same measurements for the ceramic insulator thickness hold the tighter tolerance of 0.750″ +/- 0.0001 along the entire length. Although these dimensions suggest an ideal fit, the surface finish in the bore region of the rail liner is accomplished by 400 grit belt sanding followed by 600 grit hand sanding. Hand feeding of the armatures down the bore length indicates alternating regions of binding and slipping. As a result, the final loose sliding fit was accomplished by polishing the outer armature faces. The volume of material removed by this polishing was significant: all of the as-fabricated armatures had an initial mass of 11.6 grams but the typical final armature launch mass was 11.4 grams. In general, the more material removed from the armature during polishing to provide a working fit, the more rail damage observed post-firing due to caroming of the round back and forth between the rails during launch. The extreme variation in electrical contact during launch which results from such a poor fit contributed to the rail damage as demonstrated by localized blackened aluminum and copper regions where arcing likely occurred.

In one shot, the results of which are not included in Table 3 due to occurring prior to effective diagnostics, the as-fabricated armature provided a working fit without polishing. This particular shot produced an even aluminum coating down the entire rail length with no visible damage to the underlying rail liner. Inspections of the spent armatures reveal that the highest velocity shots experience the least loss of armature mass, and the least deformation of the trailing arms. Root radius wear for the augmented higher velocity shots was grainy but retained the aluminum metallic tone whereas the root radius of the non-augmented shots was obscured by blackened deposits. Although the current levels experienced in this testing are far less than the 900 kA threshold for root radius melting observed by Francis Stefani and Trevor Watt for a 40 mm square bore railgun, visual inspection of the spent armatures suggest that the onset may occur at significantly lower currents for this small bore test platform [13].

THIS PAGE INTENTIONALLY LEFT BLANK

# VI. CONCLUSION

## A. PERFORMANCE SUMMARY AND RECOMMENDATIONS

The trend of improved velocity corresponding to engineered inductance gradients, and qualitative agreement between alternative modeling approaches indicates that there are no immediate impediments to scaling the stored energy supply in order to experiment with higher velocity regimes on this railgun test platform. However, incremental advances are recommended in order to allow the development of pulsed power supply components and diagnostics. Before moving to multi-module pulsed energy configurations, fully harnessing the stored energy of a single module must be demonstrated. As previously discussed, a 10 kV charge corresponding to a total stored energy of 83 kJ should produce nearly 500 m/s. Concurrent with fully utilizing a single module, the armatures can be loaded into a mid-bore position, reducing the effective rail length to an appropriate value such as 25 cm in order to investigate behavior when there is significant current as the armature exits the rails. This would provide the opportunity to experiment with a muzzle shunt present.

The present method of connecting the series inductor welding cable directly to the railgun conductor leads must be improved by the addition of fixed manifolds which decouple the physical stress of the inductor from the railgun itself. Such a fixed manifold could then be directly coupled to the railgun supply and return conductors via a solid copper bus-bar.

The basic mechanical containment is sound for scaling to at least 1085 m/s using Grade 2 stainless bolts.

Upgrading to Grade 8 stainless steel bolts permits scaling above 1500 m/s for all configurations. However, the likely weak points related to the mechanical design are the threaded and braised conductor connections where the augmenting rails connect to the containment penetrating conductor rods used for augmented operation, as demonstrated in Figure 12.

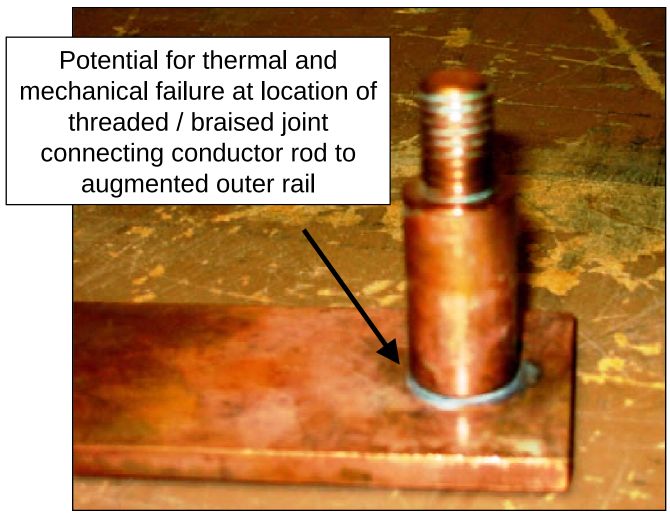


Figure 12. Augmented Rail to Conductor Threaded and Braised Joint

As adequate stored energy becomes available, in addition to targeting increases in the degree of interference fit, incorporating a bore rider in front of the armature either attached or as an independent projectile load may help both seal the bore in front of the armature to prevent blowing by of the liquid interface layer, and stabilize the armature ride within the bore, preventing the damage due to caroming which currently exists.

A variety of armature geometries, pictured in Figure 13, have been fabricated to provide options for improving the elastic response in the trailing arms in order to maintain solid to solid electrical contact with the rails.

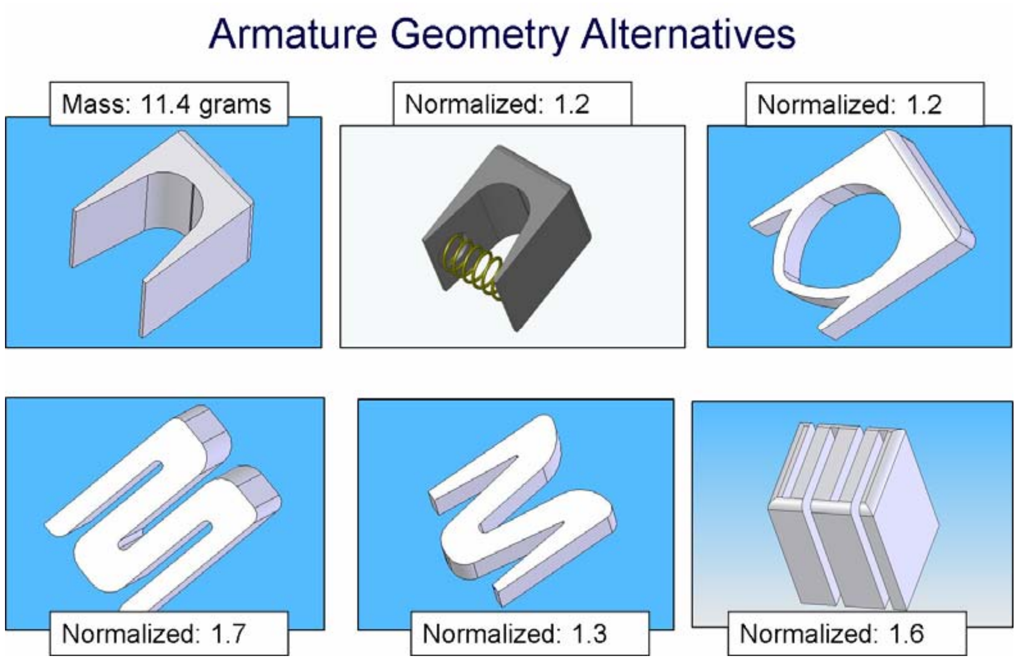

Figure 13. Armature Geometry Alternatives (Appendix B)

## B. MATERIALS PROCESSING METHODS

Anticipating the maturation of the power supply, preparations for the first application of the railgun test platform have been initiated. A collaboration between Lawrence Livermore (LLNL) and Sandia National Laboratories (SNL) is underway in order to conduct in-bore testing of laser peened [13], ion-beam surface treated [14], and untreated rail liner samples for the chromium copper, phosphor bronze, copper tungsten, and aluminum 7075 alloys discussed in Table 2.

Timothy Renk, Project Leader for Materials Applications of Ion Beams at Sandia’s Materials Modification Laboratory, has performed ion beam surface treatments on pairs of each of these materials. Tania Zaleski, Project Leader for Laser Peening at LLNL, has conducted preliminary micro-hardness testing on each material treated by a range of laser parameters in order to determine the optimal parameters to be used on the full rail liners. Following completion of the rail liner peening, and nano-hardness testing on the ion beam treated samples, LCDR Paul Clifford, USN, will conduct a series of shots at the Naval Postgraduate School in order to assess the suitability of these processes for enhancing rail life over untreated liner materials.

# APPENDIX A. MATERIAL PROPERTY DATA SHEETS

Rail liner: Chromium Copper UNS C18200, TH04

| **MatWeb Data Sheet** | | | **Date: 7/12/2005** | |
|---|---|---|---|---|
| **Chromium Copper, UNS C18200, TH04 Temper flat products, aged** | | | | |
| **KeyWords:** CDA 182, CC101, ISO CuCr1, CEN CW105C, A2/1 | | | | |
| **SubCat:** Copper Alloy, Nonferrous Metal, Metal | | | | |
| **Material Notes:** Good to excellent corrosion resistance. Excellent cold workability; good hot | | | | |
| **Applications:** resistance welding electrodes, seam welding wheels, switch gear, electrode | | | | |
| Available as flat products, wire, rod, tube, and shapes. | | | | |
| **Component** | **Value** | **Min** | **Max** | |
| Chromium, Cr | | 0.6 | 1.2 | |
| Copper, Cu | 99.1 | | | |
| Iron, Fe | | | 0.1 | |
| Lead, Pb | | | 0.05 | |
| Silicon, Si | | | 0.1 | |
| **Properties** | **Value** | **Min** | **Max** | **Comment** |
| **Physical** | | | | |
| Density, g/cc | 8.89 | -- | -- | at 20°C (68°F) |
| **Mechanical** | | | | |
| Hardness, Rockwell B | 79 | -- | -- | |
| Tensile Strength, Ultimate, MPa | 460 | -- | -- | |
| Tensile Strength, Yield, MPa | 405 | -- | -- | |
| Elongation at Break, % | 14 | -- | -- | In 50 mm |
| Modulus of Elasticity, GPa | 130 | -- | -- | |
| Poissons Ratio | 0.3 | -- | -- | |
| Machinability, % | 20 | -- | -- | UNS C36000 (free-cutting brass) = 100% |
| Shear Modulus, GPa | 50 | -- | -- | |
| **Electrical** | | | | |
| Electrical Resistivity, ohm-cm | 2.16E-06 | -- | -- | at 20°C (68°F) |
| **Thermal** | | | | |
| CTE, linear 20°C, µm/m-°C | 17.6 | -- | -- | from 20-100°C (68-212°F) |
| Heat Capacity, J/g-°C | 0.385 | -- | -- | |
| Thermal Conductivity, W/m-K | 171 | -- | -- | TB00 temper at 20°C (68°F) |
| Melting Point, °C | -- | 1070 | 1075 | |
| Solidus, °C | 1070 | -- | -- | |
| Liquidus, °C | 1075 | -- | -- | |
| **Processing** | | | | |
| Solution Temperature, °C | -- | 980 | 1000 | For 10-30 minutes, water quench |
| Aging Temperature, °C | -- | 425 | 500 | For 2-4 hours |
| Hot-Working Temperature, °C | -- | 800 | 925 | |

Table 6. Chromium Copper Rail Liner Material Properties [After Ref. 2]

Main conductor rails: OFE Copper C10100, H04

| MatWeb Data Sheet | Date: 7/12/2005 | | | |
|---|---|---|---|---|
| **Oxygen-free Electronic Copper (OFE), UNS C10100, H04 Temper, flat products** | | | | |
| **KeyWords:** BS C110, C103 , ISO Cu-OFE, CEN CW009A, oxygen-free high conductivity copper (OFHC), CDA 101 | | | | |
| **SubCat:** Copper Alloy, Nonferrous Metal, Wrought Copper, Metal | | | | |
| **Material Notes:** Flat test specimens, 1mm and 6mm thick, H04 temper. | | | | |
| **Applications:** busbars, bus conductors, waveguides, hollow conductors, lead-in wires and anodes for vacuum tubes, | | | | |
| **Processing:** Excellent hot and cold workability; good forgeability. Fabricated by bending, coining, coppersmithing, | | | | |
| **Corrosion Resistance:** Good to excellent. Susceptible to galvanic corrosion when coupled with iron, aluminum, | | | | |
| **Component** | **Value** | **Min** | **Max** | |
| Copper, Cu | | 99.99 | | |
| **Properties** | **Value** | **Min** | **Max** | **Comment** |
| **Physical** | | | | |
| Density, g/cc | 8.94 | -- | -- | at 20°C (68°F) |
| **Mechanical** | | | | |
| Hardness, Rockwell B | 50 | -- | -- | |
| Hardness, Rockwell F | 90 | -- | -- | |
| Hardness, HR30T | 57 | -- | -- | 1mm thick flat specimen |
| Tensile Strength, Ultimate, MPa | 345 | -- | -- | |
| Tensile Strength, Yield, MPa | 310 | -- | -- | 0.5% extension |
| Elongation at Break, % | 6 | -- | -- | 1mm thick flat specimen |
| Elongation at Break, % | 12 | -- | -- | 6 mm specimen. |
| Modulus of Elasticity, GPa | 115 | -- | -- | |
| Poissons Ratio | 0.31 | -- | -- | |
| Fatigue Strength, MPa | 90 | -- | -- | 1E+09 cycles, 1 mm thick flat test specimen. |
| Machinability, % | 20 | -- | -- | UNS C36000 (free-cutting brass) = 100% |
| Shear Modulus, GPa | 44 | -- | -- | |
| Shear Strength, MPa | 195 | -- | -- | |
| **Electrical** | | | | |
| Electrical Resistivity, ohm-cm | 1.71E-06 | -- | -- | at 20° C (68°F) |
| **Thermal** | | | | |
| CTE, linear 20°C, µm/m-°C | 17 | -- | -- | from 20-100°C (68-212°F) |
| CTE, linear 100°C, µm/m-°C | 17.3 | -- | -- | from 20-200°C (68-390°F) |
| CTE, linear 250°C, µm/m-°C | 17.7 | -- | -- | from 20-300°C (68-570°F) |
| Heat Capacity, J/g-°C | 0.385 | -- | -- | at 20°C (68°F) |
| Thermal Conductivity, W/m-K | 391 | -- | -- | at 20°C (68°F) |
| Melting Point, °C | 1083 | -- | -- | |
| **Processing** | | | | |
| Annealing Temperature, °C | -- | 375 | 650 | |
| Hot-Working Temperature, °C | -- | 750 | 875 | |
| Recrystallization Temperature, °C | 18.3 | -- | -- | C37700 (forging brass) = 100% |

Table 7. Oxygen Free Copper Rail Liner Material Properties [After Ref. 2]

Rail liner: Phosphor bronze C51000, H06

| MatWeb Data Sheet | Date: 7/12/2005 | | | |
|---|---|---|---|---|
| **Phosphor bronze 5% Sn, UNS C51000, H06 Temper flat products** | | | | |
| **KeyWords:** CDA 510, PB102, ISO CuSn5 | | | | |
| **SubCat:** Copper Alloy, Nonferrous Metal, Bronze, Metal | | | | |
| **Material Notes:** Good to excellent corrosion resistance. Excellent cold workability. Fabricated by blanking, | | | | |
| **Applications:** bellows, bourdon tubing, clutch discs, cotter pins, diaphragms, fasteners, lock washers, wire brushes, chemical hardware, textile machinery, welding rod. | | | | |
| Trace content of Phosphorus. | | | | |
| Test specimen: flat products - 1mm | | | | |
| **Component** | **Value** | **Min** | **Max** | |
| Copper, Cu | | 93.6 | 95.6 | |
| Iron, Fe | | | 0.1 | |
| Phosphorous, P | | 0.03 | 0.35 | |
| Lead, Pb | | | 0.05 | |
| Tin, Sn | | 4.2 | 5.8 | |
| Zinc, Zn | | | 0.3 | |
| | | | | |
| **Properties** | **Value** | **Min** | **Max** | **Comment** |
| **Physical** | | | | |
| Density, g/cc | 8.86 | -- | -- | at 20°C (68°F) |
| **Mechanical** | | | | |
| Hardness, Rockwell B | 93 | -- | -- | |
| Tensile Strength, Ultimate, MPa | 535 | -- | -- | |
| Tensile Strength, Yield, MPa | 550 | -- | -- | 0.5% extension under load |
| Elongation at Break, % | 6 | -- | -- | In 50 mm |
| Modulus of Elasticity, GPa | 110 | -- | -- | |
| Poissons Ratio | 0.341 | -- | -- | |
| Fatigue Strength, MPa | 205 | -- | -- | At 10^8 cycles, 1 mm strip |
| Machinability, % | 20 | -- | -- | UNS C36000 (free-cutting brass) = 100% |
| Shear Modulus, GPa | 41 | -- | -- | |
| **Electrical** | | | | |
| Electrical Resistivity, ohm-cm | 8.70E-06 | -- | -- | at 20°C (68°F) |
| **Thermal** | | | | |
| CTE, linear 250°C, µm/m-°C | 17.8 | -- | -- | from 20-300°C (68-570°F) |
| Heat Capacity, J/g-°C | 0.38 | -- | -- | |
| Thermal Conductivity, W/m-K | 84 | -- | -- | at 20°C (68°F) |
| Melting Point, °C | -- | 975 | 1060 | |
| Solidus, °C | 975 | -- | -- | |
| Liquidus, °C | 1060 | -- | -- | |
| **Processing** | | | | |
| Annealing Temperature, °C | -- | 475 | 675 | |

Table 8. Phosphor Bronze Rail Liner Material Properties [After Ref. 2]

Rail liner: CW 75 Class 11 25%Copper 75%Tungsten

| **MatWeb Data Sheet** | **Date: 7/12/2005** | | | |
|---|---|---|---|---|
| **CMW ELKONITE® 10W3 (Copper Tungsten) RWMA Class 11** | | | | |
| **SubCat:** Metal Matrix Composite, Copper Alloy, Tungsten Alloy, Nonferrous Metal, Metal | | | | |
| **Material Notes:** Electrical contacts resistant to arcing, power transformer switches, resistance / projection welding electrodes, and EDM electrodes | | | | |
| Information provided by CMW Inc. | | | | |
| **Component** | **Value** | **Min** | **Max** | |
| Copper, Cu | 25 | | | |
| Tungsten, W | 75 | | | |
| **Properties** | **Value** | **Min** | **Max** | **Comment** |
| **Physical** | | | | |
| Density, g/cc | 14.84 | -- | -- | |
| **Mechanical** | | | | |
| Hardness, Rockwell B | 98 | -- | -- | |
| Flexural Modulus, GPa | 1.03 | -- | -- | |
| **Electrical** | | | | |
| Electrical Resistivity, ohm-cm | 3.83E-06 | -- | -- | (45% IACS) |
| **Thermal** | | | | |
| Thermal Conductivity, W/m-K | 220 | -- | -- | |
| Melting Point, °C | -- | 1085 | 3410 | |
| Solidus, °C | 1085 | -- | -- | |
| Liquidus, °C | 3410 | -- | -- | |

Table 9. Copper Tungsten Rail Liner Properties [After Ref. 2]

Rail liner: Aluminum 7075-T651

| **MatWeb Data Sheet** | | | | **Date: 7/12/2005** |
|---|---|---|---|---|
| **Aluminum 7075-T6; 7075-T651** | | | | |
| **Material Notes:** General 7075 characteristics and uses (from Alcoa): Very high strength material used for highly stressed structural parts. The T7351 temper offers improved stress-corrosion cracking resistance. | | | | |
| **Applications:** Aircraft fittings, gears and shafts, fuse parts, meter shafts and gears, missile parts, regulating valve parts, worm gears, keys, aircraft, aerospace and defense applications; bike frames, all terrain vehicle (ATV) sprockets. | | | | |
| Data points with the AA note have been provided by the Aluminum Association, Inc. and are NOT FOR DESIGN. | | | | |
| **Component** | **Value** | **Min** | **Max** | |
| Aluminum, Al | | 87.1 | 91.4 | |
| Chromium, Cr | | 0.18 | 0.28 | |
| Copper, Cu | | 1.2 | 2 | |
| Iron, Fe | | | 0.5 | |
| Magnesium, Mg | | 2.1 | 2.9 | |
| Manganese, Mn | | | 0.3 | |
| Silicon, Si | | | 0.4 | |
| Titanium, Ti | | | 0.2 | |
| Zinc, Zn | | 5.1 | 6.1 | |
| **Properties** | **Value** | **Min** | **Max** | **Comment** |
| **Physical** | | | | |
| Density, g/cc | 2.81 | -- | -- | AA; Typical |
| **Mechanical** | | | | |
| Hardness, Brinell | 150 | -- | -- | AA; Typical; 500 g load; 10 mm ball |
| Hardness, Knoop | 191 | -- | -- | Converted from Brinell Hardness Value |
| Hardness, Rockwell A | 53.5 | -- | -- | Converted from Brinell Hardness Value |
| Hardness, Rockwell B | 87 | -- | -- | Converted from Brinell Hardness Value |
| Hardness, Vickers | 175 | -- | -- | Converted from Brinell Hardness Value |
| Ultimate Tensile Strength, MPa | 572 | -- | -- | AA; Typical |
| Tensile Yield Strength, MPa | 503 | -- | -- | AA; Typical |
| Elongation at Break, % | 11 | -- | -- | AA; Typical; 1/16 in. (1.6 mm) Thickness |
| Elongation at Break, % | 11 | -- | -- | AA; Typical; 1/2 in. (12.7 mm) Diameter |
| Modulus of Elasticity, GPa | 71.7 | -- | -- | AA; Typical; Average of tension and compression. Compression modulus is about 2% greater than tensile modulus. |
| Poissons Ratio | 0.33 | -- | -- | |
| Fatigue Strength, MPa | 159 | -- | -- | AA; 500,000,000 cycles completely reversed stress; RR Moore machine/specimen |
| Fracture Toughness, MPa-m½ | 29 | -- | -- | K(IC) in L-T Direction |
| Fracture Toughness, MPa-m½ | 20 | -- | -- | K(IC) in S-L Direction |
| Fracture Toughness, MPa-m½ | 25 | -- | -- | K(IC) in T-L Direction |
| Machinability, % | 70 | -- | -- | 0-100 Scale of Aluminum Alloys |
| Shear Modulus, GPa | 26.9 | -- | -- | |
| Shear Strength, MPa | 331 | -- | -- | AA; Typical |
| **Electrical** | | | | |
| Electrical Resistivity, ohm-cm | 5.15E-06 | -- | -- | AA; Typical at 68°F |
| **Thermal** | | | | |
| CTE, linear 68°F, µm/m-°C | 23.6 | -- | -- | AA; Typical; Average over 68-212°F range. |
| CTE, linear 250°C, µm/m-°C | 25.2 | -- | -- | Average over the range 20-300ºC |
| Heat Capacity, J/g-°C | 0.96 | -- | -- | |
| Thermal Conductivity, W/m-K | 130 | -- | -- | AA; Typical at 77°F |
| Melting Point, °C | -- | 477 | 635 | AA; Typical |
| Solidus, °C | 477 | -- | -- | AA; Typical |
| Liquidus, °C | 635 | -- | -- | AA; Typical |

Table 10. Aluminum 7075 T-651 Rail Liner Material Properties [After Ref. 2]

Armature: Aluminum 6063-T5

| **MatWeb Data Sheet** | **Date: 7/12/2005** | | | |
|---|---|---|---|---|
| **Aluminum 6063-T5** UNS A96063; ISO AlMg0.5Si; Aluminium 6063-T5; AA6063-T5 | | | | |
| **KeyWords:** UNS A96063; ISO AlMg0.5Si; Aluminium 6063-T5; AA6063-T5 | | | | |
| **SubCat:** Aluminum Alloy, Nonferrous Metal, 6000 Series Aluminum Alloy, Metal | | | | |
| **Material Notes:** Data points with the AA note have been provided by the Aluminum Association, Inc. and are | | | | |
| **Component** | **Value** | **Min** | **Max** | |
| Aluminum, Al | | | 97.5 | |
| Chromium, Cr | | | 0.1 | |
| Copper, Cu | | | 0.1 | |
| Iron, Fe | | | 0.35 | |
| Magnesium, Mg | | 0.45 | 0.9 | |
| Manganese, Mn | | | 0.1 | |
| Silicon, Si | | 0.2 | 0.6 | |
| Titanium, Ti | | | 0.1 | |
| Zinc, Zn | | | 0.1 | |
| **Properties** | **Value** | **Min** | **Max** | **Comment** |
| **Physical** | | | | |
| Density, g/cc | 2.7 | -- | -- | AA; Typical |
| **Mechanical** | | | | |
| Hardness, Brinell | 60 | -- | -- | AA; Typical; 500 g load; 10 mm ball |
| Hardness, Knoop | 83 | -- | -- | Converted from Brinell Hardness Value |
| Hardness, Vickers | 70 | -- | -- | Converted from Brinell Hardness Value |
| Ultimate Tensile Strength, MPa | 186 | -- | -- | AA; Typical |
| Tensile Yield Strength, MPa | 145 | -- | -- | AA; Typical |
| Elongation at Break, % | 12 | -- | -- | AA; Typical; 1/16 in. (1.6 mm) Thickness |
| Modulus of Elasticity, GPa | 68.9 | -- | -- | AA; Typical; Average of tension and compression. Compression modulus is about 2% greater than tensile modulus. |
| Poissons Ratio | 0.33 | -- | -- | |
| Fatigue Strength, MPa | 68.9 | -- | -- | AA; 500,000,000 cycles completely reversed stress; RR Moore machine/specimen |
| Shear Modulus, GPa | 25.8 | -- | -- | |
| Shear Strength, MPa | 117 | -- | -- | AA; Typical |
| **Electrical** | | | | |
| Electrical Resistivity, ohm-cm | 3.16E-06 | -- | -- | AA; Typical at 68°F |
| **Thermal** | | | | |
| CTE, linear 68°F, µm/m-°C | 23.4 | -- | -- | AA; Typical; Average over 68-212°F range. |
| CTE, linear 250°C, µm/m-°C | 25.6 | -- | -- | Average over the range 20-300ºC |
| Heat Capacity, J/g-°C | 0.9 | -- | -- | |
| Thermal Conductivity, W/m-K | 209 | -- | -- | AA; Typical at 77°F |
| Melting Point, °C | -- | 616 | 654 | AA; Typical range based on typical composition for wrought products 1/4 inch thickness or greater |
| Solidus, °C | 616 | -- | -- | AA; Typical |
| Liquidus, °C | 654 | -- | -- | AA; Typical |
| **Processing** | | | | |
| Annealing Temperature, °C | 413 | -- | -- | hold at temperature for 2 to 3 hr; cool at 50 °F |
| Solution Temperature, °C | 521 | -- | -- | |
| Aging Temperature, °C | 204 | -- | -- | hold at temperature for 1 hr |
| Aging Temperature, °C | 182 | -- | -- | hold at temperature for 1 hr |

Table 11. Aluminum 6063 T-5 Armature Material Properties [After Ref. 2]

Containment: G-11 FR-5 Glass-reinforced epoxy

| | |
|---|---|
| **G-11 NEMA Grade FR5** | |
| **Glass reinforced, high temperature epoxy, laminate** | |
| **Tensile Strength** | |
| lengthwise, PSI | 40,000 |
| crosswise, PSI | 35,000 |
| **Compressive Strength** | |
| flatwise, PSI | 60,000 |
| edgewise, PSI | 35,000 |
| **Flexural Strength** | |
| lengthwise, PSI | 55,000 |
| crosswise, PSI | 45,000 |
| | |
| **Modulus of Elasticity in flex** | |
| lengthwise, PSI x $10^{6}$ | 2.7 |
| crosswise, PSI x $10^{6}$ | 2.2 |
| **Shear Strength, PSI** | 19,000 |
| **IZOD Impact** | |
| flatwise, ft lb per inch of notch | 7 |
| edgewise, ft lb per inch of notch | 5.5 |
| **Rockwell Hardness M scale** | 110 |
| **Specific Gravity** | 1.82 |
| **Coefficient of Thermal Expansion** | |
| cm/cm/ deg C x $10^{-5}$ | 0.9 |
| **Water Absorption** | |
| .062" thick, % per 24 hrs | 0.25 |
| .125" thick, % per 24 hrs | 0.15 |
| .500" thick, % per 24 hrs | 0.1 |
| **Dielectric Strength, volt/mil** | |
| perpendicular to laminations; short | |
| .062" thick | 500 |
| .125" thick | 400 |
| **Dissipation Factor** | |
| condition A, 1 megacycle | 0.025 |
| **Dielectric Constant** | |
| condition A, 1 megacycle | 5.2 |
| | |
| **Insulation Resistance** | |
| Condition: | |
| 96 hours at 90% | |
| relative humidity | |
| (in mega ohms) | 200,000 |
| **Flame Resistance** | |
| Underwriter Labs, Classification | 94V-0 |
| **Bond Strength, in lbs** | 1,600 |
| **Max Continuous Operating Temperature All Phenolics can withstand -100º F** | |
| Approximate degrees F | 300 |
| sheet mil spec: | |
| Mil-I-24768 / _ _ | 28 |

Table 12. G-11 FR-5 Containment Material Properties [After Ref 10]

Insulator: CoorsTek AD-96 alumina ceramic

| **AD-96 Alumina Material Properties** | | | | **2/23/2006** |
|---|---|---|---|---|
| **Trade Name: AD-96** | | | | |
| **Composition: Nominal 96% $Al_2O_3$ Color: White** | | | | |
| **Property** | | **Units** | **Test** | **Value** |
| Density | | gm/cc | ASTM-C20 | 3.72 |
| Crystal Size | | Microns | Thin-Section | 6 |
| Water Absorption | | % | ASTM-373 | 0 |
| Gas Permeability | | | | 0 |
| Flexural Strength (MOR), 20 degrees C | | -- | -- | 358 (52) |
| Elastic Modulus, 20 degrees C | | GPa (psi x $10^6$) | ASTM-F417 | 303 (44) |
| Poisson's Ratio, 20 degrees C | | -- | ASTM-C848 | 0.21 |
| Compressive Strenght | | MPa(psi x $10^3$) | ASTM-C773 | 2068 (300) |
| Hardness | | GPa(kg/$mm^2$) | KNOOP 1000 gm | 11.5 (1175) |
| | | | Rockwell 45 N | 78 |
| Tensile Strength, 25 degrees C | | MPa (psi x $10^3$) | ACMA TEST #4 | 221 (32) |
| Fracture Toughness K(Ic) | | Mpa $m^{1/2}$ | NOTCHED BEAM | 5-Apr |
| Thermal Conductivity, 20 degrees C | | Wm degrees K | ASTM-C408 | 24.7 |
| Coefficient of Thermal Expansion, 25-1000 degrees C | | 1 x $10^{-6}$/degrees C | ASTM-C372 | 8.2 |
| Specific Heat, 100 degrees C | | J/kg*K | ASTM-E1269 | 880 |
| Thermal Shock Resistance, (delta)Tc | | degrees C | NOTE 3 | 250 |
| Maximum Use Temperature | | degrees C | NO-LOAD COND. | 1700 |
| Dielectric Stength | | ac-kV/mm (acV/mil) | ASTM-D116 | 8.3 (210) |
| Dielectric Constant, 1MHz | | 25 degrees C | ASTM-D150 | 9 |
| Dielectric Loss (tan delta) 1MHz | | 25 degrees C | ASTM-D2520 | 0.0002 |
| Volume Resistivity | 25 degrees C | ohm-cm | ASTM-D1829 | $>10^{14}$ |
| | 500 degrees C | ohm-cm | ASTM-D1829 | 4 x $10^9$ |
| | 1000 degrees C | ohm-cm | ASTM-D1829 | 1 x $10^6$ |
| Impingement | | -- | Note 4 | 0.5 |
| Rubbing | | -- | Note 4 | 0.6 |

Table 13. Ceramic Insulator Material Properties [After Ref. 11]

Augmenting Rail Insulator: Mylar (polyester)

## Material Specifications for Mylar® (Polyester) Film

| Property | Value | Test Method |
|---|---|---|
| **DC Dielectric Strength** | **Typical Value for Mylar® 92 EL/C*** | ¼ in upper electrode and flat plate lower electrode. 500 V/sec rate of rise. |
| 25°C (77°F) | 11.0 kV/mil | |
| **Gauge and Type at 25°C (77°F)** | **Minimum Values for Mylar® C Film** | |
| 6C | 0.225 kV | |
| 7C | 0.300 kV | |
| 8C | 0.320 kV | |
| 10C | 0.490 kV | Minimum average voltage of 20 film-foil capacitors, 0.5 μF each |
| 12C | 0.650 kV | |
| 14C | 0.825 kV | |
| 20C | 1.500 kV | |
| 24C | 2.000 kV | |
| 32C | 3.100 kV | 100 V/sec rate of rise |
| 40C | 4.100 kV | |
| 48C | 4.900 kV | |
| 75C | 5.500 kV | |
| 95C | 6.000 kV | |
| **AC Dielectric Strength** | **Typical Value for Mylar® 92 EL/C*** | ASTM D149 and ASTM D2305 60 Hz 500 V/sec rate of rise |
| 25°C (77°F) | 7.0 kV/mil | |
| **Gauge and Type at 25°C (77°F)** | **Minimum Values for Mylar® EL Film** | |
| 48EL | 2.8 kV | |
| 75EL | 3.5 kV | |
| 92EL | 4.0 kV | ASTM D149 and D2305 |
| 142EL | 5.5 kV | Minimum average voltage of 10 sheet samples |
| 200EL | 7.7 kV | |
| 300EL | 10.0 kV | |
| 500EL | 13.5 kV | 60 Hz |
| 750EL | 17.5 kV | 500 V/sec rate of rise |
| 900EL | 18.4 kV | |
| 1000EL | 19.0 kV | |
| 1400EL | 20.0 kV | |
| **Dielectric Constant** | **Typical Value for Mylar® 92 EL/C*** | |
| 25°C (77°F) – 60 Hz | 3.3 | |
| 25°C (77°F) – 1 kHz | 3.25 | ASTM D150 |
| 25°C (77°F) – 1 MHz | 3.0 | |
| 25°C (77°F) – 1 GHz | 2.8 | |
| 150°C (302°F) – 60 Hz | 3.7 | |
| **Dissipation Factor** | **Typical Value for Mylar® 92 EL/C** | |
| 25°C (77°F) – 60 Hz | 0.0025 | |
| 25°C (77°F) – 1 kHz | 0.0050 | |
| 25°C (77°F) – 1 MHz | 0.016 | ASTM D150 |
| 25°C (77°F) – 1 GHz | 0.008 | |
| 150°C (302°F) – 60 Hz | 0.004 | |
| -269°C (-452°F) – 1 kHz (in Helium) | 0.0002 | |
| **Volume Resistivity** | **Typical Value for Mylar® 92 EL/C** | |
| 25°C (77°F) | $10^{18}$ ohm-cm | |
| 150°C (302°F) (Type C Film) | $10^{13}$ ohm-cm | |
| **Surface Resistivity** | | ASTM D257 and D2305 |
| 23°C (73°F) – 30% RH | $10^{16}$ ohm/sq | |
| 23°C (302°F) – 80% RH | $10^{12}$ ohm/sq | |
| **Insulation Resistance** | | |
| 35°C (95°F) – 90% RH | $10^{12}$ ohm | |
| **Capacitor Insulation Resistance** | **Typical Value for Mylar® 92 C** | Based on 0.5 μF film-foil capacitor sections, using single layer, 92 Mylar® C |
| 100°C (212°F) | 30,000 MΩ-μF | |
| 125°C (257°F) | 1,000 MΩ-μF | |
| 150°C (302°F) | 100 MΩ-μF | |

Table 14. Mylar Film Insulator Material Properties [After Ref. 12]

THIS PAGE INTENTIONALLY LEFT BLANK

# APPENDIX B. PRODUCTION DRAWINGS

Top Containment Half

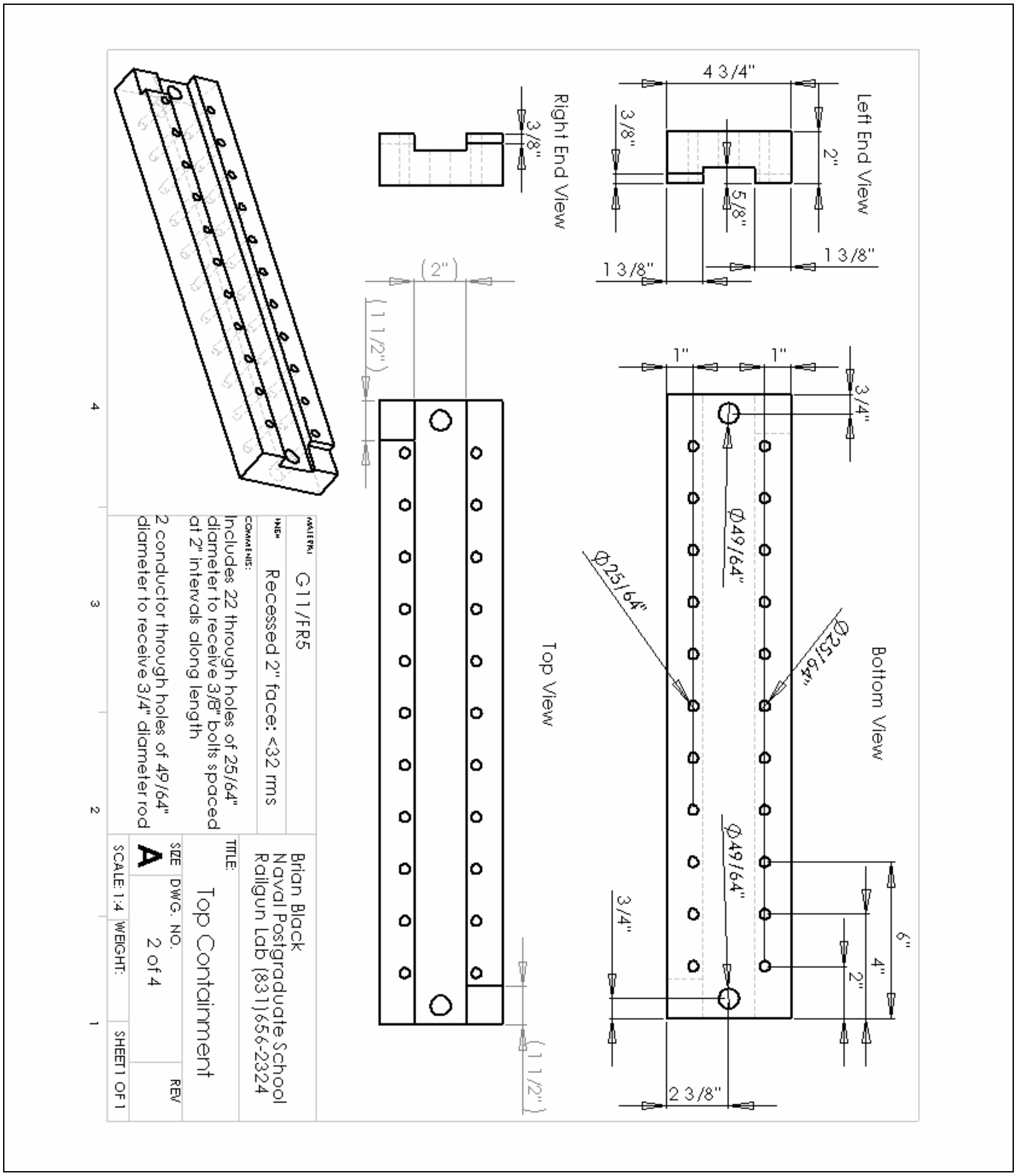


Figure 14. Top Containment Half

Bottom Containment Half

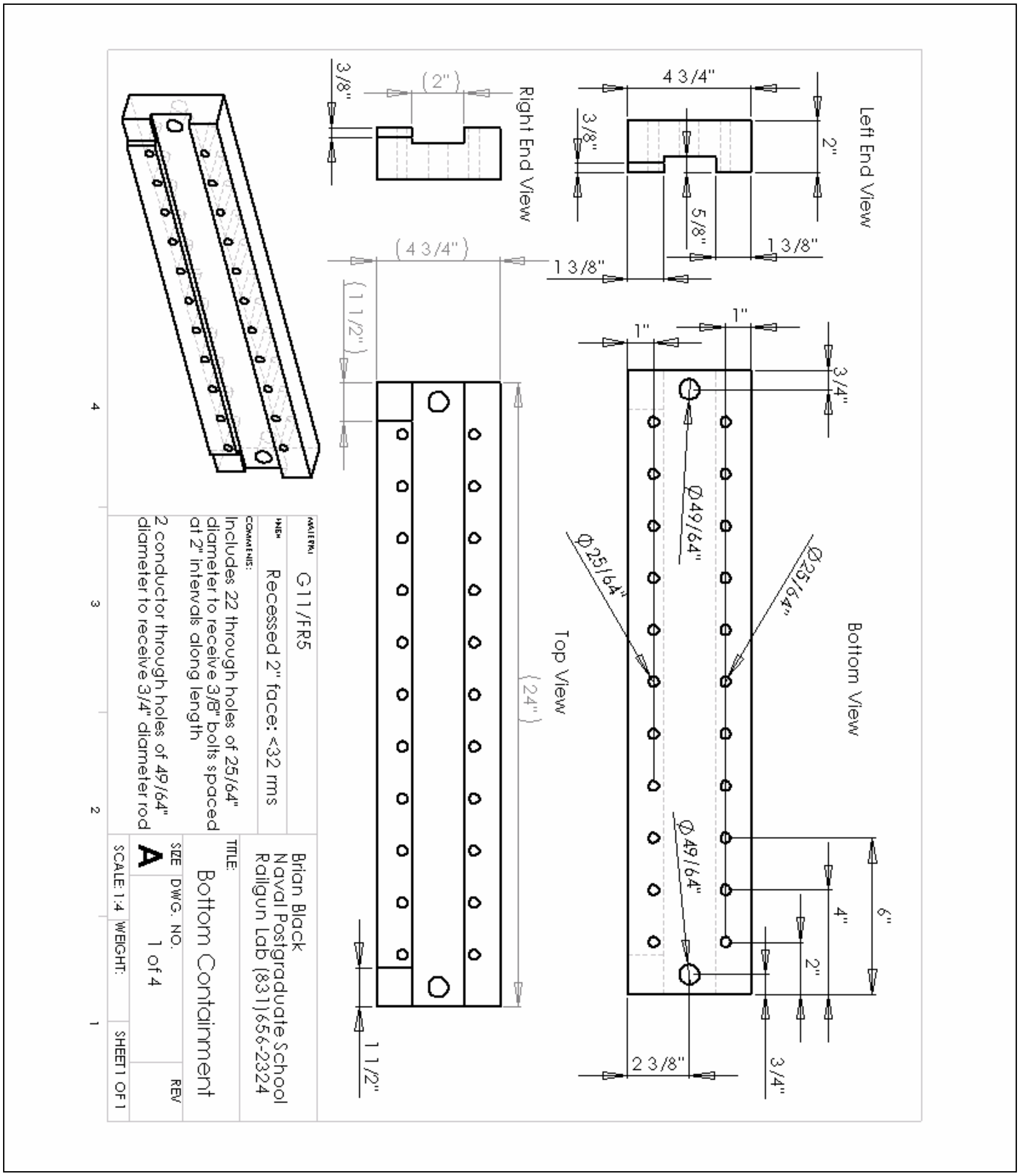

Figure 15. Bottom Containment Half

Solid Primary Conductor Rails

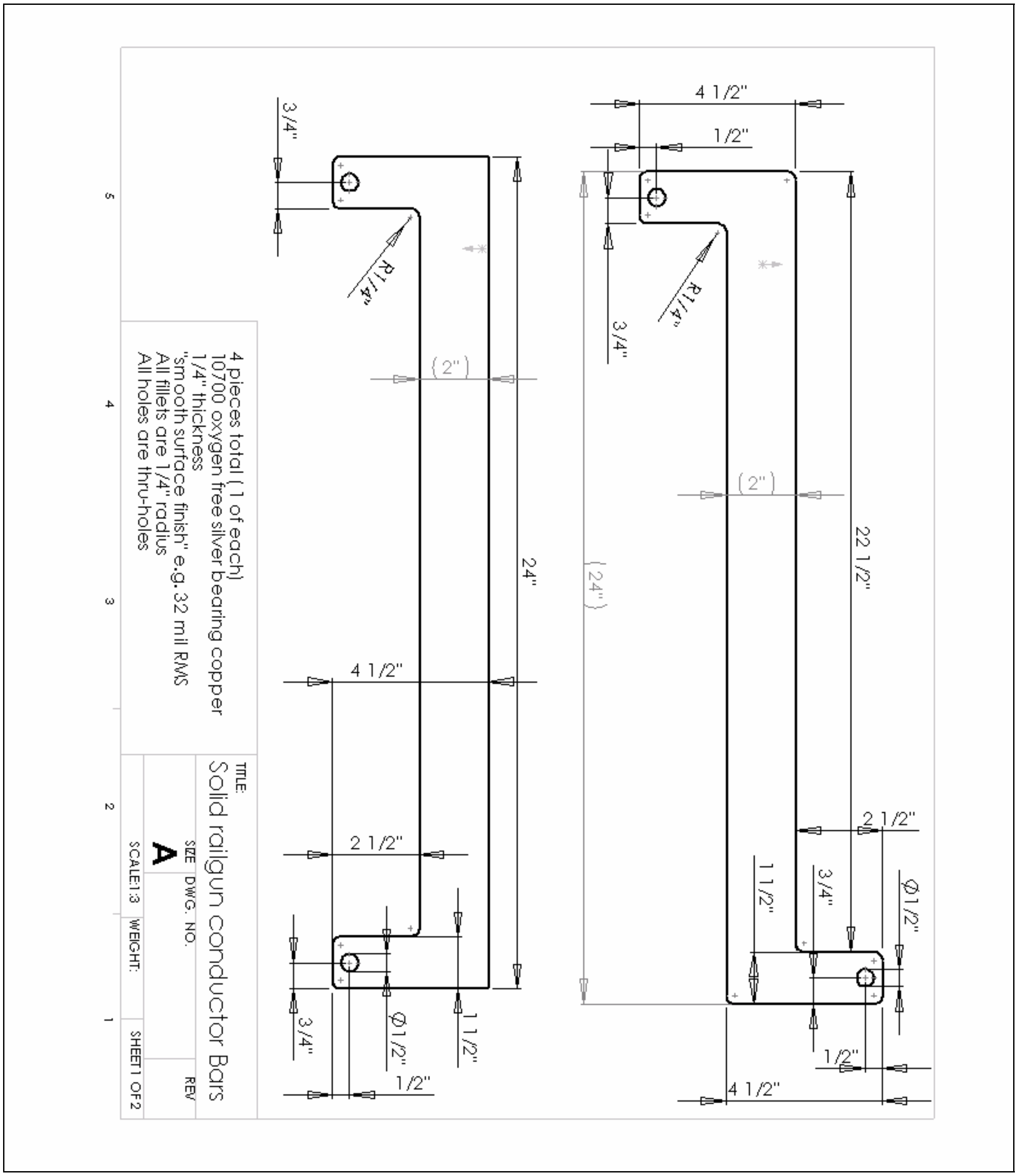


Figure 16. Solid Primary Conductor Rails

Slotted Primary Conductor Rails

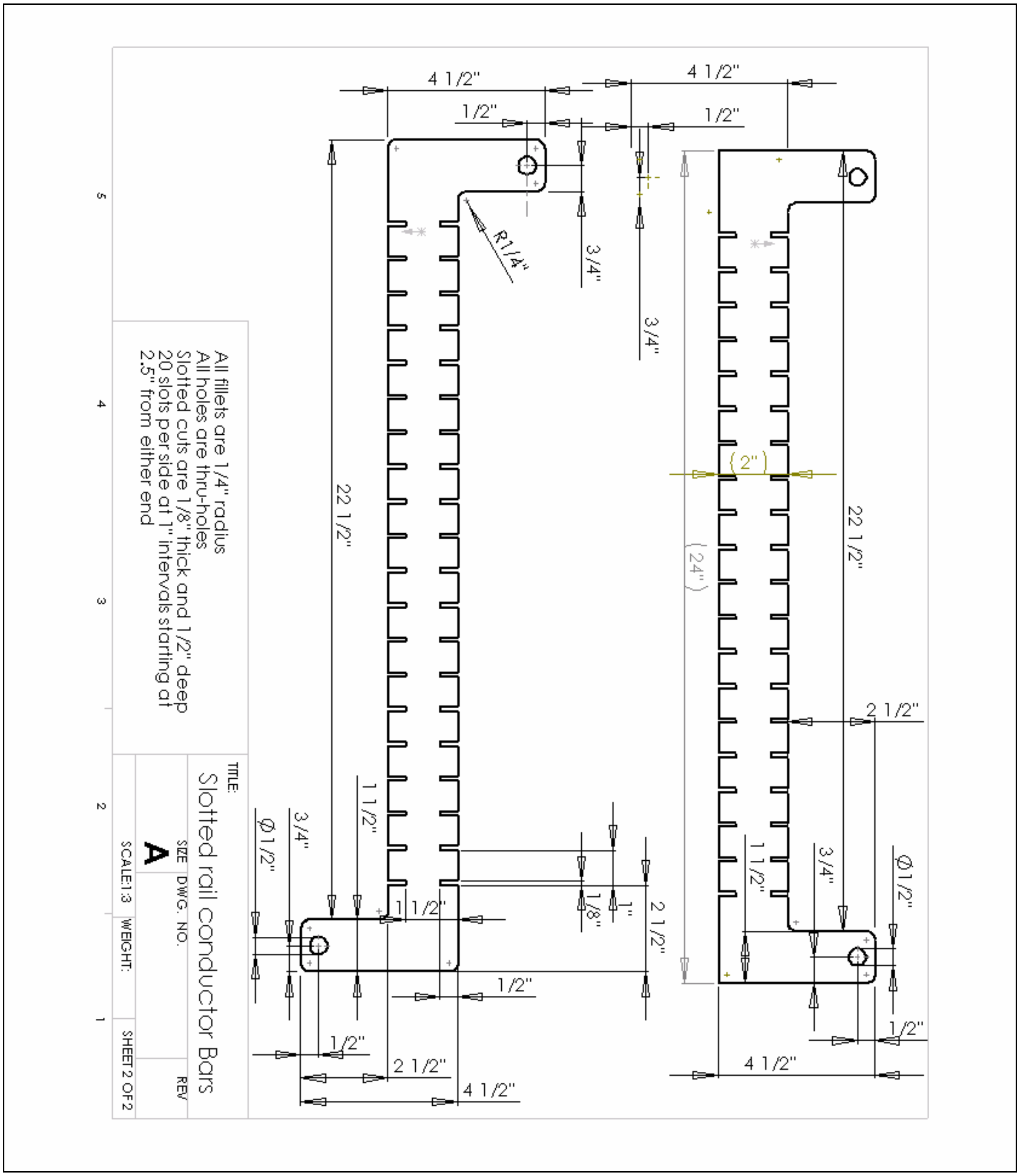


Figure 17. Slotted Primary Conductor Rails

Ceramic Insulator

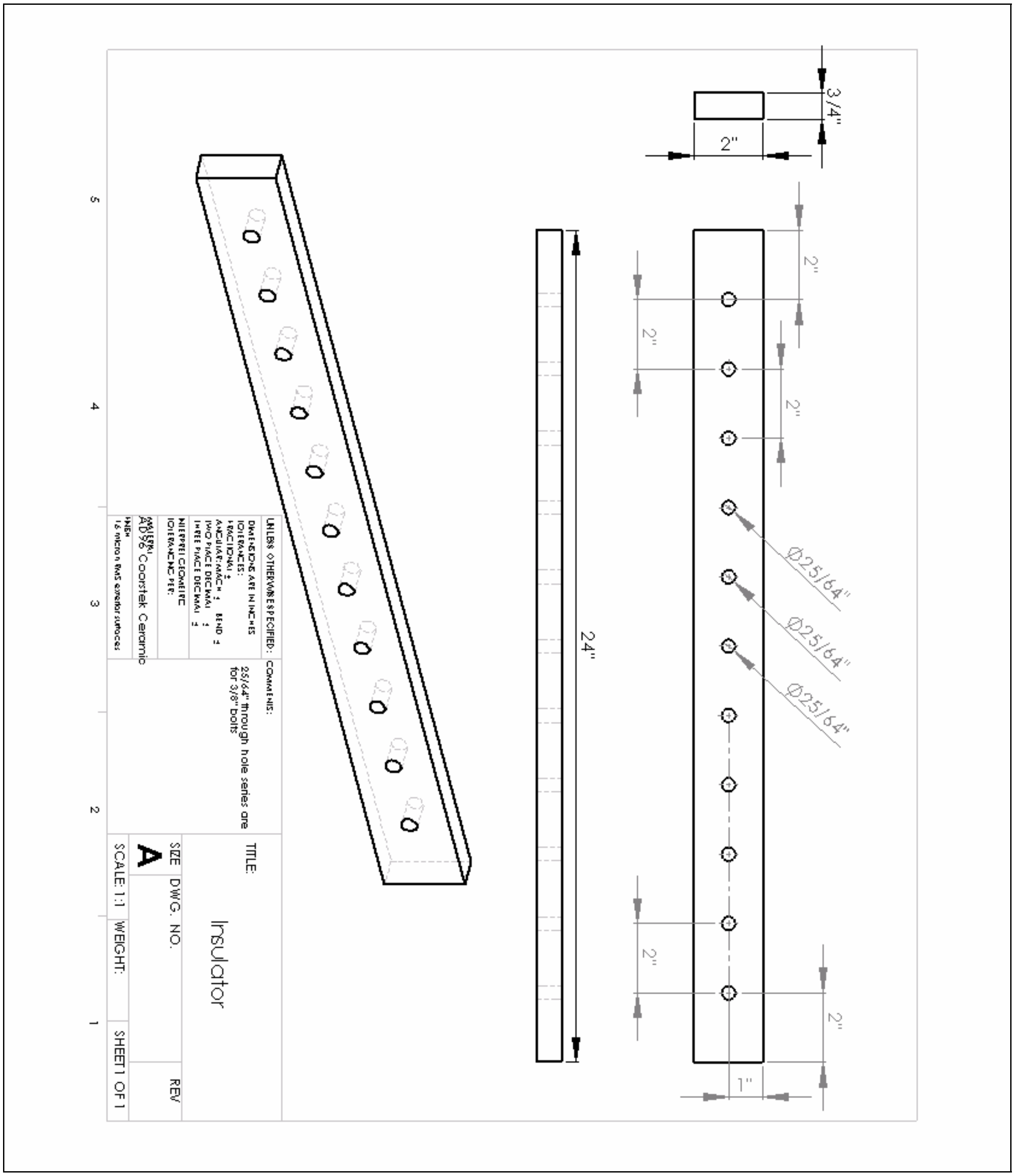


Figure 18. Ceramic Insulators

Augmented Rails, Rail liners, and Spacer

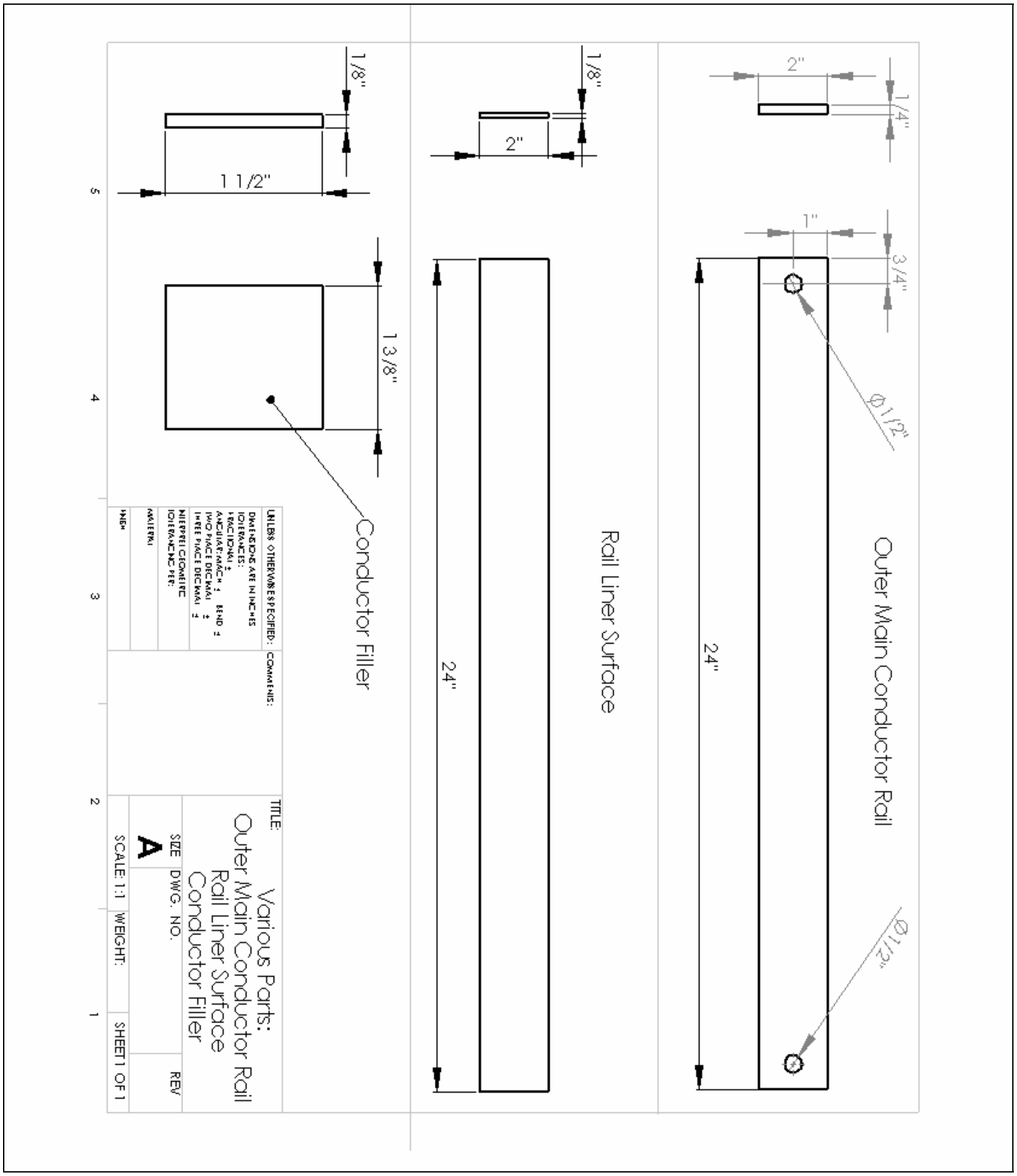


Figure 19. Augmented Rails, Rail liners, and Spacer

Augmenting Conductor Components

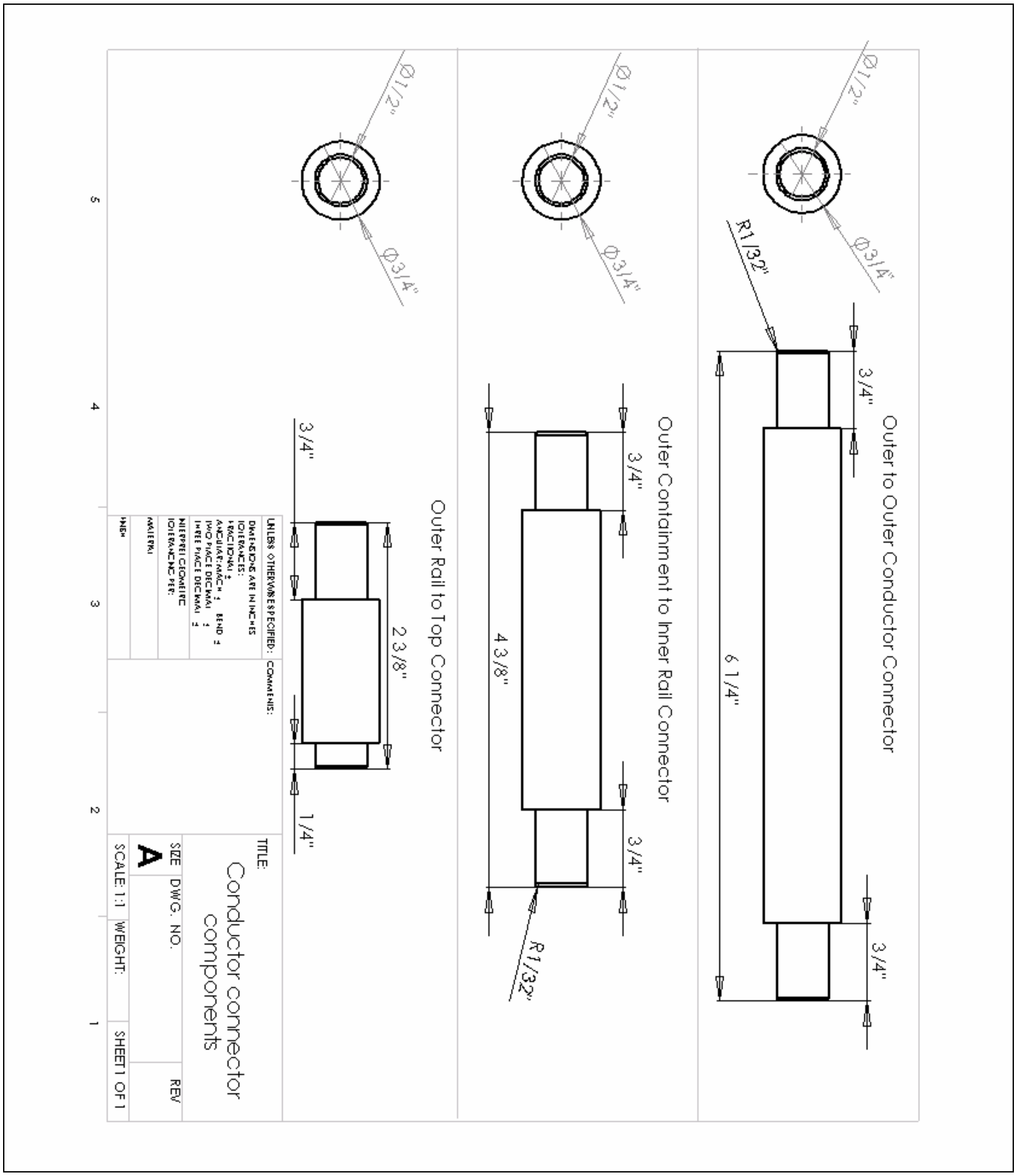


Figure 20. Augmenting Conductor Components

External Conductor Connectors and Muzzle Shunt

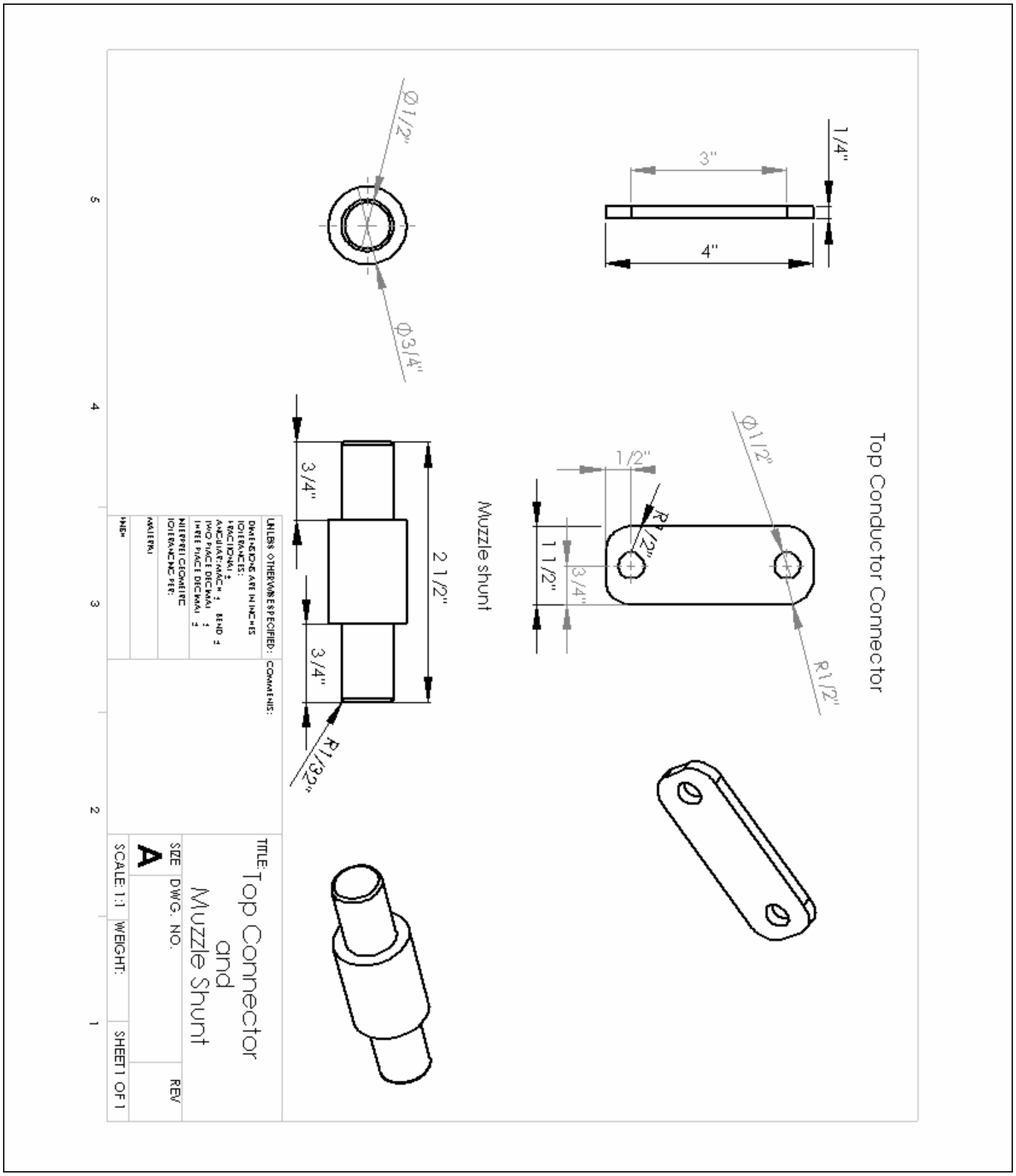


Figure 21. External Conductor Connectors and Muzzle Shunt

Full Conductor Assembly

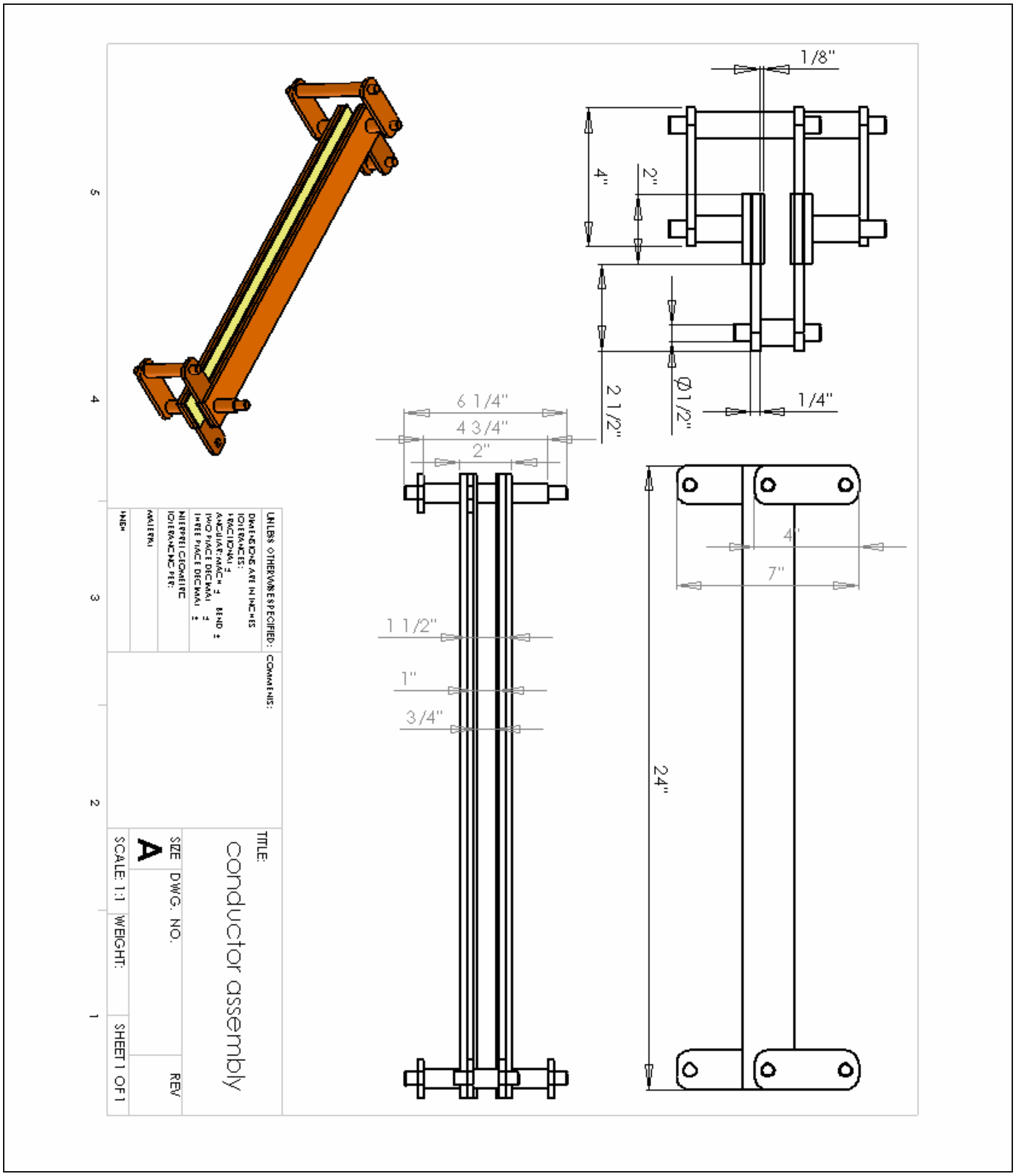


Figure 22. Full Conductor Assembly

Full Assembly CAD Model and Finished Result

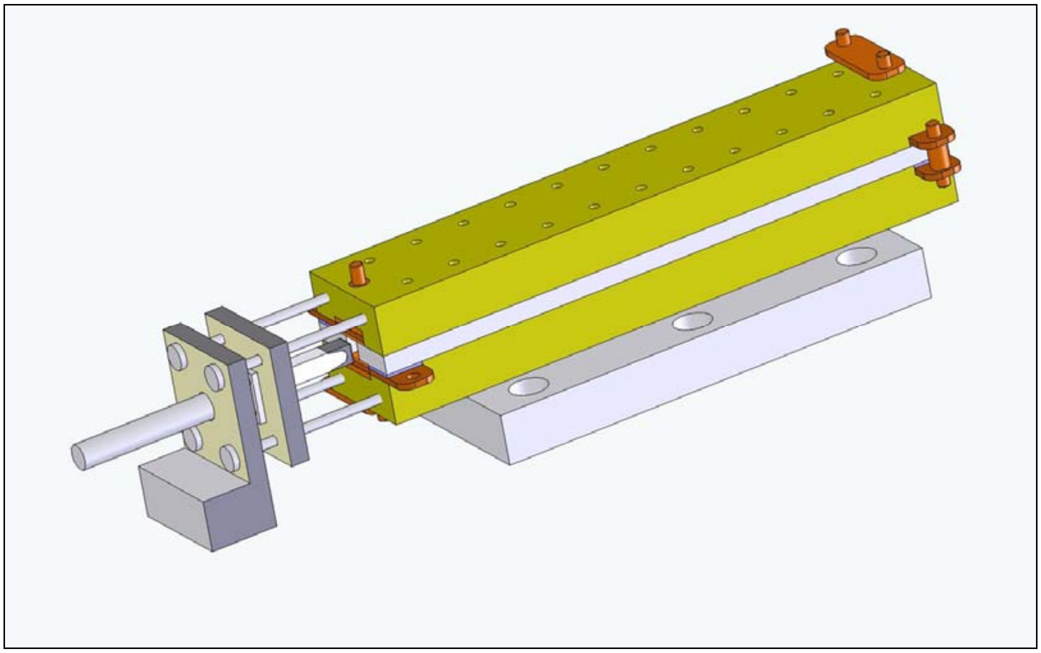

Figure 23. Full CAD Assembly with Loader and Muzzle Shunt

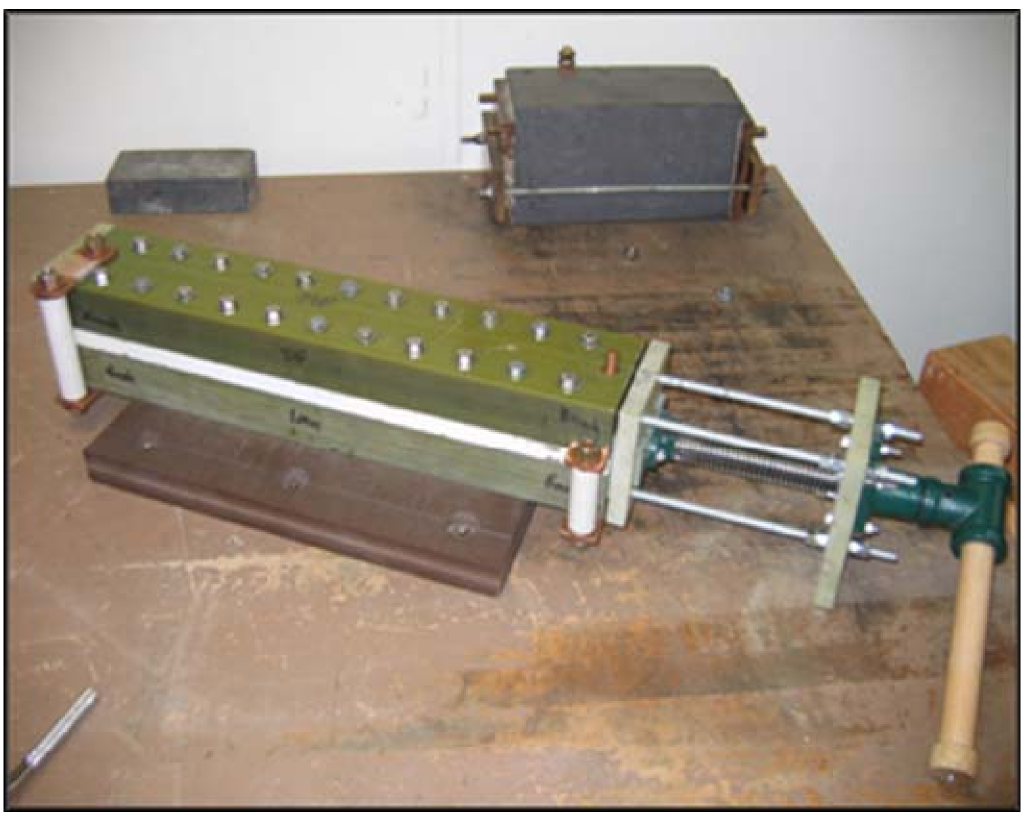

Figure 24. Full Assembled Railgun with Loader

Basic U-shape Armature

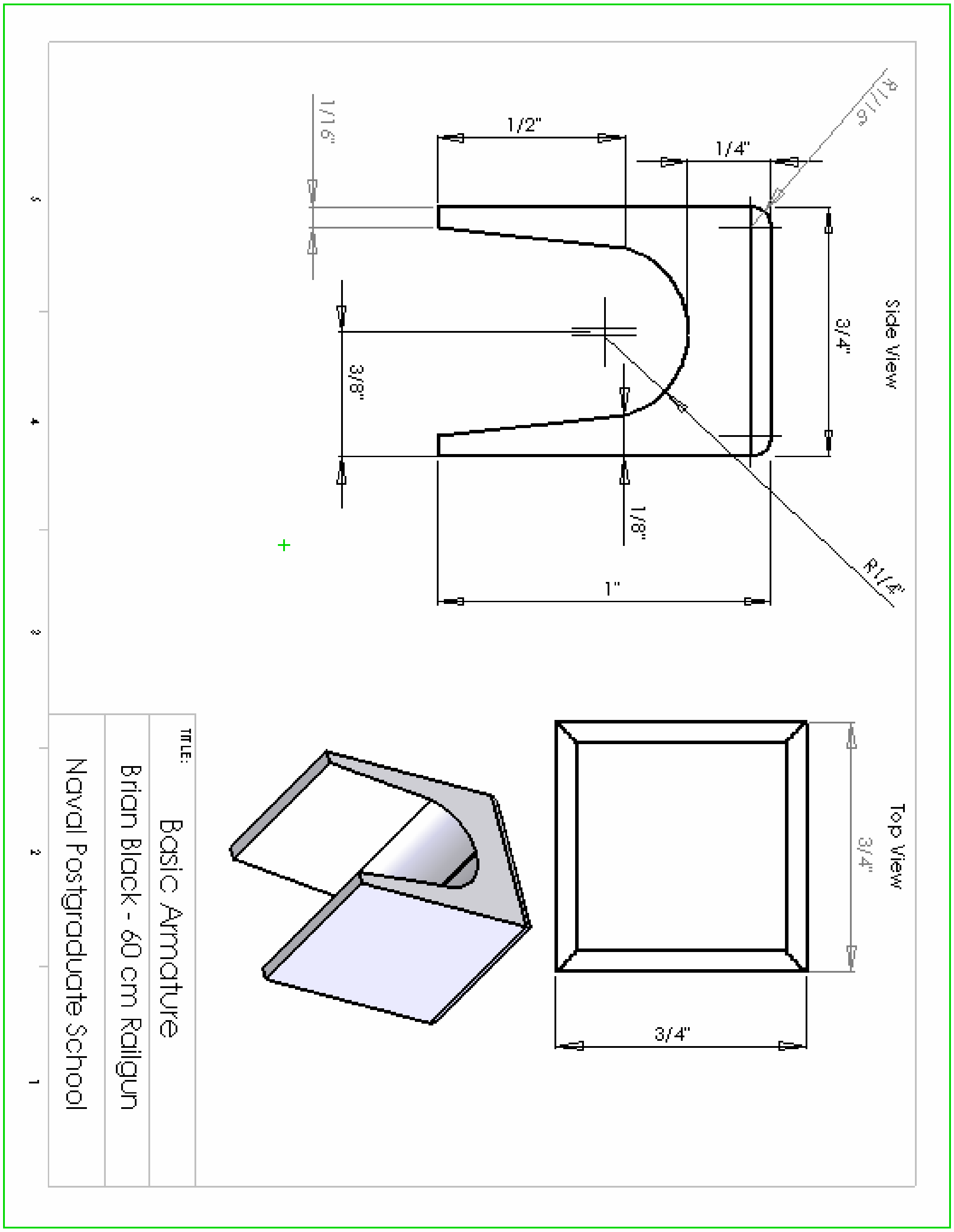


Figure 25. Basic U-Shape Armature

Flared M-shape Armature

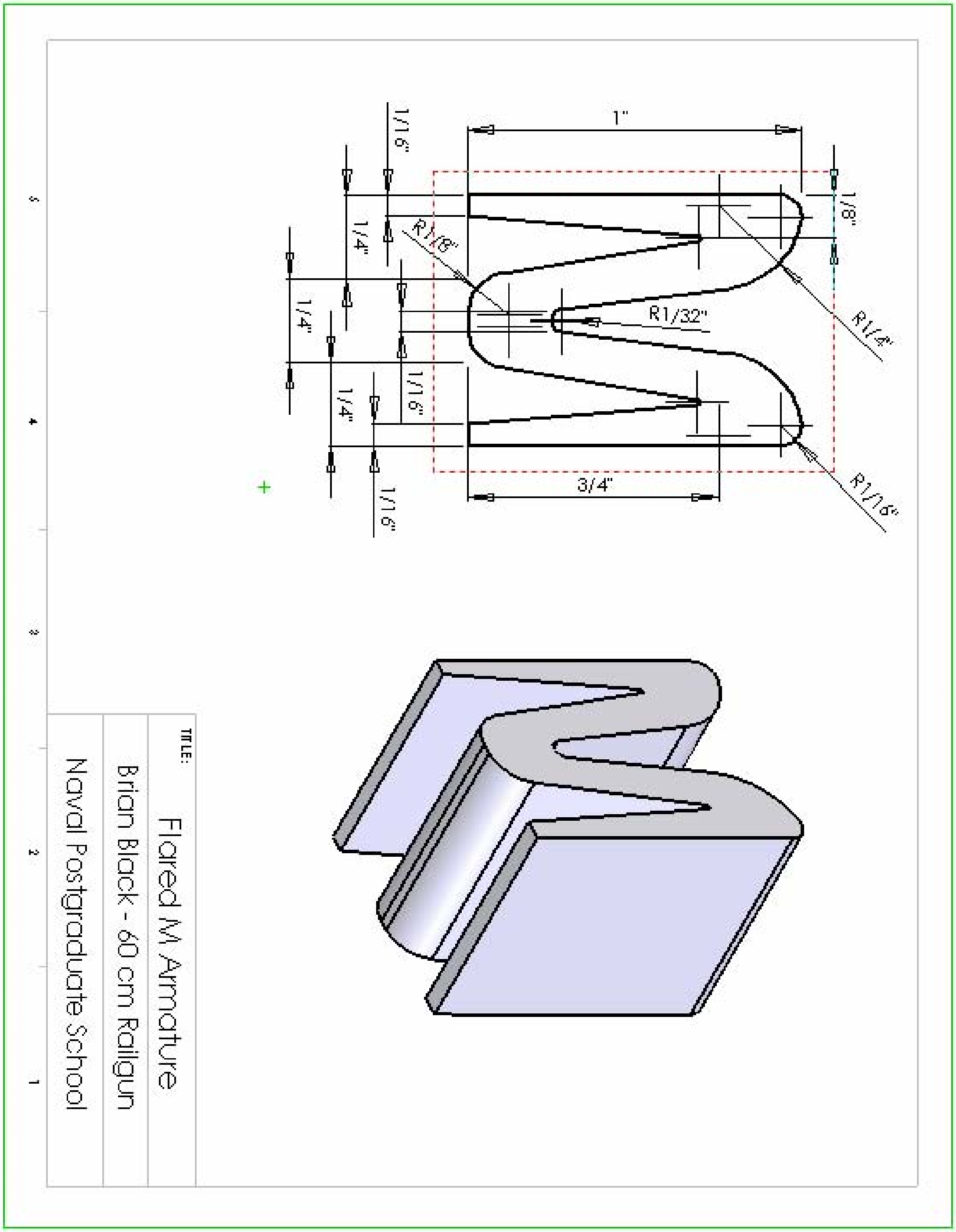


Figure 26. Flared M-shape Armature

Square M-shape Armature

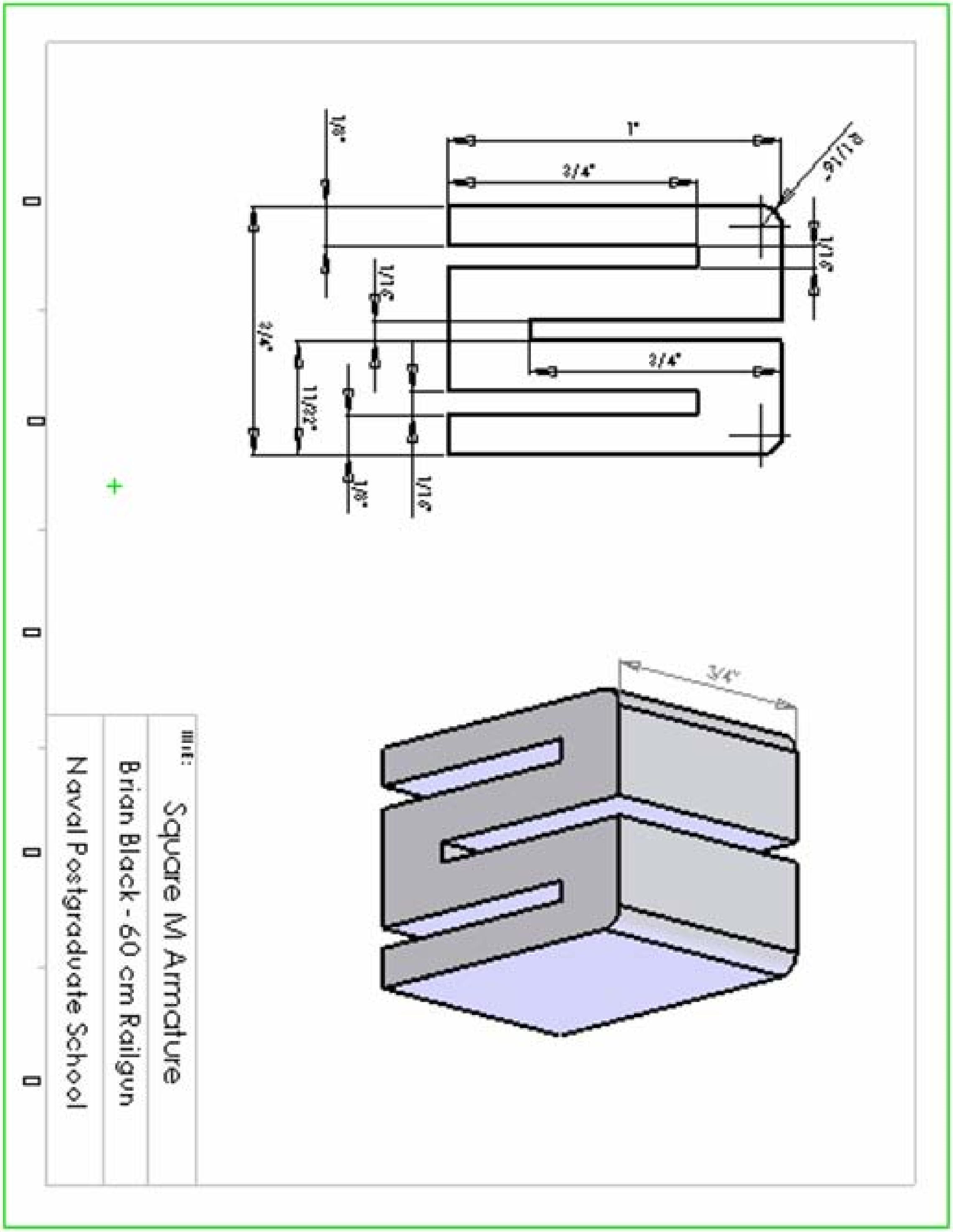


Figure 27. Square M-shape Armature

Altered U-shape Armature with Center Hollow

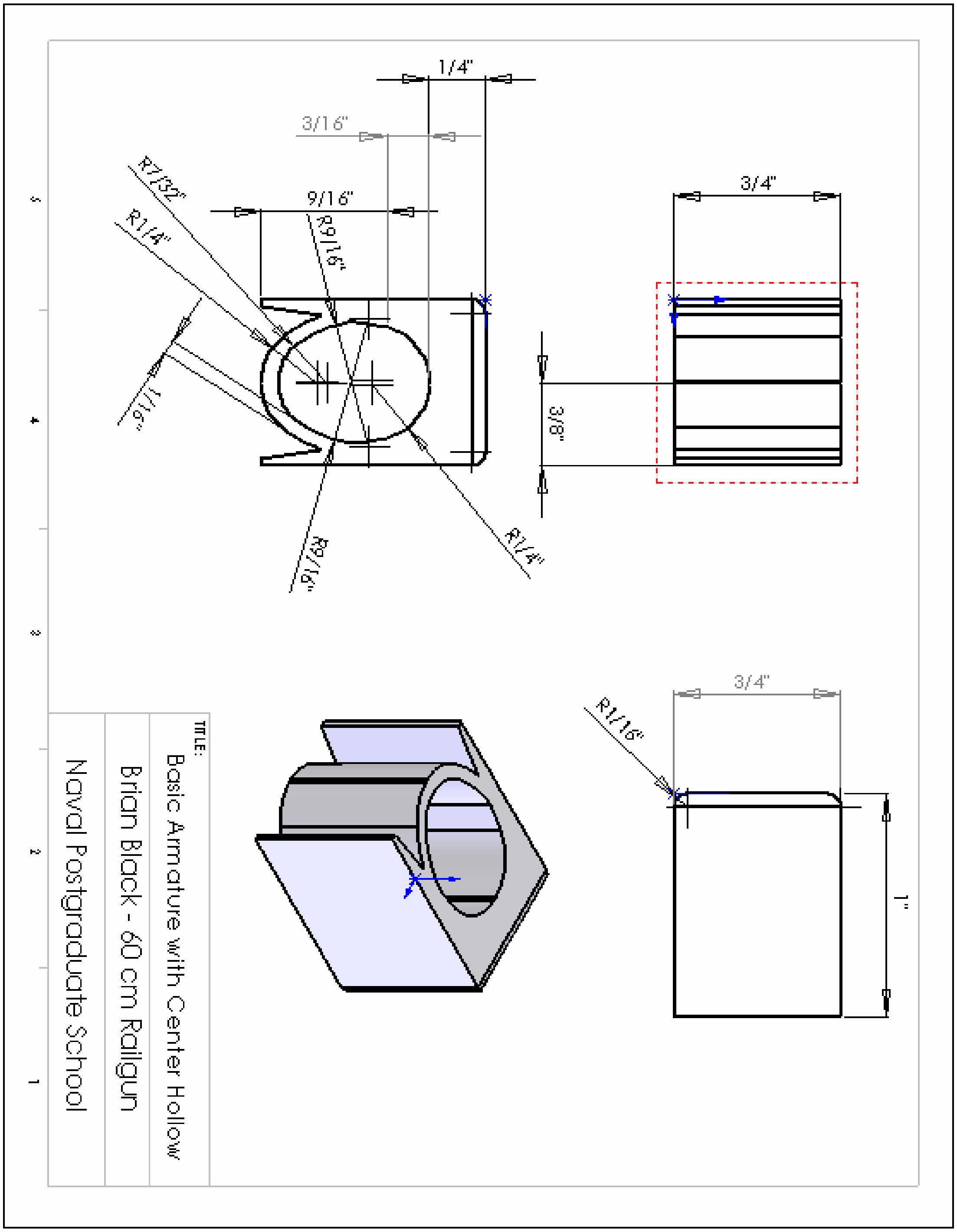


Figure 28. Altered U-shape Armature with Center Hollow

Railgun Mounting Base

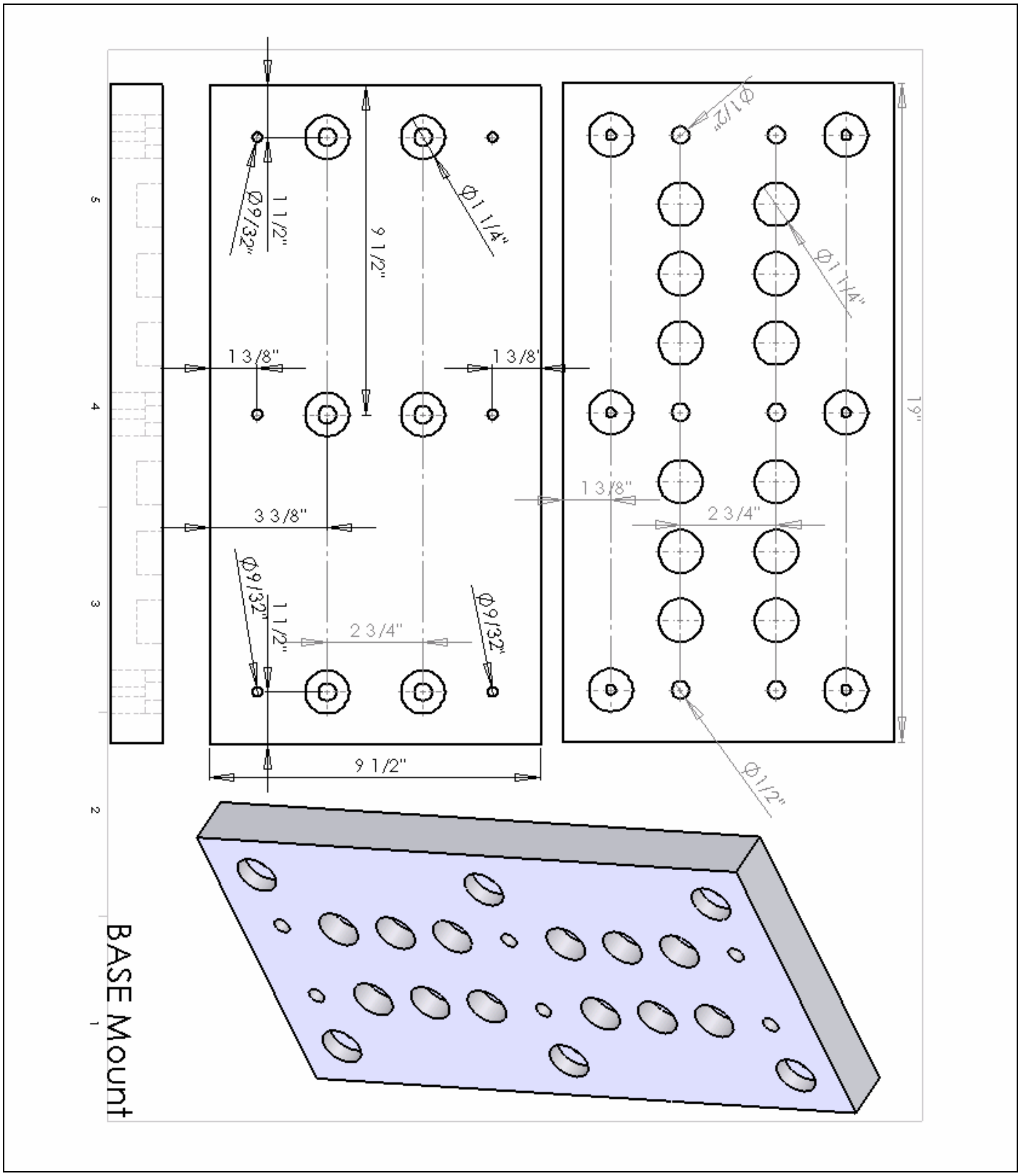


Figure 29. Railgun Mounting Base

The mounting base is fabricated from a 1.5” thick slab of insulating phenolic. Three pairs of the containment bolts extend through the base for mounting. The base itself is then bolted directly to the firing line table.

THIS PAGE INTENTIONALLY LEFT BLANK

# APPENDIX C. MODELING

## A. KERRISK'S METHOD SPREADSHEETS [3]

Inductance Gradient Calculations for Solid and Non-slotted Rail Geometries

| Kerrisk's Method for L' Determination - Los Alamos National Laboratory 1981 [Ref.2] | | | | |
|---|---|---|---|---|
| L' = [A + B*ln(1 + a1*(w/h) + a2*(w/h)*(s/h))*ln(b1 + b2*(s/h) + b3*(w/h) + b4*(s/h)*(w/h)] | | | | |
| s = bore spacing(mm) | | | h = rail height (mm) | w = rail width (mm) |
| ( NOTE: Augmented configurations apply gain factor of 1.55 over their respective non-augmented L' ) | | | | |
| **Solid Rails** | | **Slotted Rails** | **Solid Augmented** | **Slotted Augmented** |
| A | 0.440641 | 0.440641 | 0.440641 | 0.440641 |
| B | -0.07771 | -0.07771 | -0.07771 | -0.07771 |
| a1 | 3.397143 | 3.397143 | 3.397143 | 3.397143 |
| a2 | -0.06603 | -0.06603 | -0.06603 | -0.06603 |
| b1 | 1.07719 | 1.07719 | 1.07719 | 1.07719 |
| b2 | 2.743651 | 2.743651 | 2.743651 | 2.743651 |
| b3 | 0.022093 | 0.022093 | 0.022093 | 0.022093 |
| b4 | 0.263739 | 0.263739 | 0.263739 | 0.263739 |
| s | 19 | 19 | 19 | 19 |
| h | 50.8 | 25.4 | 50.8 | 25.4 |
| w | 9.5 | 9.5 | 9.5 | 9.5 |
| s/h | 0.374015748 | 0.748031496 | 0.374015748 | 0.748031496 |
| w/h | 0.187007874 | 0.374015748 | 0.187007874 | 0.374015748 |
| **Solid Rail L'** | | **Slotted L'** | **Solid augmented L'** | **Slotted Augmented L'** |
| **0.30368** | | **0.44051** | **0.47070** | **0.68279** |

Table 15. Kerrisk's Method and Augmentation Adjusted Inductance Gradient (L') Calculations

Table 14 input parameters of bore spacing (s), rail height (h), and rail width (w) are demonstrated in Figure 28 below.

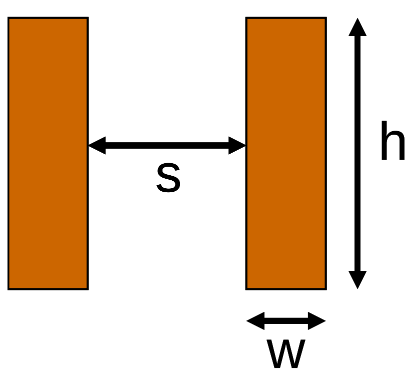


Figure 30. Kerrisk's Method Rail Parameters [After Ref. 2]

## B. PARAMETER BASED MODELING [7]

1500 m/s Solid Non-Augmented Parameter Modeling

| Solid Rail Non-Augmented Parameter Model | | | | | |
|---|---|---|---|---|---|
| **L'** | **0.30368** | **μH/m** | | | |
| **Target velocity:** | | **1500** | m/s | | |
| Projectile mass: | | 11.4 | grams | | |
| Effective length: | | 50 | cm | | |
| Armature height: | | 19 | mm | | |
| t = 2x/(delta v) | | t (ms) | 0.67 | | |
| $a_{avg} = 2x/(t^2)$ | | 2.25E+06 | $a_{avg}$ (m/s$^2$) | | |
| | | 225 | $a_{avg}$ (kG's) | | |
| Avg. Current: $I_{avg} = (2ma/L')^{0.5}$ | | 411.01 | k-Amps | Assume: average acceleration is 70% of peak acceleration and this ratio is proportional to $(I_{avg}^2/I_{peak}^2)$ | |
| Peak Current $I_{peak} = (I_{avg}^2/0.7)^{0.5}$ | | 491.25 | k-Amps | | |
| Linear current density: $I_{peak}' = I_{peak}$ / armature height | | 25.86 | (kA/mm) | Note: linear current densities > 45 kA/mm are regarded as unstable for railgun design | |
| Electrical Action: G=2mv/L' | | 1.13E+08 | Amp$^2$s | Electrical Action is a measure of heating due to current flow | |
| $\Delta T = (\rho_e/\rho_m C_p)*(G/A^2)$ | | 40.00 | Kelvin (K) | Based on thumbrule of a delta T of 40 K across the rail due to resistive heating, where A = conductor cross-sectional area | |
| Conductor Area = $[(\rho_e/\rho_m C_p)(G/\Delta T)]^{0.5}$ | | 118.65 | mm$^2$ | The expression $(\rho_e/\rho_m C_p)$ is a ratio of electrical resistivity to the product of mass density and specific heat capacity, a typical value for the ratio for copper is 0.005 (K/Amp$^2$s)/mm$^4$. | |
| Required rail width (mm) | | 6.24 | mm | | |
| Actual rail width (1/4" rail + 1/8" rail liner) | | 9.53 | mm | | |
| Lorentz Force at peak current: $F = (1/2)L'I_{peak}^2$ | | 36642.86 | N | 8238 | lbf |
| Bore Area (m$^2$) | | 0.000361 | m$^2$ | 0.56 | square inches |
| Base Pressure = F/A | | 102 | Mpa | 14.73 | ksi |
| Repulsion force per unit length (Base Pressure x Bore height) | | 1.93 | MN/m | 11.05 | kip/in |
| Grade 2 SAE J429 3/8" diameter stainless steel bolts Minimum Yield Strength | | | | 57000 | psi |
| Individual bolt area required to avoid exceeding Yield Strength for static longitudinal repulsion force along entire 24" rail length distributed between 22 bolts | | | | 0.21 | square inches |
| Minimum Bolt Diameter Required | | | | 0.519 | inches |
| Actual Bolt Diameter | | | | 0.375 | inches |

Table 16. 1500 m/s Solid Non-Augmented Parameter Model

1500 m/s Slotted Non-Augmented Parameter Modeling

| **Slotted Rail Non-Augmented Parameter Model** | | | | | |
|---|---|---|---|---|---|
| **L'** | **0.44051** | **$\mu$H/m** | | | |
| **Target velocity:** | | **1500** | m/s | | |
| Projectile mass: | | 11.4 | grams | | |
| Effective length: | | 50 | cm | | |
| Armature height: | | 19 | mm | | |
| t = 2x/(delta v) | | t (ms) | 0.67 | | |
| $a_{avg} = 2x/(t^2)$ | | 2.25E+06 | $a_{avg}$ (m/s$^2$) | | |
| | | 225 | $a_{avg}$ (kG's) | | |
| Avg. Current: $I_{avg} = (2ma/L')^{0.5}$ | | 341.26 | k-Amps | Assume: average acceleration is 70% of peak acceleration and this ratio is proportional to $(I_{avg}^2/I_{peak}^2)$ | |
| Peak Current $I_{peak} = (I_{avg}^2/0.7)^{0.5}$ | | 407.88 | k-Amps | | |
| Linear current density: $I_{peak}' = I_{peak}$ / armature height | | 21.47 | (kA/mm) | Note: linear current densities > 45 kA/mm are regarded as unstable for railgun design | |
| Electrical Action: G=2mv/L' | | 7.76E+07 | Amp$^2$s | Electrical Action is a measure of heating due to current flow | |
| $\Delta T = (\rho_e/\rho_m C_p)*(G/A^2)$ | | 40.00 | Kelvin (K) | Based on thumbrule of a delta T of 40 K across the rail due to resistive heating, where | |
| Conductor Area = $[(\rho_e/\rho_m C_p)(G/\Delta T)]^{0.5}$ | | 98.51 | mm$^2$ | The expression $(\rho_e/\rho_m C_p)$ is a ratio of electrical resistivity to the product of mass density and specific heat capacity, a typical value for the ratio for copper is 0.005 (K/Amp$^2$s)/mm$^4$. | |
| Required rail width (mm) | | 5.18 | mm | | |
| Actual rail width (1/4" rail + 1/8" rail liner) | | 9.53 | mm | | |
| Lorentz Force at peak current: $F = (1/2)L'I_{peak}^2$ | | 36642.86 | N | 8238 | lbf |
| Bore Area (m$^2$) | | 0.000361 | m$^2$ | 0.56 | square inches |
| Base Pressure = F/A | | 102 | Mpa | 14.73 | ksi |
| Repulsion force per unit length (Base Pressure x Bore height) | | 1.93 | MN/m | 11.05 | kip/in |
| Grade 2 SAE J429 3/8" diameter stainless steel bolts Minimum Yield Strength | | | | 57000 | psi |
| Individual bolt area required to avoid exceeding Yield Strength for static longitudinal repulsion force along entire 24" rail length distributed between 22 bolts | | | | 0.21 | square inches |
| Minimum Bolt Diameter Required | | | | 0.519 | inches |
| Actual Bolt Diameter | | | | 0.375 | inches |

Table 17. 1500 m/s Slotted Non-Augmented Parameter Model

1500 m/s Solid Augmented Parameter Modeling

| **Solid Rail Augmented Parameter Model** | | | | |
|---|---|---|---|---|
| **L'** **0.47070** | **μH/m** | | | |
| **Target velocity:** | **1500** | m/s | | |
| Projectile mass: | 11.4 | grams | | |
| Effective length: | 50 | cm | | |
| Armature height: | 19 | mm | | |
| t = 2x/(delta v) | t (ms) | 0.67 | | |
| $a_{avg} = 2x/(t^2)$ | 2.25E+06 | $a_{avg}$ (m/s$^2$) | | |
| | 225 | $a_{avg}$ (kG's) | | |
| Avg. Current: $I_{avg} = (2ma/L')^{0.5}$ | 330.13 | k-Amps | Assume: average acceleration is 70% of peak acceleration and this ratio is proportional to $(I_{avg}^2/I_{peak}^2)$ | |
| Peak Current $I_{peak} = (I_{avg}^2/0.7)^{0.5}$ | 394.58 | k-Amps | | |
| Linear current density: $I_{peak}' = I_{peak}$ / armature height | 20.77 | (kA/mm) | Note: linear current densities > 45 kA/mm are regarded as unstable for railgun design | |
| Electrical Action: G=2mv/L' | 7.27E+07 | Amp$^2$s | Electrical Action is a measure of heating due to current flow | |
| $\Delta T = (\rho_e/\rho_m C_p)*(G/A^2)$ | 40.00 | Kelvin (K) | Based on thumbrule of a delta T of 40 K across the rail due to resistive heating, where | |
| Conductor Area = $[(\rho_e/\rho_m C_p)(G/\Delta T)]^{0.5}$ | 95.30 | mm$^2$ | The expression $(\rho_e/\rho_m C_p)$ is a ratio of electrical resistivity to the product of mass density and specific heat capacity, a typical value for the ratio for copper is 0.005 (K/Amp$^2$s)/mm$^4$. | |
| Required rail width (mm) | 5.02 | mm | | |
| Actual rail width (1/4" rail + 1/8" rail liner) | 9.53 | mm | | |
| Lorentz Force at peak current: $F = (1/2)L'I_{peak}^2$ | 36642.86 | N | 8238 | lbf |
| Bore Area (m$^2$) | 0.000361 | m$^2$ | 0.56 | square inches |
| Base Pressure = F/A | 102 | Mpa | 14.73 | ksi |
| Repulsion force per unit length (Base Pressure x Bore height) | 1.93 | MN/m | 11.05 | kip/in |
| Grade 2 SAE J429 3/8" diameter stainless steel bolts Minimum Yield Strength | | | 57000 | psi |
| Individual bolt area required to avoid exceeding Yield Strength for static longitudinal repulsion force along entire 24" rail length distributed between 22 bolts | | | 0.21 | square inches |
| Grade 2 Minimum Bolt Diameter Required | | | 0.519 | inches |
| Grade 8 SAE J429 3/8" diameter stainless steel bolts Minimum Yield Strength | | | 130000 | psi |
| Individual bolt area required to avoid exceeding Yield Strength for static longitudinal repulsion force along 2" rail length distributed between 4 bolts | | | 0.09 | square inches |
| Grade 8 Minimum Bolt Diameter Required | | | 0.344 | inches |
| Actual Bolt Diameter | | | 0.375 | inches |

Table 18. 1500 m/s Solid Augmented Parameter Model

1500 m/s Slotted Augmented Parameter Modeling

| Slotted Rail Augmented Parameter Model | | | | |
|---|---|---|---|---|
| **L'** | **0.68279** | **µH/m** | | |
| **Target velocity:** | **1500** | m/s | | |
| Projectile mass: | 11.4 | grams | | |
| Effective length: | 50 | cm | | |
| Armature height: | 19 | mm | | |
| t = 2x/(delta v) | t (ms) | 0.67 | | |
| $a_{avg} = 2x/(t^2)$ | 2.25E+06 | $a_{avg}$ (m/s$^2$) | | |
| | 225 | $a_{avg}$ (kG's) | | |
| Avg. Current: $I_{avg} = (2ma/L')^{0.5}$ | 274.10 | k-Amps | Assume: average acceleration is 70% of peak acceleration and this ratio is proportional to $(I_{avg}^2/I_{peak}^2)$ | |
| Peak Current $I_{peak} = (I_{avg}^2/0.7)^{0.5}$ | 327.62 | k-Amps | | |
| Linear current density: $I_{peak}' = I_{peak}$ / armature height | 17.24 | (kA/mm) | Note: linear current densities > 45 kA/mm are regarded as unstable for railgun design | |
| Electrical Action: G=2mv/L' | 5.01E+07 | Amp$^2$s | Electrical Action is a measure of heating due to current flow | |
| $\Delta T = (\rho_e/\rho_m C_p)*(G/A^2)$ | 40.00 | Kelvin (K) | Based on thumbrule of a delta T of 40 K across the rail due to resistive heating, where | |
| Conductor Area = $[(\rho_e/\rho_m C_p)(G/\Delta T)]^{0.5}$ | 79.13 | mm$^2$ | The expression $(\rho_e/\rho_m C_p)$ is a ratio of electrical resistivity to the product of mass density and specific heat capacity, a typical value for the ratio for copper is 0.005 (K/Amp$^2$s)/mm$^4$. | |
| Required rail width (mm) | 4.16 | mm | | |
| Actual rail width (1/4" rail + 1/8" rail liner) | 9.53 | mm | | |
| Lorentz Force at peak current: $F = (1/2)L'I_{peak}^2$ | 36642.86 | N | 8238 | lbf |
| Bore Area (m$^2$) | 0.000361 | m$^2$ | 0.56 | square inches |
| Base Pressure = F/A | 102 | Mpa | 14.73 | ksi |
| Repulsion force per unit length (Base Pressure x Bore height) | 1.93 | MN/m | 11.05 | kip/in |
| Grade 2 SAE J429 3/8" diameter stainless steel bolts Minimum Yield Strength | | | 57000 | psi |
| Individual bolt area required to avoid exceeding Yield Strength for static longitudinal repulsion force along entire 24" rail length distributed between 22 bolts | | | 0.21 | square inches |
| Grade 2 Minimum Bolt Diameter Required | | | 0.519 | inches |
| Grade 8 SAE J429 3/8" diameter stainless steel bolts Minimum Yield Strength | | | 130000 | psi |
| Individual bolt area required to avoid exceeding Yield Strength for static longitudinal repulsion force along 2" rail length distributed between 4 bolts | | | 0.09 | square inches |
| Grade 8 Minimum Bolt Diameter Required | | | 0.344 | inches |
| Actual Bolt Diameter | | | 0.375 | inches |

Table 19. 1500 m/s Slotted Augmented Parameter Model

265 m/s Solid Augmented Parameter Modeling

| **Solid Rail Augmented Parameter Model for Experimental Velocity Result: 265 m/s** | | | | |
|---|---|---|---|---|
| **L'** | **0.47070** | **μH/m** | | |
| **Target velocity:** | **265** | m/s | | |
| Projectile mass: | 11.4 | grams | | |
| Effective length: | 50 | cm | | |
| Armature height: | 19 | mm | | |
| t = 2x/(delta v) | t (ms) | 3.77 | | |
| $a_{avg} = 2x/(t^2)$ | 7.02E+04 | $a_{avg}$ (m/s$^2$) | | |
| | 7.0225 | $a_{avg}$ (kG's) | | |
| Avg. Current: $I_{avg} = (2ma/L')^{0.5}$ | 58.32 | k-Amps | Assume: average acceleration is 70% of peak acceleration and this ratio is proportional to $(I_{avg}^2/I_{peak}^2)$ | |
| Peak Current $I_{peak} = (I_{avg}^2/0.7)^{0.5}$ | 69.71 | k-Amps | | |
| Linear current density: $I_{peak}' = I_{peak}$ / armature height | 3.67 | (kA/mm) | Note: linear current densities > 45 kA/mm are regarded as unstable for railgun design | |
| Electrical Action: G=2mv/L' | 1.28E+07 | Amp$^2$s | Electrical Action is a measure of heating due to current flow | |
| $\Delta T = (\rho_e/\rho_m C_p)*(G/A^2)$ | 40.00 | Kelvin (K) | Based on thumbrule of a delta T of 40 K across the rail due to resistive heating, where | |
| Conductor Area = $[(\rho_e/\rho_m C_p)(G/\Delta T)]^{0.5}$ | 40.06 | mm$^2$ | The expression $(\rho_e/\rho_m C_p)$ is a ratio of electrical resistivity to the product of mass density and specific heat capacity, a typical value for the ratio for copper is 0.005 (K/Amp$^2$s)/mm$^4$. | |
| Required rail width (mm) | 2.11 | mm | | |
| Actual rail width (1/4" rail + 1/8" rail liner) | 9.53 | mm | | |
| Lorentz Force at peak current: $F = (1/2)L'I_{peak}^2$ | 1143.66 | N | 257 | lbf |
| Bore Area (m$^2$) | 0.000361 | m$^2$ | 0.56 | square inches |
| Base Pressure = F/A | 3 | Mpa | 0.46 | ksi |
| Repulsion force per unit length (Base Pressure x Bore height) | 0.06 | MN/m | 0.34 | kip/in |
| Grade 2 SAE J429 3/8" diameter stainless steel bolts Minimum Yield Strength | | | 57000 | psi |
| Individual bolt area required to avoid exceeding Yield Strength for static longitudinal repulsion force along entire 24" rail length distributed between 22 bolts | | | 0.01 | square inches |
| Grade 2 Minimum Bolt Diameter Required | | | 0.092 | inches |
| Grade 8 SAE J429 3/8" diameter stainless steel bolts Minimum Yield Strength | | | 130000 | psi |
| Individual bolt area required to avoid exceeding Yield Strength for static longitudinal repulsion force along 2" rail length distributed between 4 bolts | | | 0.00 | square inches |
| Grade 8 Minimum Bolt Diameter Required | | | 0.061 | inches |
| Actual Bolt Diameter | | | 0.375 | inches |

Table 20. 265 m/s Solid Augmented Parameter Model

290 m/s Slotted Augmented Parameter Model

| Slotted Rail Augmented Parameter Model for Experimental Velocity Result: 290 m/s | | | | |
|---|---|---|---|---|
| **L'** | **0.68279** | **μH/m** | | |
| **Target velocity:** | **290** | m/s | | |
| Projectile mass: | 11.4 | grams | | |
| Effective length: | 50 | cm | | |
| Armature height: | 19 | mm | | |
| t = 2x/(delta v) | t (ms) | 3.45 | | |
| $a_{avg} = 2x/(t^2)$ | 8.41E+04 | $a_{avg}$ (m/s$^2$) | | |
| | 8.41 | $a_{avg}$ (kG's) | | |
| Avg. Current: $I_{avg} = (2ma/L')^{0.5}$ | 52.99 | k-Amps | Assume: average acceleration is 70% of peak acceleration and this ratio is proportional to $(I_{avg}^2/I_{peak}^2)$ | |
| Peak Current $I_{peak} = (I_{avg}^2/0.7)^{0.5}$ | 63.34 | k-Amps | | |
| Linear current density: $I_{peak}' = I_{peak}$ / armature height | 3.33 | (kA/mm) | Note: linear current densities > 45 kA/mm are regarded as unstable for railgun design | |
| Electrical Action: G=2mv/L' | 9.68E+06 | Amp$^2$s | Electrical Action is a measure of heating due to current flow | |
| $\Delta T = (\rho_e/\rho_m C_p)*(G/A^2)$ | 40.00 | Kelvin (K) | Based on thumbrule of a delta T of 40 K across the rail due to resistive heating, where | |
| Conductor Area = $[(\rho_e/\rho_m C_p)(G/\Delta T)]^{0.5}$ | 34.79 | mm$^2$ | The expression $(\rho_e/\rho_m C_p)$ is a ratio of electrical resistivity to the product of mass density and specific heat capacity, a typical value for the ratio for copper is 0.005 (K/Amp$^2$s)/mm$^4$. | |
| Required rail width (mm) | 1.83 | mm | | |
| Actual rail width (1/4" rail + 1/8" rail liner) | 9.53 | mm | | |
| Lorentz Force at peak current: $F = (1/2)L'I_{peak}^2$ | 1369.63 | N | 308 | lbf |
| Bore Area (m$^2$) | 0.000361 | m$^2$ | 0.56 | square inches |
| Base Pressure = F/A | 4 | Mpa | 0.55 | ksi |
| Repulsion force per unit length (Base Pressure x Bore height) | 0.07 | MN/m | 0.41 | kip/in |
| Grade 2 SAE J429 3/8" diameter stainless steel bolts Minimum Yield Strength | | | 57000 | psi |
| Individual bolt area required to avoid exceeding Yield Strength for static longitudinal repulsion force along entire 24" rail length distributed between 22 bolts | | | 0.01 | square inches |
| Grade 2 Minimum Bolt Diameter Required | | | 0.100 | inches |
| Grade 8 SAE J429 3/8" diameter stainless steel bolts Minimum Yield Strength | | | 130000 | psi |
| Individual bolt area required to avoid exceeding Yield Strength for static longitudinal repulsion force along 2" rail length distributed between 4 bolts | | | 0.00 | square inches |
| Grade 8 Minimum Bolt Diameter Required | | | 0.066 | inches |
| Actual Bolt Diameter | | | 0.375 | inches |

Table 21. 290 m/s Slotted Augmented Parameter Model

Solid Non-Augmented Parameter Model for Peak Current, Maximum Velocity for Grade 2 Bolt Diameter

| Solid Rail Non-Augmented Parameter Model for Actual Grade 2 Bolt Design | | | | | |
|---|---|---|---|---|---|
| **L'** **0.30368** | | **μH/m** | | | |
| **Target velocity:** | **1085** | m/s | | | |
| Projectile mass: | 11.4 | grams | | | |
| Effective length: | 50 | cm | | | |
| Armature height: | 19 | mm | | | |
| t = 2x/(delta v) | t (ms) | 0.92 | | | |
| $a_{avg} = 2x/(t^2)$ | 1.18E+06 | $a_{avg}$ ($m/s^2$) | | | |
| | 117.7225 | $a_{avg}$ (kG's) | | | |
| Avg. Current: $I_{avg} = (2ma/L')^{0.5}$ | 297.30 | k-Amps | Assume: average acceleration is 70% of peak acceleration and this ratio is proportional to $(I_{avg}^2/I_{peak}^2)$ | | |
| Peak Current $I_{peak} = (I_{avg}^2/0.7)^{0.5}$ | **355.34** | k-Amps | | | |
| Linear current density: $I_{peak}' = I_{peak}$ / armature height | 18.70 | (kA/mm) | Note: linear current densities > 45 kA/mm are regarded as unstable for railgun design | | |
| Electrical Action: G=2mv/L' | 8.15E+07 | $Amp^2s$ | Electrical Action is a measure of heating due to current flow | | |
| $\Delta T = (\rho_e/\rho_m C_p)*(G/A^2)$ | 40.00 | Kelvin (K) | Based on thumbrule of a delta T of 40 K across the rail due to resistive heating, where A = conductor cross-sectional area | | |
| Conductor Area = $[(\rho_e/\rho_m C_p)(G/\Delta T)]^{0.5}$ | 100.91 | $mm^2$ | The expression $(\rho_e/\rho_m C_p)$ is a ratio of electrical resistivity to the product of mass density and specific heat capacity, a typical value for the ratio for copper is 0.005 $(K/Amp^2s)/mm^4$. | | |
| Required rail width (mm) | 5.31 | mm | | | |
| Actual rail width (1/4" rail + 1/8" rail liner) | 9.53 | mm | | | |
| Lorentz Force at peak current: $F = (1/2)L'I_{peak}^2$ | 19171.95 | N | 4310 | lbf | |
| Bore Area ($m^2$) | 0.000361 | $m^2$ | 0.56 | square inches | |
| Base Pressure = F/A | 53 | Mpa | 7.71 | ksi | |
| Repulsion force per unit length (Base Pressure x Bore height) | 1.01 | MN/m | 5.78 | kip/in | |
| Grade 2 SAE J429 3/8" diameter stainless steel bolts Minimum Yield Strength | | | 57000 | psi | |
| Individual bolt area required to avoid exceeding Yield Strength for static longitudinal repulsion force along entire 24" rail length distributed between 22 bolts | | | 0.11 | square inches | |
| Grade 2 Minimum Bolt Diameter Required | | | **0.375** | inches | |
| Grade 8 SAE J429 3/8" diameter stainless steel bolts Minimum Yield Strength | | | 130000 | psi | |
| Individual bolt area required to avoid exceeding Yield Strength for static longitudinal repulsion force along 2" rail length distributed between 4 bolts | | | 0.05 | square inches | |
| Grade 8 Minimum Bolt Diameter Required | | | 0.249 | inches | |
| Actual Bolt Diameter | | | **0.375** | inches | |

Table 22. Parameter Estimate of Peak Current and Final Velocity for 3/8” diameter Grade 2 Bolts

## C. CONSERVATION OF ENERGY INTEGRATION [4]

35 kJ Solid Non-Augmented Velocity Integration

**Rail length as an integral function of velocity for solid/non-augmented input parameters:**

$$\int dx = \frac{1}{2a}\ln\left(av^2+bv+c\right)-\frac{b}{2a}\left[\frac{1}{\sqrt{b^2-4ac}}\ln\left(\frac{2av+b-\sqrt{b^2-4ac}}{2av+b+\sqrt{b^2-4ac}}\right)\right]+D$$

Table integral form: $V = av^2 + bv + c$

| Input Parameters: | | Velocity (m/s) | First Term: | Second Term: | Required Rail Length (m): |
|---|---|---|---|---|---|
| mass (g) | 0.0114 | 120 | -9.17E+01 | -6.23E+01 | 0.12 |
| C (farads) | 1.66E-03 | 121 | -9.13E+01 | -6.28E+01 | 0.13 |
| L (Henries) | 5.50E-06 | 122 | -9.08E+01 | -6.32E+01 | 0.13 |
| R (ohms) | 3.30E-03 | 123 | -9.03E+01 | -6.37E+01 | 0.14 |
| Volts | 6.50E+03 | 124 | -8.98E+01 | -6.43E+01 | 0.14 |
| $W_0$ (J) | 3.51E+04 | 125 | -8.92E+01 | -6.48E+01 | 0.15 |
| L' (H/m) | 3.04E-07 | 126 | -8.86E+01 | -6.54E+01 | 0.16 |
| **Integral factors:** | | 127 | -8.80E+01 | -6.60E+01 | 0.16 |
| a = -L'/L | -5.52E-02 | 128 | -8.73E+01 | -6.67E+01 | 0.17 |
| b= -2R/L | -1.20E+03 | 129 | -8.65E+01 | -6.75E+01 | 0.18 |
| c =(L' $W_o$)/(mL) | 1.70E+05 | 130 | -8.57E+01 | -6.83E+01 | 0.19 |
| 4ac | -3.75E+04 | 131 | -8.48E+01 | -6.91E+01 | 0.20 |
| $b^2$ | 1.44E+06 | 132 | -8.38E+01 | -7.01E+01 | 0.21 |
| b / 2a | 1.09E+04 | 133 | -8.27E+01 | -7.12E+01 | 0.23 |
| **Square Root ($b^2$ - 4ac)** | | 134 | -8.14E+01 | -7.25E+01 | 0.24 |
| 1.22E+03 | | 135 | -8.00E+01 | -7.39E+01 | 0.26 |
| **1/Square Root($b^2$ - 4ac)** | | 136 | -7.82E+01 | -7.57E+01 | 0.28 |
| 8.23E-04 | | 137 | -7.60E+01 | -7.79E+01 | 0.31 |
| **D = Integration Constant:** | | 138 | -7.31E+01 | -8.08E+01 | 0.35 |
| 154.17 | | 139 | -6.87E+01 | -8.50E+01 | 0.40 |
| | | **140** | **-6.01E+01** | **-9.36E+01** | **0.51** |
| | | 141 | -5.54E+01 | -9.82E+01 | 0.57 |

Table 23. 35 kJ Velocity Integral, Solid Non-Augmented.

35 kJ Slotted Non-Augmented Velocity Integration

**Rail length as an integral function of velocity for slotted/non-augmented input parameters:**

$$\int dx = \frac{1}{2a}\ln\left(av^2+bv+c\right)-\frac{b}{2a}\left[\frac{1}{\sqrt{b^2-4ac}}\ln\left(\frac{2av+b-\sqrt{b^2-4ac}}{2av+b+\sqrt{b^2-4ac}}\right)\right]+D$$

Table integral form: $V = av^2 + bv + c$

| Input Parameters: | | Velocity (m/s) | First Term: | Second Term: | Required Rail Length (m): |
|---|---|---|---|---|---|
| mass (g) | 0.0114 | 160 | -6.78E+01 | -3.58E+01 | 0.13 |
| C (farads) | 1.66E-03 | 162 | -6.75E+01 | -3.61E+01 | 0.13 |
| L (Henries) | 5.50E-06 | 164 | -6.72E+01 | -3.64E+01 | 0.14 |
| R (ohms) | 3.30E-03 | 166 | -6.69E+01 | -3.67E+01 | 0.15 |
| Volts | 6.50E+03 | 168 | -6.65E+01 | -3.71E+01 | 0.15 |
| $W_0$ (J) | 3.51E+04 | 170 | -6.62E+01 | -3.74E+01 | 0.16 |
| L' (H/m) | 4.41E-07 | 172 | -6.58E+01 | -3.78E+01 | 0.17 |
| **Integral factors:** | | 174 | -6.53E+01 | -3.82E+01 | 0.18 |
| a = -L'/L | -8.01E-02 | 176 | -6.49E+01 | -3.87E+01 | 0.19 |
| b= -2R/L | -1.20E+03 | 178 | -6.44E+01 | -3.91E+01 | 0.20 |
| c =(L' $W_o$)/(mL) | 2.46E+05 | 180 | -6.39E+01 | -3.97E+01 | 0.21 |
| 4ac | -7.89E+04 | 182 | -6.33E+01 | -4.02E+01 | 0.23 |
| $b^2$ | 1.44E+06 | 184 | -6.27E+01 | -4.08E+01 | 0.24 |
| b / 2a | 7.49E+03 | 186 | -6.19E+01 | -4.15E+01 | 0.26 |
| **Square Root ($b^2$ - 4ac)** | | 188 | -6.11E+01 | -4.23E+01 | 0.28 |
| 1.23E+03 | | 190 | -6.02E+01 | -4.32E+01 | 0.30 |
| **1/Square Root($b^2$ - 4ac)** | | 192 | -5.91E+01 | -4.43E+01 | 0.33 |
| 8.11E-04 | | 194 | -5.78E+01 | -4.55E+01 | 0.36 |
| **D = Integration Constant:** | | 196 | -5.62E+01 | -4.72E+01 | 0.40 |
| 103.74 | | **198** | **-5.39E+01** | **-4.94E+01** | **0.46** |
| | | **200** | **-5.03E+01** | **-5.29E+01** | **0.55** |
| | | 202 | -4.09E+01 | -6.20E+01 | 0.80 |

Table 24. 35 kJ Velocity Integral, Slotted Non-Augmented.

35 kJ Solid Augmented Velocity Integration

**Rail length as an integral function of velocity for solid/augmented input parameters:**

$$\int dx = \frac{1}{2a}\ln\left(av^2+bv+c\right)-\frac{b}{2a}\left[\frac{1}{\sqrt{b^2-4ac}}\ln\left(\frac{2av+b-\sqrt{b^2-4ac}}{2av+b+\sqrt{b^2-4ac}}\right)\right]+D$$

Table integral form: $V = av^2 + bv + c$

| Input Parameters: | | Velocity (m/s) | First Term: | Second Term: | Required Rail Length (m): |
|---|---|---|---|---|---|
| mass (g) | 0.0114 | 150 | -6.61E+01 | -3.05E+01 | 0.08 |
| C (farads) | 1.66E-03 | 152 | -6.59E+01 | -3.07E+01 | 0.09 |
| L (Henries) | 5.50E-06 | 154 | -6.57E+01 | -3.09E+01 | 0.09 |
| R (ohms) | 3.30E-03 | 156 | -6.55E+01 | -3.11E+01 | 0.09 |
| Volts | 6.50E+03 | 158 | -6.53E+01 | -3.12E+01 | 0.10 |
| $W_0$ (J) | 3.51E+04 | 160 | -6.51E+01 | -3.14E+01 | 0.10 |
| L' (H/m) | 4.71E-07 | 162 | -6.49E+01 | -3.17E+01 | 0.11 |
| **Integral factors:** | | 164 | -6.47E+01 | -3.19E+01 | 0.11 |
| a = -L'/L | -8.56E-02 | 166 | -6.44E+01 | -3.21E+01 | 0.12 |
| b= -2R/L | -1.20E+03 | 168 | -6.42E+01 | -3.23E+01 | 0.12 |
| c =(L' $W_o$)/(mL) | 2.63E+05 | 170 | -6.40E+01 | -3.26E+01 | 0.13 |
| 4ac | -9.01E+04 | 172 | -6.37E+01 | -3.28E+01 | 0.13 |
| $b^2$ | 1.44E+06 | 174 | -6.34E+01 | -3.31E+01 | 0.14 |
| b / 2a | 7.01E+03 | 176 | -6.31E+01 | -3.34E+01 | 0.15 |
| **Square Root ($b^2$ - 4ac)** | | 178 | -6.28E+01 | -3.36E+01 | 0.16 |
| 1.24E+03 | | 180 | -6.25E+01 | -3.40E+01 | 0.16 |
| **1/Square Root($b^2$ - 4ac)** | | 182 | -6.22E+01 | -3.43E+01 | 0.17 |
| 8.08E-04 | | 184 | -6.18E+01 | -3.46E+01 | 0.18 |
| **D = Integration Constant:** | | 186 | -6.15E+01 | -3.50E+01 | 0.19 |
| 96.65 | | 188 | -6.11E+01 | -3.54E+01 | 0.20 |
| | | 190 | -6.06E+01 | -3.58E+01 | 0.21 |
| | | 192 | -6.02E+01 | -3.63E+01 | 0.22 |
| | | 194 | -5.97E+01 | -3.67E+01 | 0.24 |
| | | 196 | -5.91E+01 | -3.73E+01 | 0.25 |
| | | 198 | -5.85E+01 | -3.79E+01 | 0.27 |
| | | 200 | -5.78E+01 | -3.86E+01 | 0.29 |
| | | 202 | -5.70E+01 | -3.93E+01 | 0.31 |
| | | 204 | -5.61E+01 | -4.02E+01 | 0.34 |
| | | 206 | -5.51E+01 | -4.12E+01 | 0.37 |
| | | 208 | -5.38E+01 | -4.25E+01 | 0.40 |
| | | **210** | **-5.21E+01** | **-4.41E+01** | **0.45** |
| | | **212** | **-4.98E+01** | **-4.64E+01** | **0.52** |
| | | 214 | -4.58E+01 | -5.02E+01 | 0.64 |

Table 25. 35 kJ Velocity Integral, Solid Augmented.

35 kJ Slotted Augmented Velocity Integration

| Rail length as an integral function of velocity for slotted/augmented input parameters: | | | | | |
|---|---|---|---|---|---|
| $\int dx = \frac{1}{2a}\ln\left(av^2+bv+c\right)-\frac{b}{2a}\left[\frac{1}{\sqrt{b^2-4ac}}\ln\left(\frac{2av+b-\sqrt{b^2-4ac}}{2av+b+\sqrt{b^2-4ac}}\right)\right]+D$ | | | | | |
| Table integral form: $V = av^2 + bv + c$ | | | | | |
| **Input Parameters:** | | **Velocity (m/s)** | **First Term:** | **Second Term:** | **Required Rail Length (m):** |
| mass (g) | 0.0114 | 150 | -4.91E+01 | -1.57E+01 | 0.05 |
| C (farads) | 1.66E-03 | 155 | -4.90E+01 | -1.59E+01 | 0.05 |
| L (Henries) | 5.50E-06 | 160 | -4.89E+01 | -1.60E+01 | 0.05 |
| R (ohms) | 3.30E-03 | 165 | -4.87E+01 | -1.61E+01 | 0.06 |
| Volts | 6.50E+03 | 170 | -4.86E+01 | -1.63E+01 | 0.06 |
| $W_0$ (J) | 3.51E+04 | 175 | -4.85E+01 | -1.64E+01 | 0.07 |
| L' (H/m) | 6.83E-07 | 180 | -4.83E+01 | -1.65E+01 | 0.07 |
| **Integral factors:** | | 185 | -4.82E+01 | -1.67E+01 | 0.08 |
| a = -L'/L | -1.24E-01 | 190 | -4.80E+01 | -1.69E+01 | 0.09 |
| b= -2R/L | -1.20E+03 | 195 | -4.78E+01 | -1.70E+01 | 0.09 |
| c =(L' $W_o$)/(mL) | 3.82E+05 | 200 | -4.76E+01 | -1.72E+01 | 0.10 |
| 4ac | -1.90E+05 | 205 | -4.74E+01 | -1.74E+01 | 0.11 |
| $b^2$ | 1.44E+06 | 210 | -4.72E+01 | -1.76E+01 | 0.12 |
| b / 2a | 4.83E+03 | 215 | -4.70E+01 | -1.78E+01 | 0.12 |
| **Square Root ($b^2$ - 4ac)** | | 220 | -4.68E+01 | -1.80E+01 | 0.13 |
| 1.28E+03 | | 225 | -4.66E+01 | -1.82E+01 | 0.14 |
| **1/Square Root($b^2$ - 4ac)** | | 230 | -4.63E+01 | -1.84E+01 | 0.16 |
| 7.83E-04 | | 235 | -4.61E+01 | -1.87E+01 | 0.17 |
| **D = Integration Constant:** | | 240 | -4.58E+01 | -1.90E+01 | 0.18 |
| 64.93 | | 245 | -4.55E+01 | -1.92E+01 | 0.20 |
| | | 250 | -4.52E+01 | -1.96E+01 | 0.21 |
| | | 255 | -4.48E+01 | -1.99E+01 | 0.23 |
| | | 260 | -4.44E+01 | -2.03E+01 | 0.25 |
| | | 265 | -4.40E+01 | -2.07E+01 | 0.27 |
| | | 270 | -4.35E+01 | -2.12E+01 | 0.30 |
| | | 275 | -4.29E+01 | -2.17E+01 | 0.33 |
| | | 280 | -4.23E+01 | -2.23E+01 | 0.36 |
| | | 285 | -4.15E+01 | -2.30E+01 | 0.41 |
| | | **290** | **-4.05E+01** | **-2.39E+01** | **0.46** |
| | | **295** | **-3.93E+01** | **-2.51E+01** | **0.53** |
| | | 300 | -3.74E+01 | -2.69E+01 | 0.64 |
| | | 305 | -3.37E+01 | -3.03E+01 | 0.86 |
| | | 310 | -3.07E+01 | -3.32E+01 | 1.03 |

Table 26. 35 kJ Velocity Integral, Slotted Augmented.

## 83 kJ Slotted Augmented Velocity Integration

**Rail length as an integral function of velocity for slotted/augmented input parameters:**

$$\int dx = \frac{1}{2a}\ln\left(av^2+bv+c\right)-\frac{b}{2a}\left[\frac{1}{\sqrt{b^2-4ac}}\ln\left(\frac{2av+b-\sqrt{b^2-4ac}}{2av+b+\sqrt{b^2-4ac}}\right)\right]+D$$

Table integral form: $V = av^2 + bv + c$

| **Input Parameters:** | | **Velocity (m/s)** | **First Term:** | **Second Term:** | **Required Rail Length (m):** |
|---|---|---|---|---|---|
| mass (g) | 0.0114 | 350 | -5.26E+01 | -1.20E+01 | 0.10 |
| C (farads) | 1.66E-03 | 355 | -5.25E+01 | -1.21E+01 | 0.33 |
| L (Henries) | 5.50E-06 | 360 | -5.25E+01 | -1.21E+01 | 0.34 |
| R (ohms) | 3.30E-03 | 365 | -5.24E+01 | -1.22E+01 | 0.34 |
| Volts | 1.00E+04 | 370 | -5.24E+01 | -1.22E+01 | 0.34 |
| $W_0$ (J) | 8.30E+04 | 375 | -5.23E+01 | -1.23E+01 | 0.35 |
| L' (H/m) | 6.83E-07 | 380 | -5.22E+01 | -1.23E+01 | 0.35 |
| **Integral factors:** | | 385 | -5.22E+01 | -1.24E+01 | 0.36 |
| a = -L'/L | -1.24E-01 | 390 | -5.21E+01 | -1.24E+01 | 0.36 |
| b= -2R/L | -1.20E+03 | 395 | -5.21E+01 | -1.25E+01 | 0.37 |
| c =(L' $W_o$)/(mL) | 9.04E+05 | 400 | -5.20E+01 | -1.26E+01 | 0.37 |
| 4ac | -4.49E+05 | 405 | -5.19E+01 | -1.26E+01 | 0.38 |
| $b^2$ | 1.44E+06 | 410 | -5.19E+01 | -1.27E+01 | 0.38 |
| b / 2a | 4.83E+03 | 415 | -5.18E+01 | -1.27E+01 | 0.39 |
| **Square Root ($b^2$ - 4ac)** | | 420 | -5.17E+01 | -1.28E+01 | 0.39 |
| 1.37E+03 | | 425 | -5.17E+01 | -1.29E+01 | 0.40 |
| **1/Square Root($b^2$ - 4ac)** | | 430 | -5.16E+01 | -1.29E+01 | 0.40 |
| 7.28E-04 | | 435 | -5.15E+01 | -1.30E+01 | 0.41 |
| **D = Integration Constant:** | | 440 | -5.14E+01 | -1.31E+01 | 0.42 |
| 64.93 | | 445 | -5.14E+01 | -1.31E+01 | 0.42 |
| | | 450 | -5.13E+01 | -1.32E+01 | 0.43 |
| | | 455 | -5.12E+01 | -1.33E+01 | 0.44 |
| | | 460 | -5.11E+01 | -1.34E+01 | 0.44 |
| | | 465 | -5.10E+01 | -1.34E+01 | 0.45 |
| | | 470 | -5.10E+01 | -1.35E+01 | 0.46 |
| | | 475 | -5.09E+01 | -1.36E+01 | 0.46 |
| | | 480 | -5.08E+01 | -1.37E+01 | 0.47 |
| | | 485 | -5.07E+01 | -1.38E+01 | 0.48 |
| | | 490 | -5.06E+01 | -1.38E+01 | 0.49 |
| | | **495** | **-5.05E+01** | **-1.39E+01** | **0.50** |
| | | 500 | -5.04E+01 | -1.40E+01 | 0.51 |
| | | 505 | -5.03E+01 | -1.41E+01 | 0.52 |
| | | 510 | -5.02E+01 | -1.42E+01 | 0.53 |

Table 27. 83 kJ Velocity Integral, Slotted Augmented.

## D. STRUCTURAL DESIGN VERIFICATION

Rail containment deflection is modeled based on static loading from 500 kA peak current conditions predicted for the solid non-augmented configuration in Table 15. The railgun test platform cross-sectional geometry is simplified by considering the rail liner, primary, and augmenting conducting rails as a single solid oxygen free copper conducting bar. The homogenous beam bending model considers only the 1-3/8" G-11 material from the outer face of the augmenting conductor rail to the top of the containment. The resultant combined rail and containment geometry contributing to the beam bending model are represented in Figure 30.

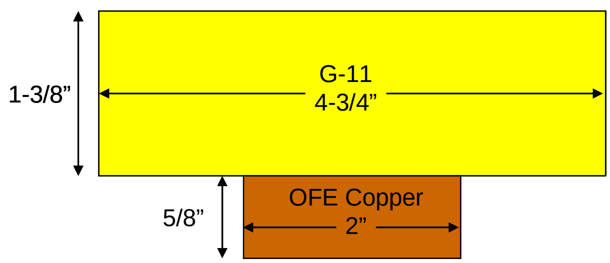


Figure 31. Simplified Beam Geometry (Not to scale)

The transformed geometry after expressing the copper in terms of G-11 for purposes of calculated the rectangular moment of inertia is depicted by Figure 31.

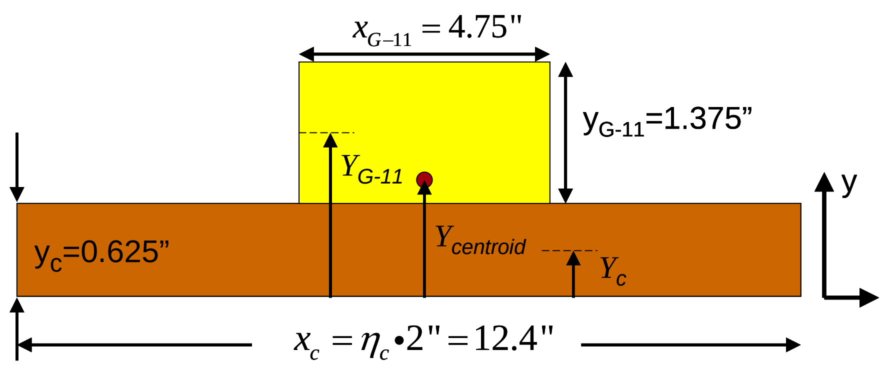


Figure 32. Transformed Homogenous Beam Geometry (Not to Scale)

The centroid and moment of inertia for the transformed geometry of Figure 31 are based on the following equations.

$$Y_{centroid} = \left( \frac{y_c A_c + y_{G-11} A_{G-11}}{A_c + A_{G-11}} \right)$$

$$I = \sum \left[ \frac{1}{12} x_i y_i^3 + A_i \left| Y_{centroid} - Y_i \right|^2 \right]$$

Table 27 lists the values used in the previous equations to calculate the rectangular moment of inertia for the transformed cross-section.

| Centroid and Moment of Inertia Calculations for Equivalent Homogenous Beam | | | | | | |
|---|---|---|---|---|---|---|
| Section | Elasticity Modulus (psi) | Area ( $in^2$ ) | y (in) | yA ( $in^3$ ) | Centroid ( in ) | Moment of Inertia ( $in^4$ ) |
| Copper | 1.67E+07 | 7.75 | 0.1875 | 1.453 | 0.6448 | 8.370 |
| G-11 | 2.70E+06 | 6.5313 | 1.1875 | 7.756 | | |

Table 28. Transformed Geometry Moment of Inertia Calculation

THIS PAGE INTENTIONALLY LEFT BLANK

# APPENDIX D. MAGNETIC FIELD AND CIRCUIT SIMULATIONS

## A. COMSOL MULTIPHYSICS MODELING

100 k-Amp DC, Solid Non-Augmented

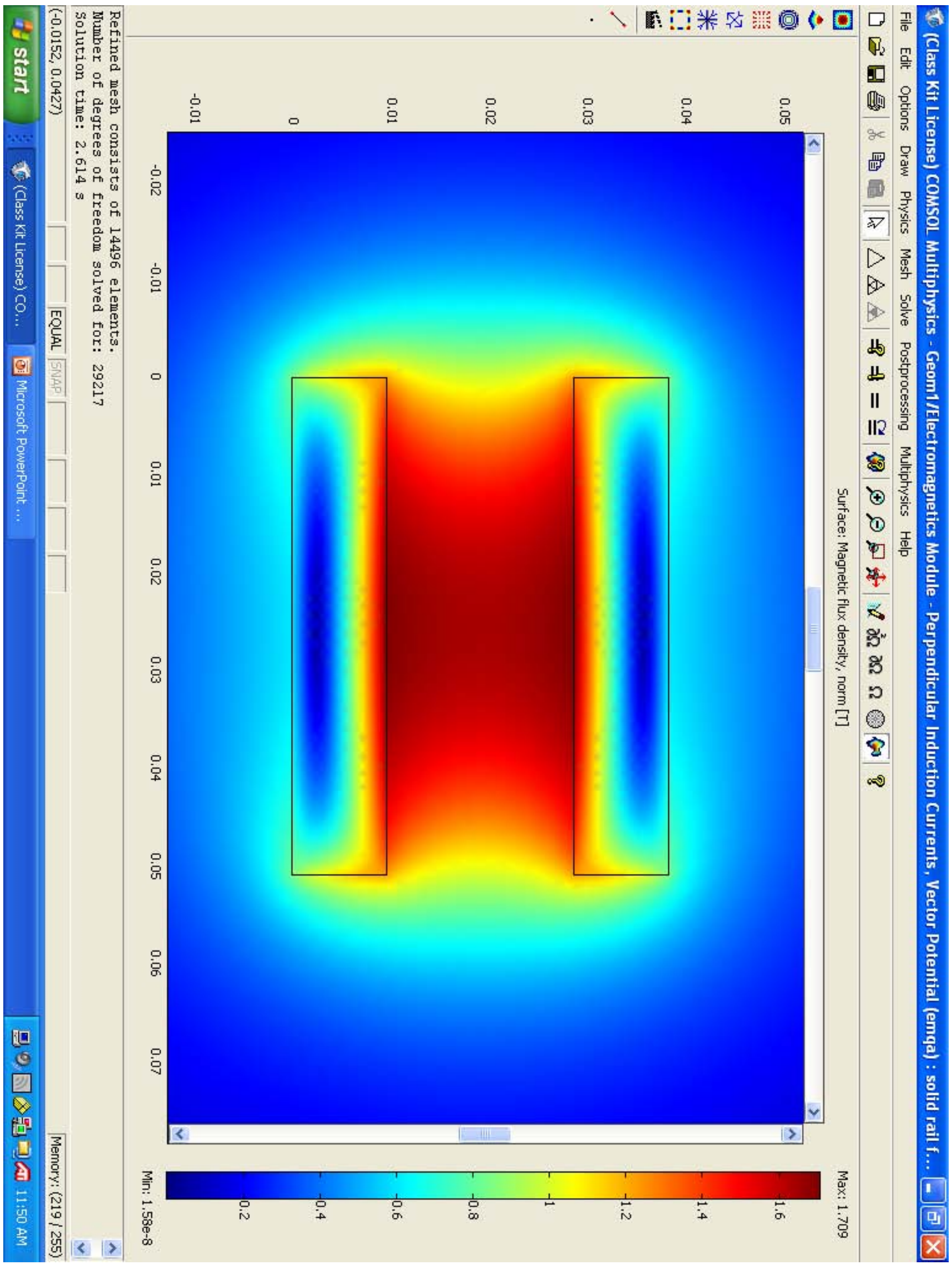


Figure 33. Solid Non-Augmented Magnetic Flux Density

X and Y axes units are in meters.

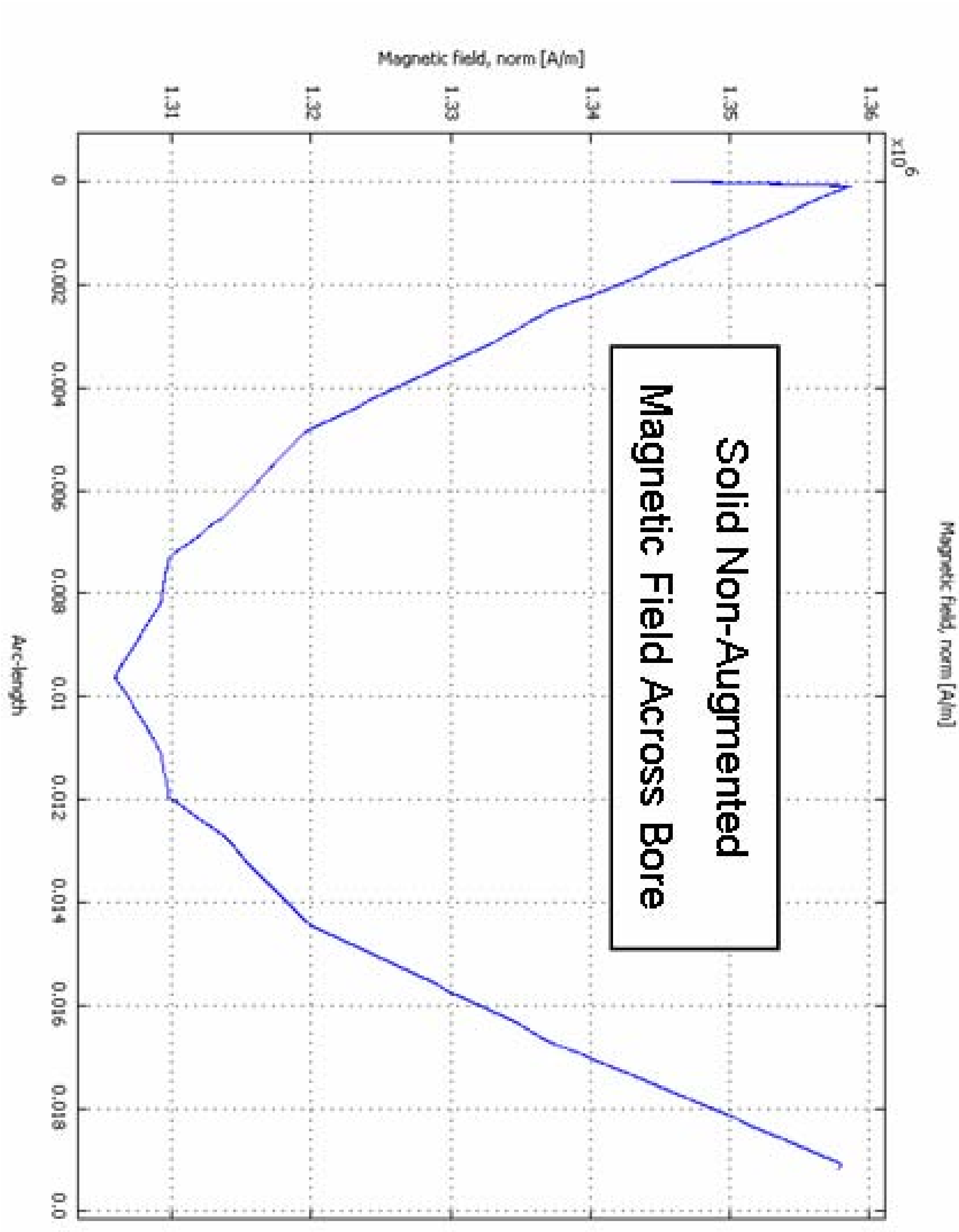


Figure 34. Solid Non-Augmented Magnetic Field Across Bore

X axis is in units of meters, Y axis is Magnetic field strength A/m.

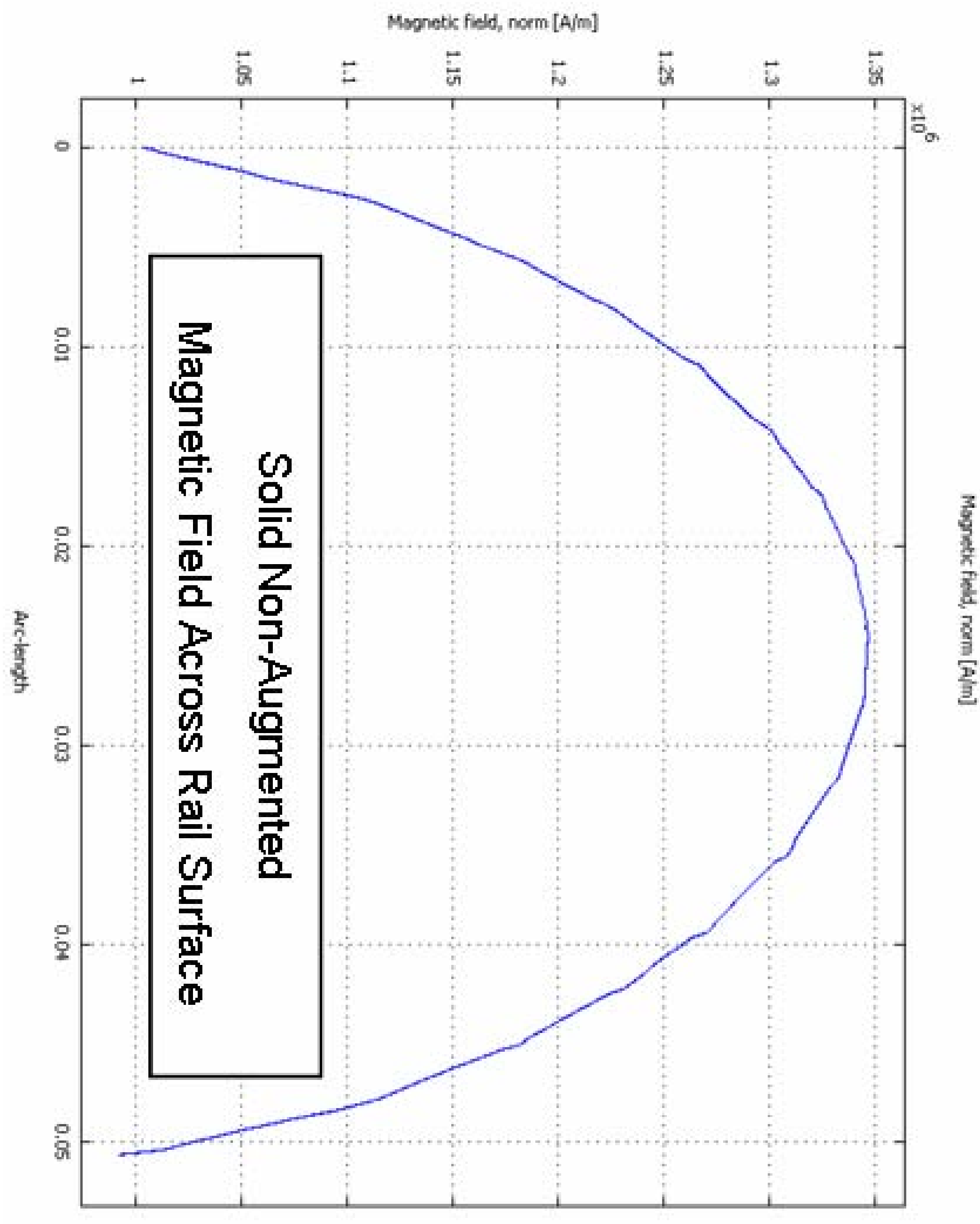


Figure 35. Solid Non-Augmented Magnetic Field Across Rail Surface

X axis is in units of meters, Y axis is Magnetic field strength A/m.

100 k-Amp DC, Slotted Rail, Non-Augmented

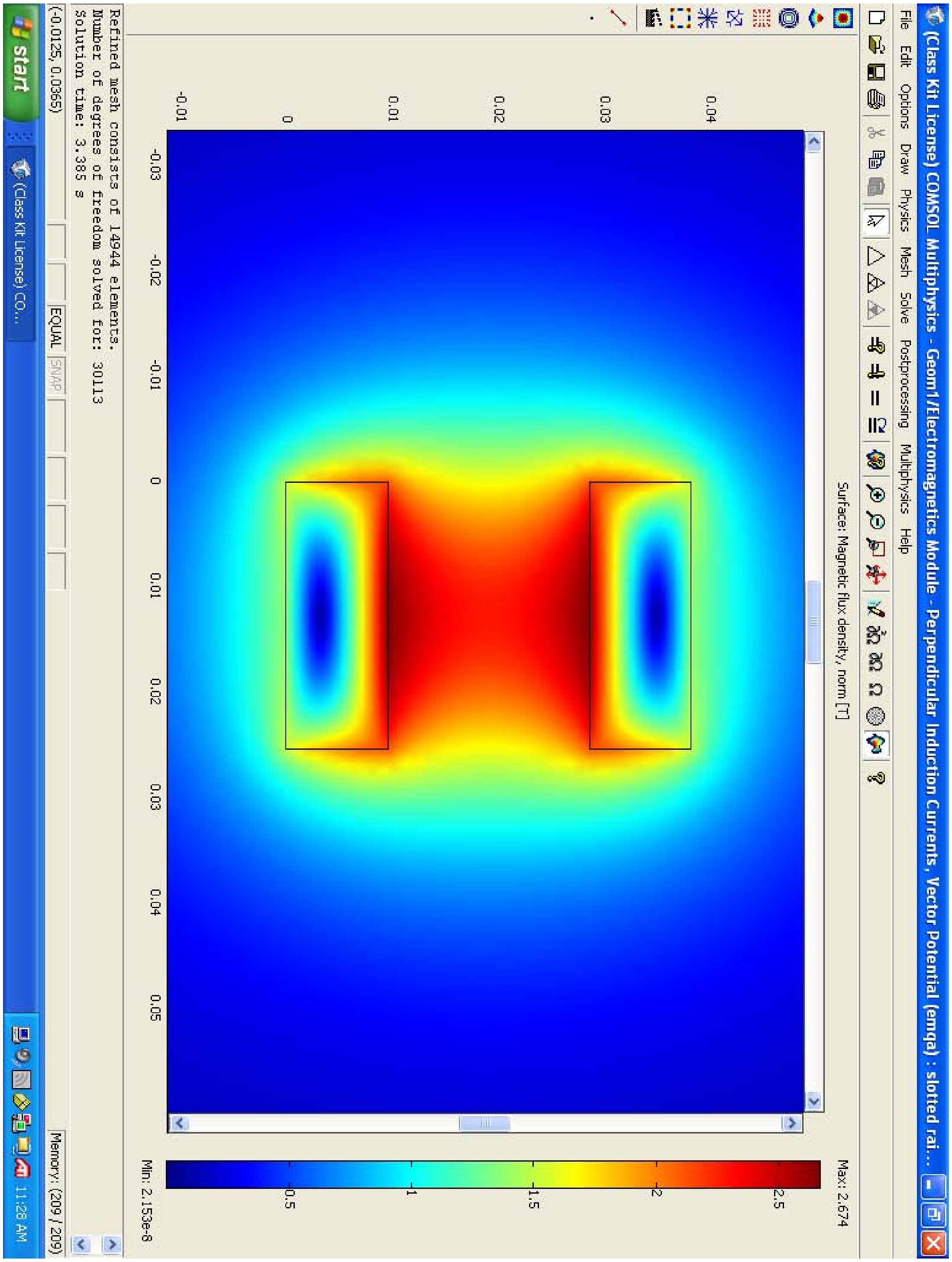


Figure 36. Slotted Non-Augmented Magnetic Flux Density

X and Y axes units are in meters.

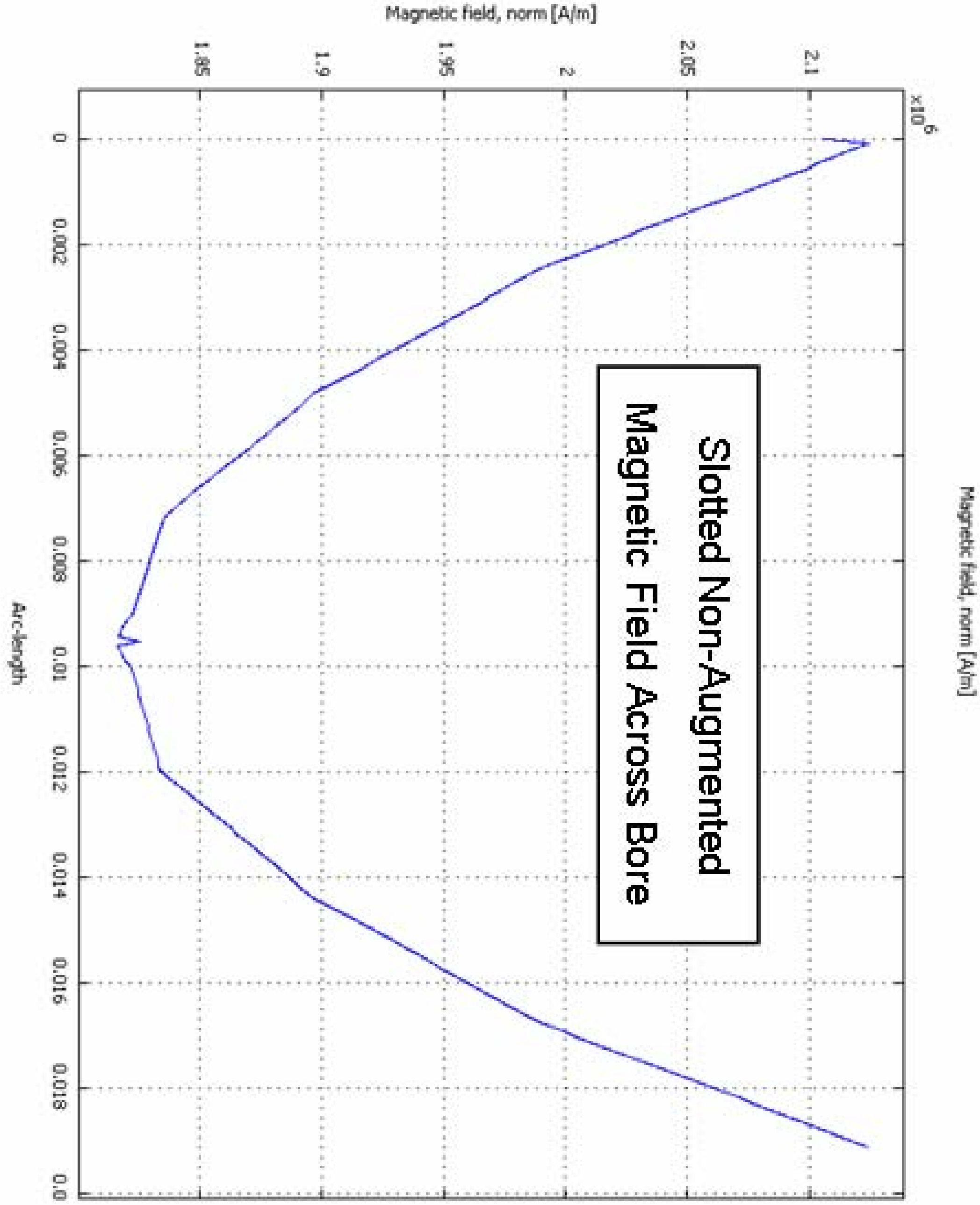


Figure 37. Slotted Non-Augmented Magnetic Field Across Bore

X axis is in units of meters, Y axis is Magnetic field strength A/m.

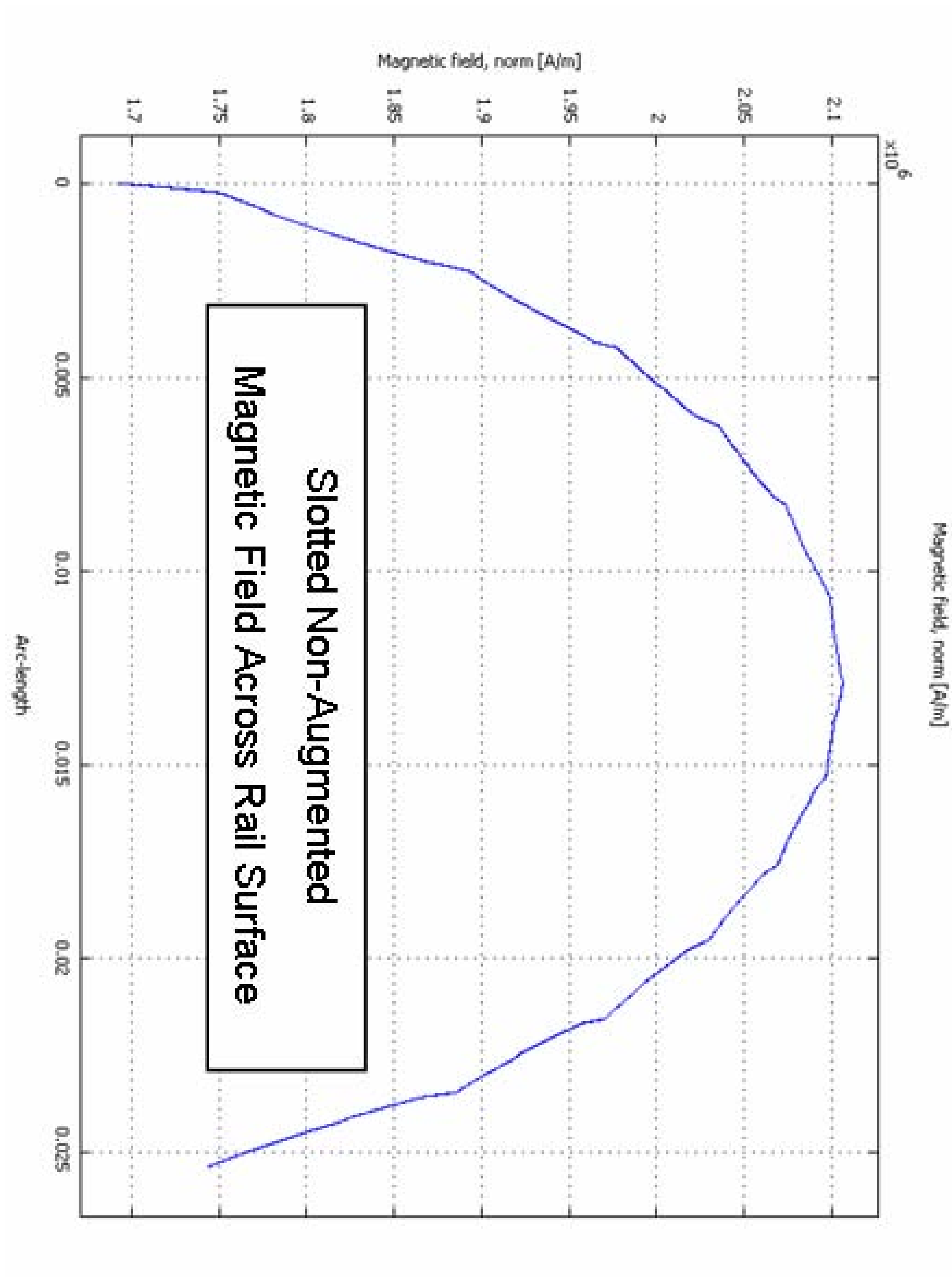


Figure 38. Slotted Non-Augmented Magnetic Field Across Rail Surface

X axis is in units of meters, Y axis is Magnetic field strength A/m.

100 k-Amp DC, Solid Rail, Augmented

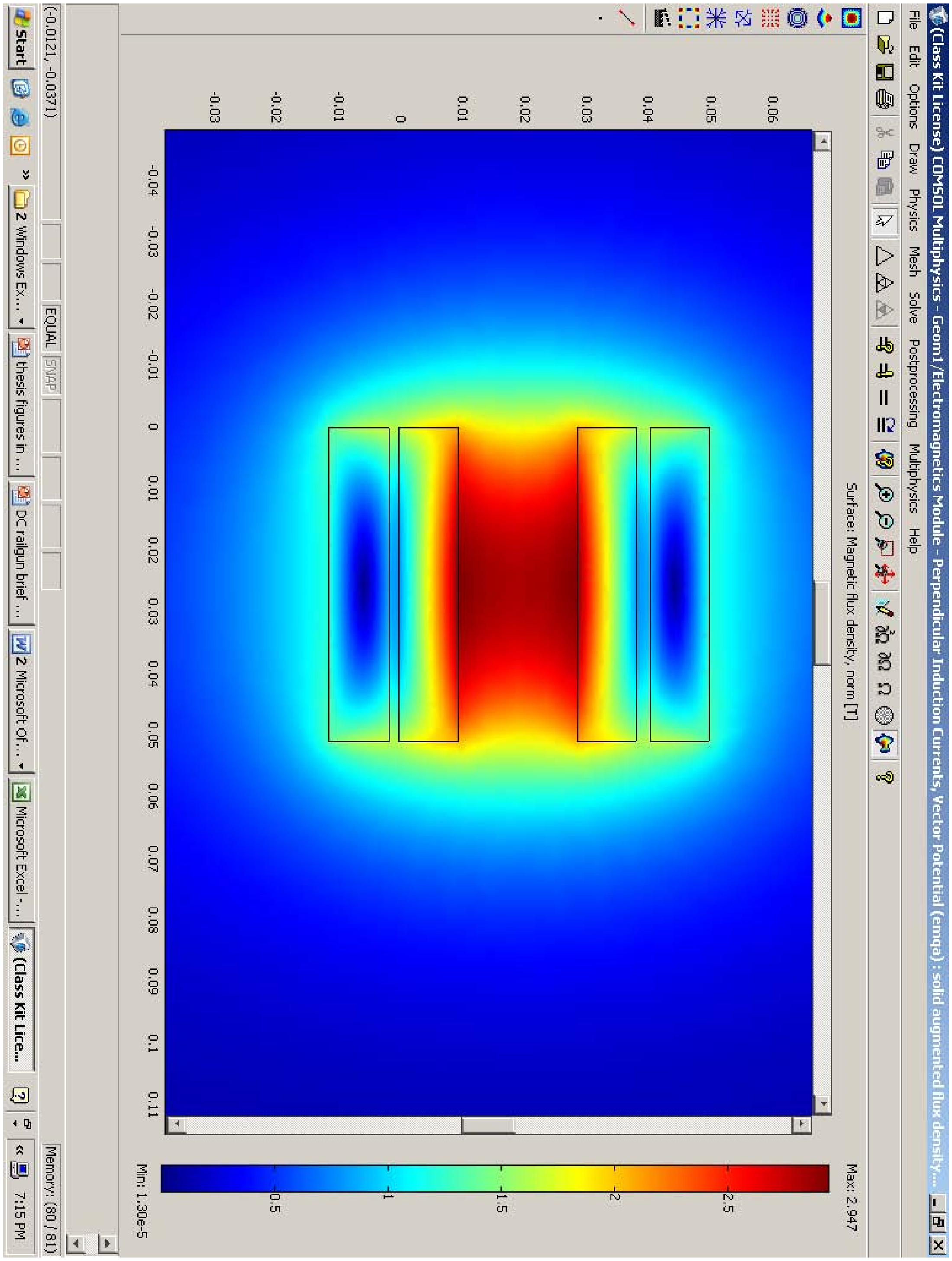


Figure 39. Solid, Augmented Magnetic Flux Density

X and Y axes are units are in meters.

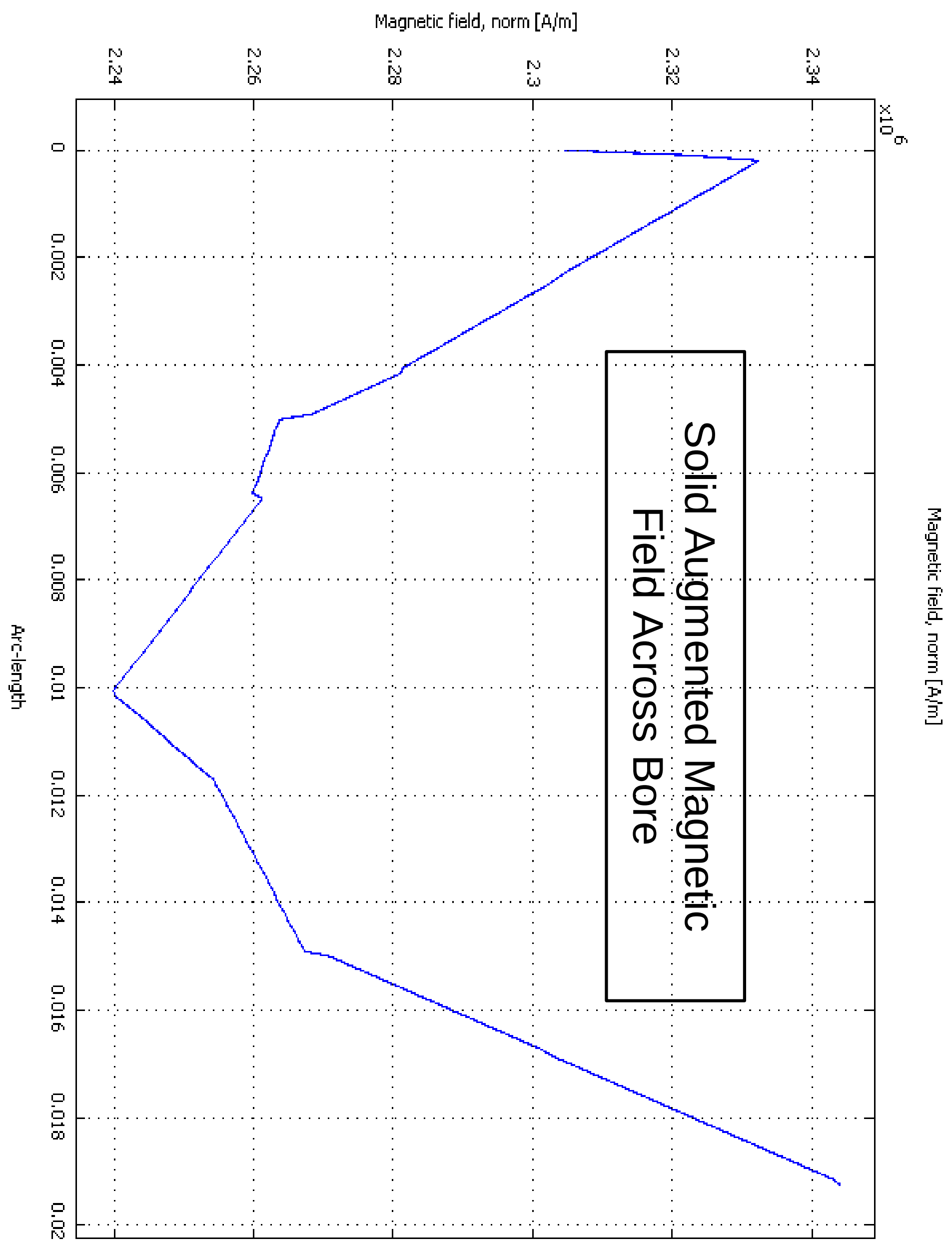


Figure 40. Solid Augmented Magnetic Field Across Bore

X axis is in units of meters, Y axis is Magnetic field strength A/m.

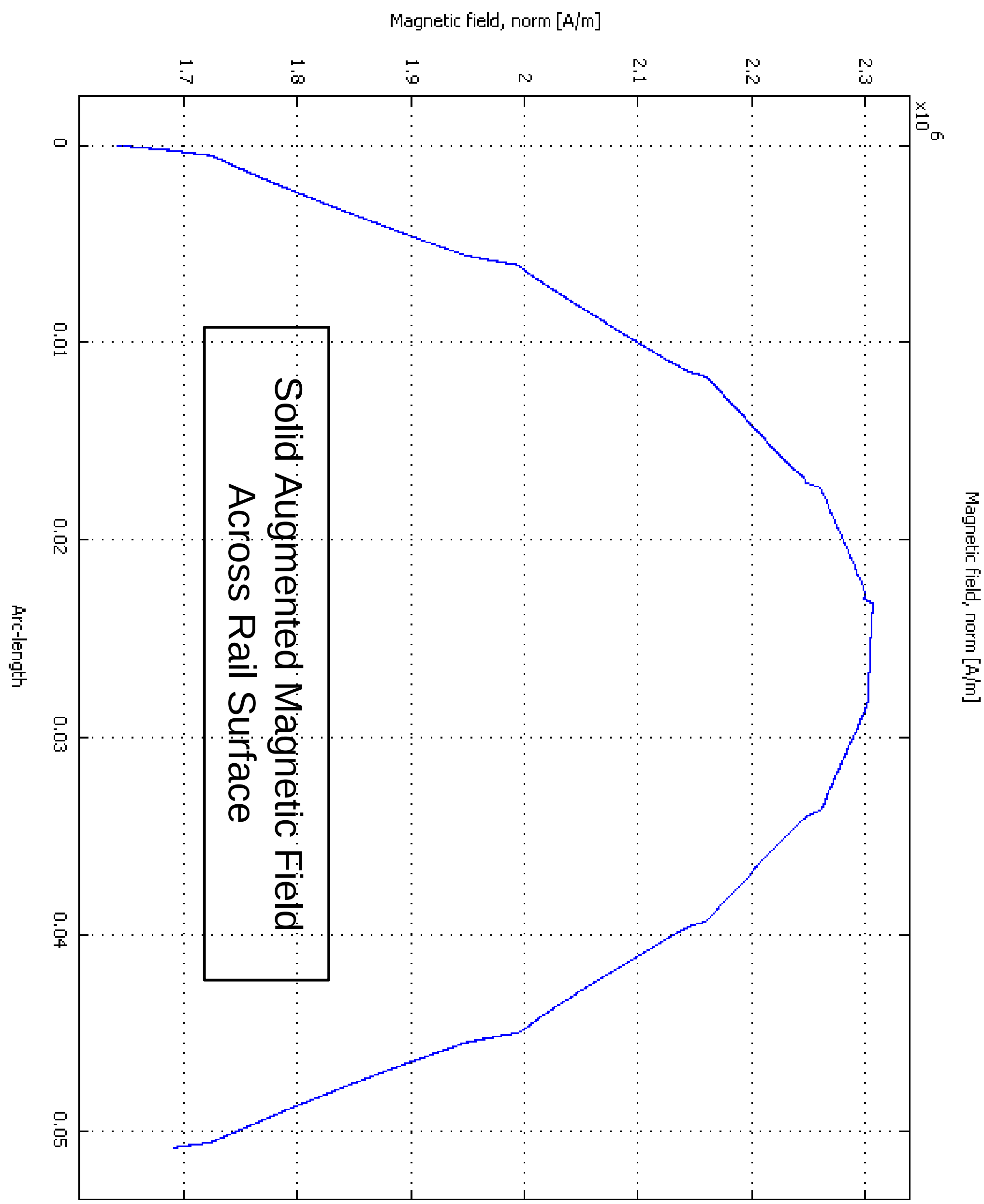


Figure 41. Solid, Augmented Magnetic Field Across Rail Surface

X axis is in units of meters, Y axis is Magnetic field strength A/m.

100 k-Amp DC, Slotted Rail, Augmented

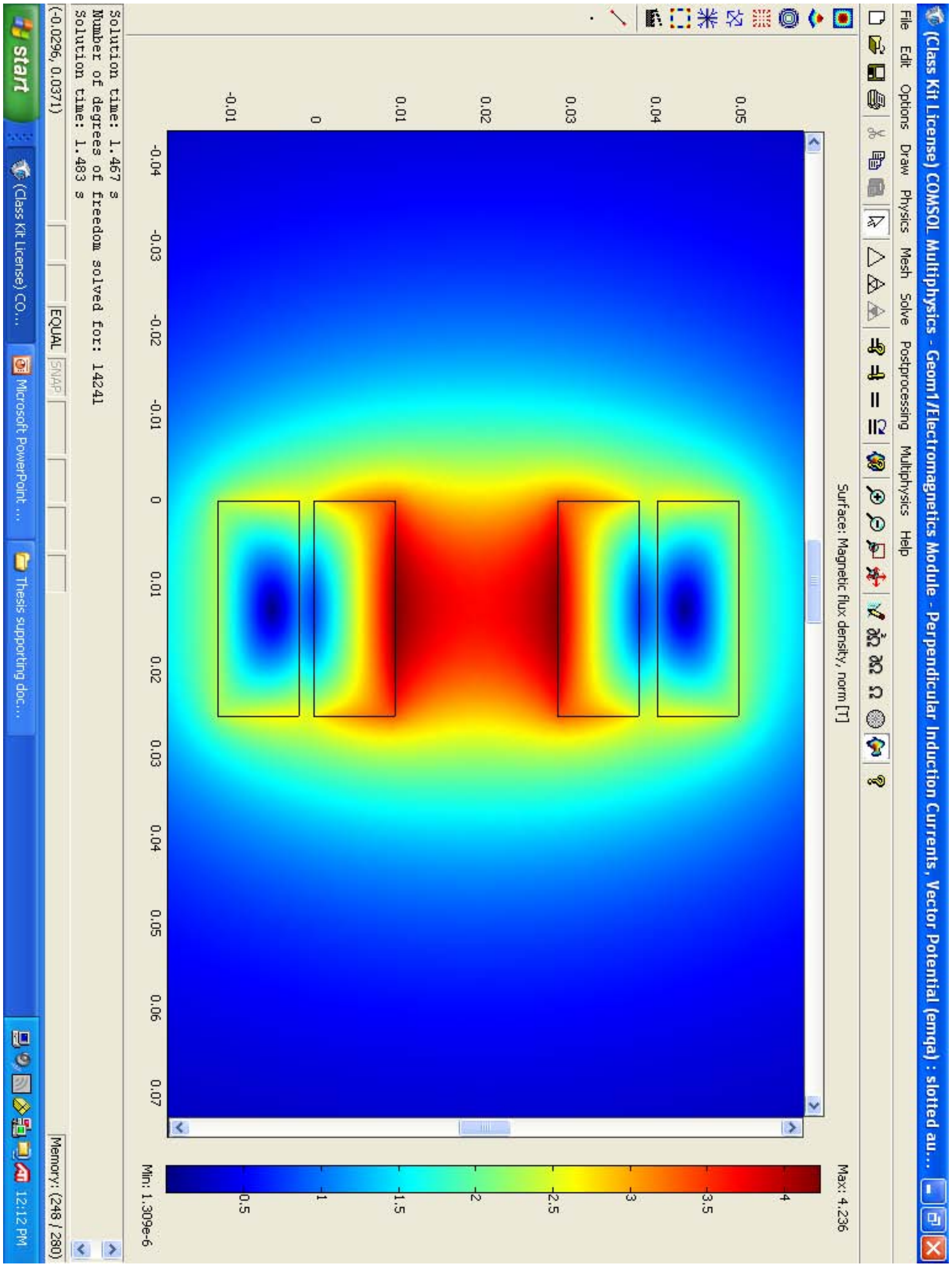


Figure 42. Slotted Augment Magnetic Flux Density

X and Y axes units are in meters.

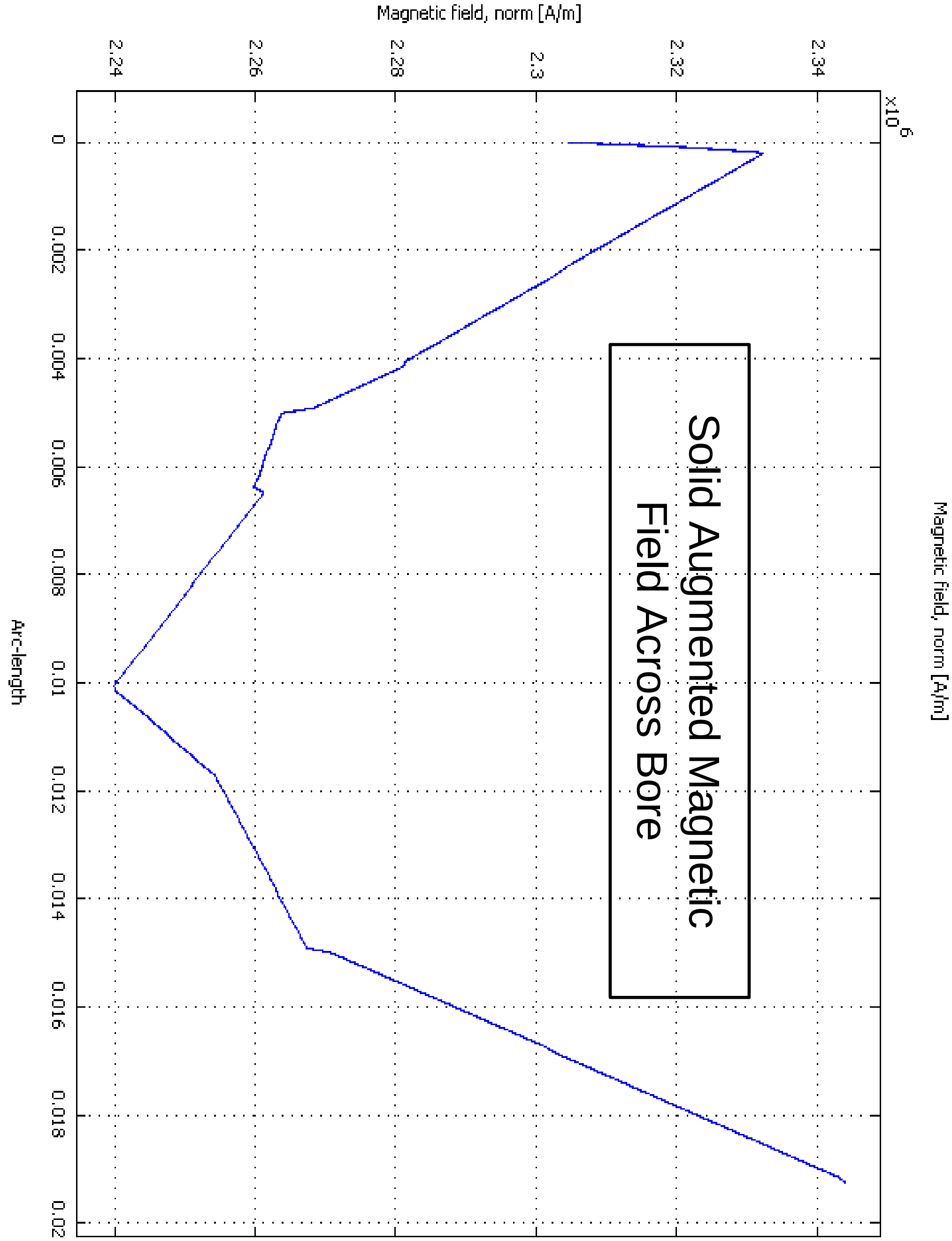


Figure 43. Solid Augmented Magnetic Field Across Bore

X axis is in units of meters, Y axis is Magnetic field strength A/m.

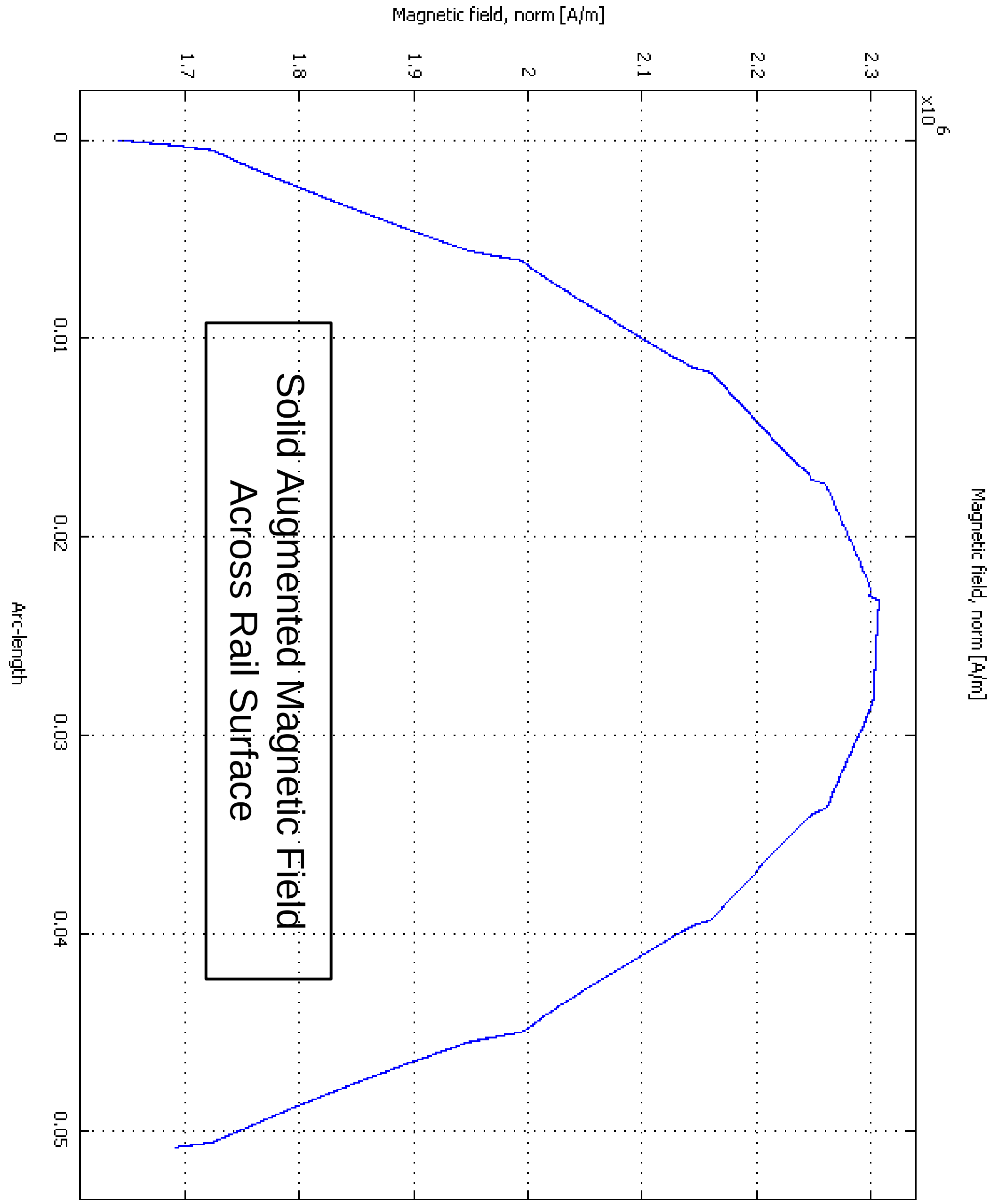


Figure 44. Solid Augmented Magnetic Field Across Rail Surface

X axis is in units of meters, Y axis is Magnetic field strength A/m.

## B. ORCAD 10.3 P-SPICE CIRCUIT MODELING

LRC Model of the existing power supply, and resultant current profile at 35 kJ

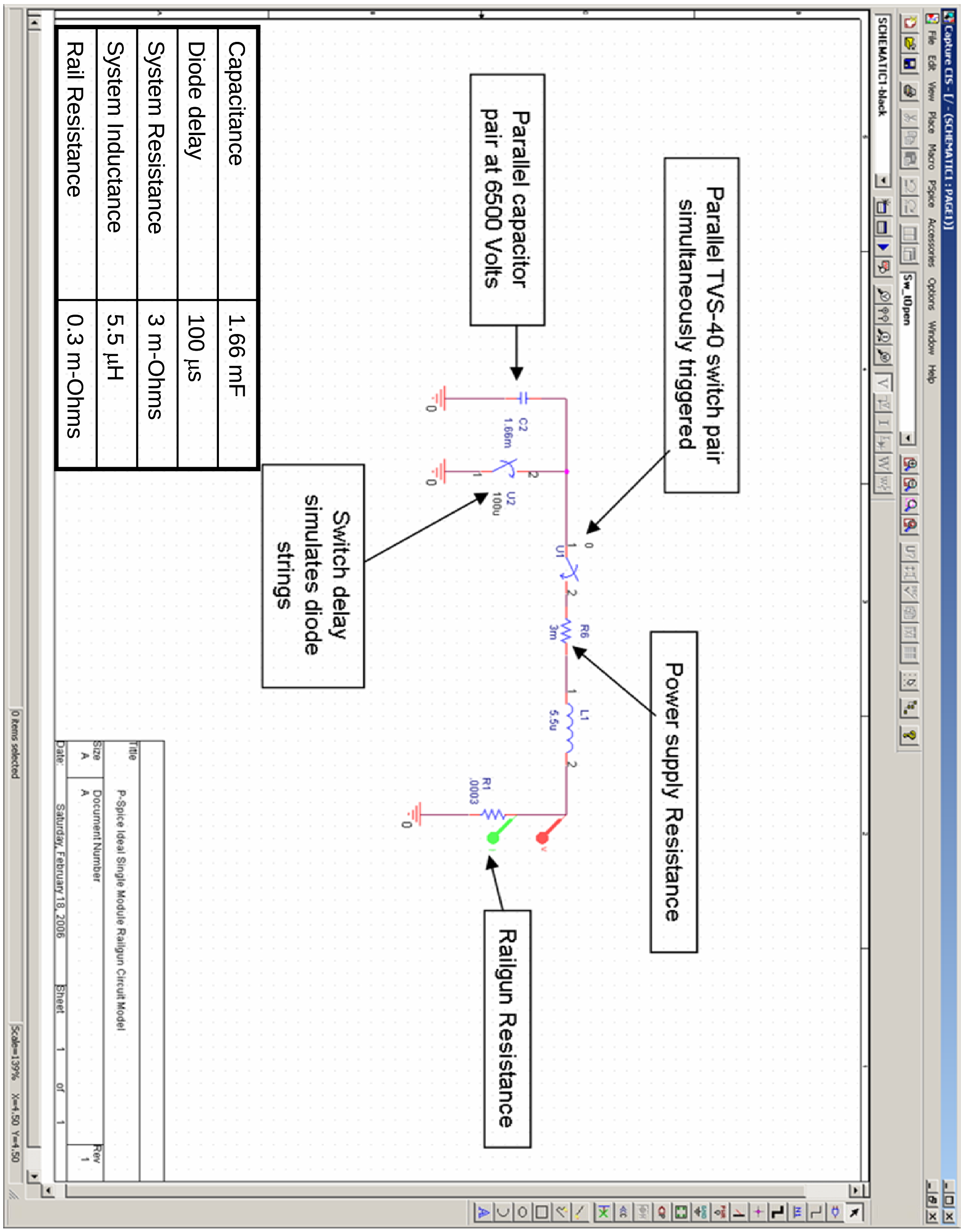


Figure 45. P-SPICE Single Module LRC Circuit Model

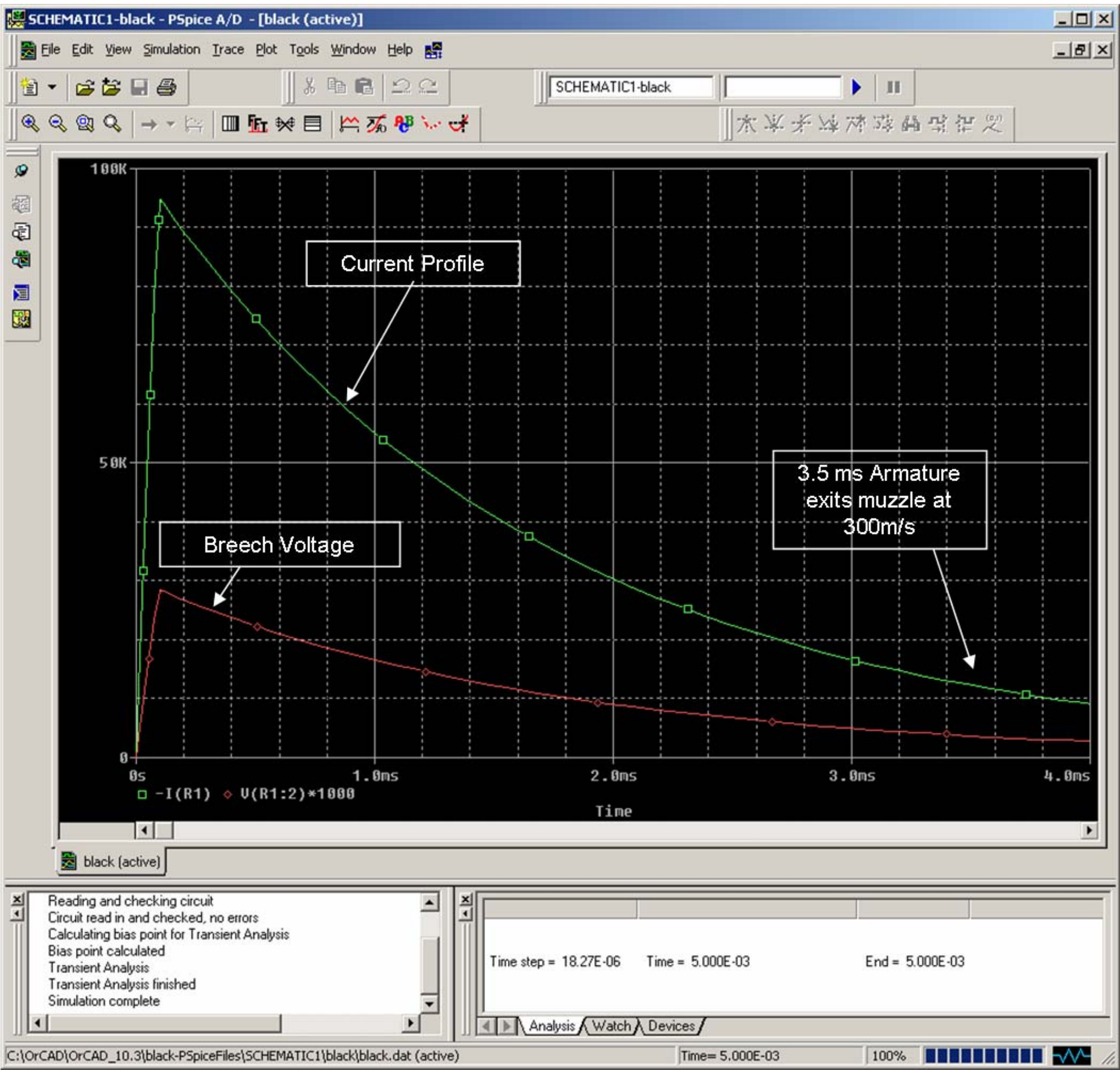


Figure 46. Single Power Module Current Profile

Four-Module Ripple Fired 332-kJ Circuit Model

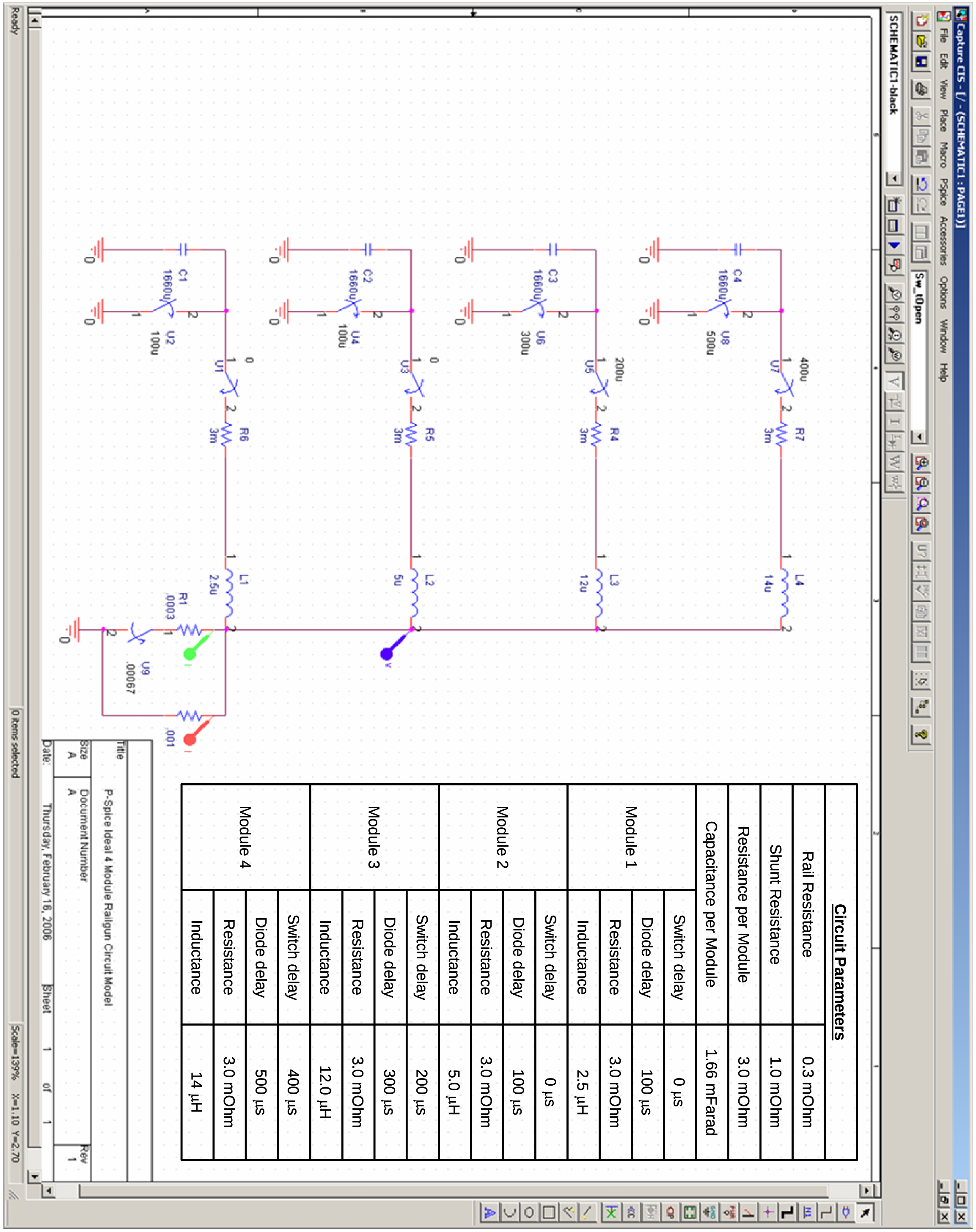

| Circuit Parameters | | |
|---|---|---|
| Rail Resistance | | 0.3 mOhm |
| Shunt Resistance | | 1.0 mOhm |
| Resistance per Module | | 3.0 mOhm |
| Capacitance per Module | | 1.66 mFarad |
| Module 1 | Switch delay | 0 µs |
| | Diode delay | 100 µs |
| | Resistance | 3.0 mOhm |
| | Inductance | 2.5 µH |
| Module 2 | Switch delay | 0 µs |
| | Diode delay | 100 µs |
| | Resistance | 3.0 mOhm |
| | Inductance | 5.0 µH |
| Module 3 | Switch delay | 200 µs |
| | Diode delay | 300 µs |
| | Resistance | 3.0 mOhm |
| | Inductance | 12.0 µH |
| Module 4 | Switch delay | 400 µs |
| | Diode delay | 500 µs |
| | Resistance | 3.0 mOhm |
| | Inductance | 14 µH |



Figure 47. P-SPICE Four-Module LRC Circuit Model

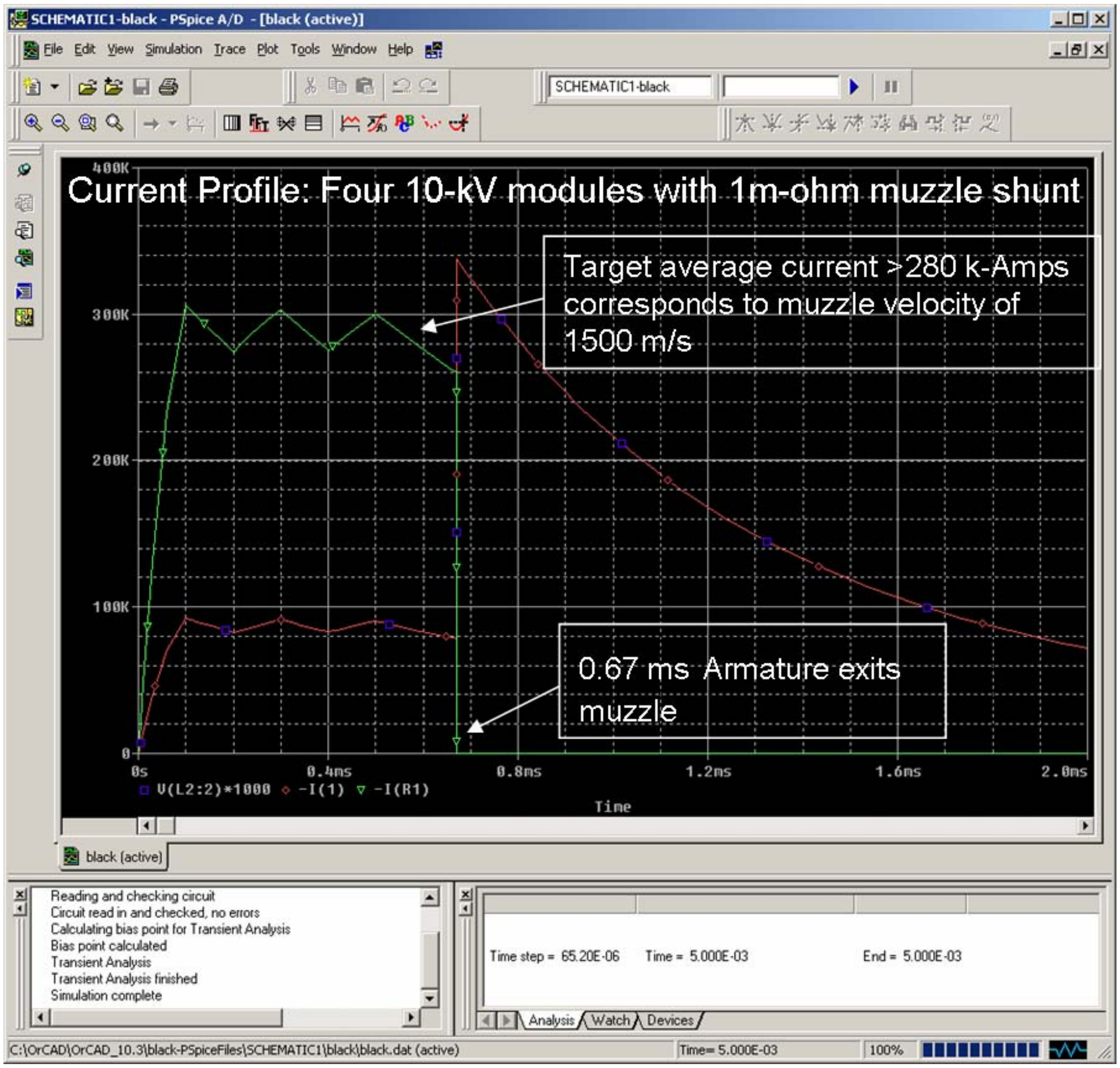


Figure 48. Four-Module Current Profile Output from Figure 46 Circuit Model

# APPENDIX E. BREAK SCREEN AND CURRENT PROFILE SCREEN CAPTURES

6500 Volts, Solid Rail, Non-augmented

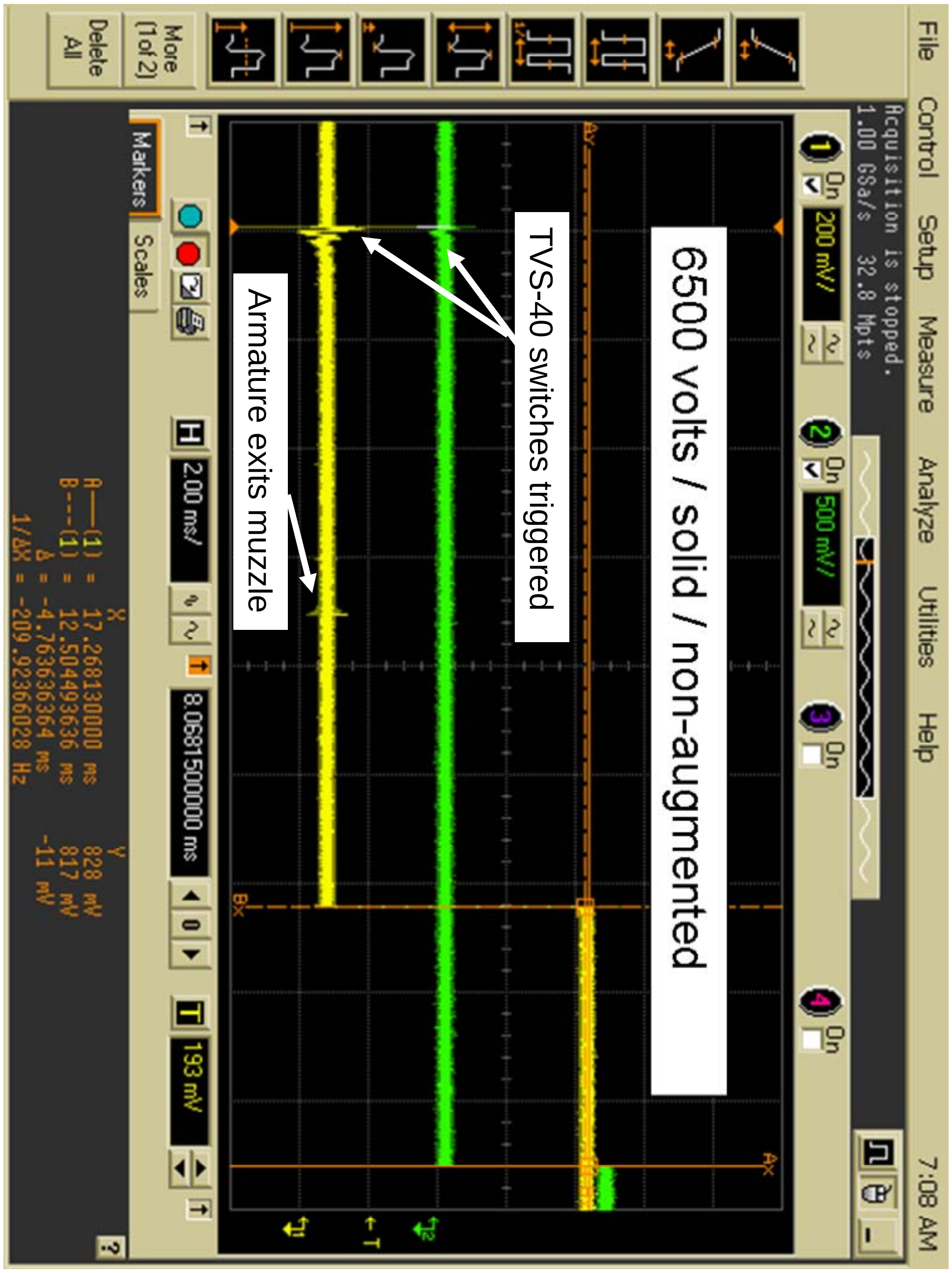


Figure 49. Solid Non-Augmented Velocity Measurement

Green and yellow traces are from break screens located at 0.5 meter interval for velocity measurement.

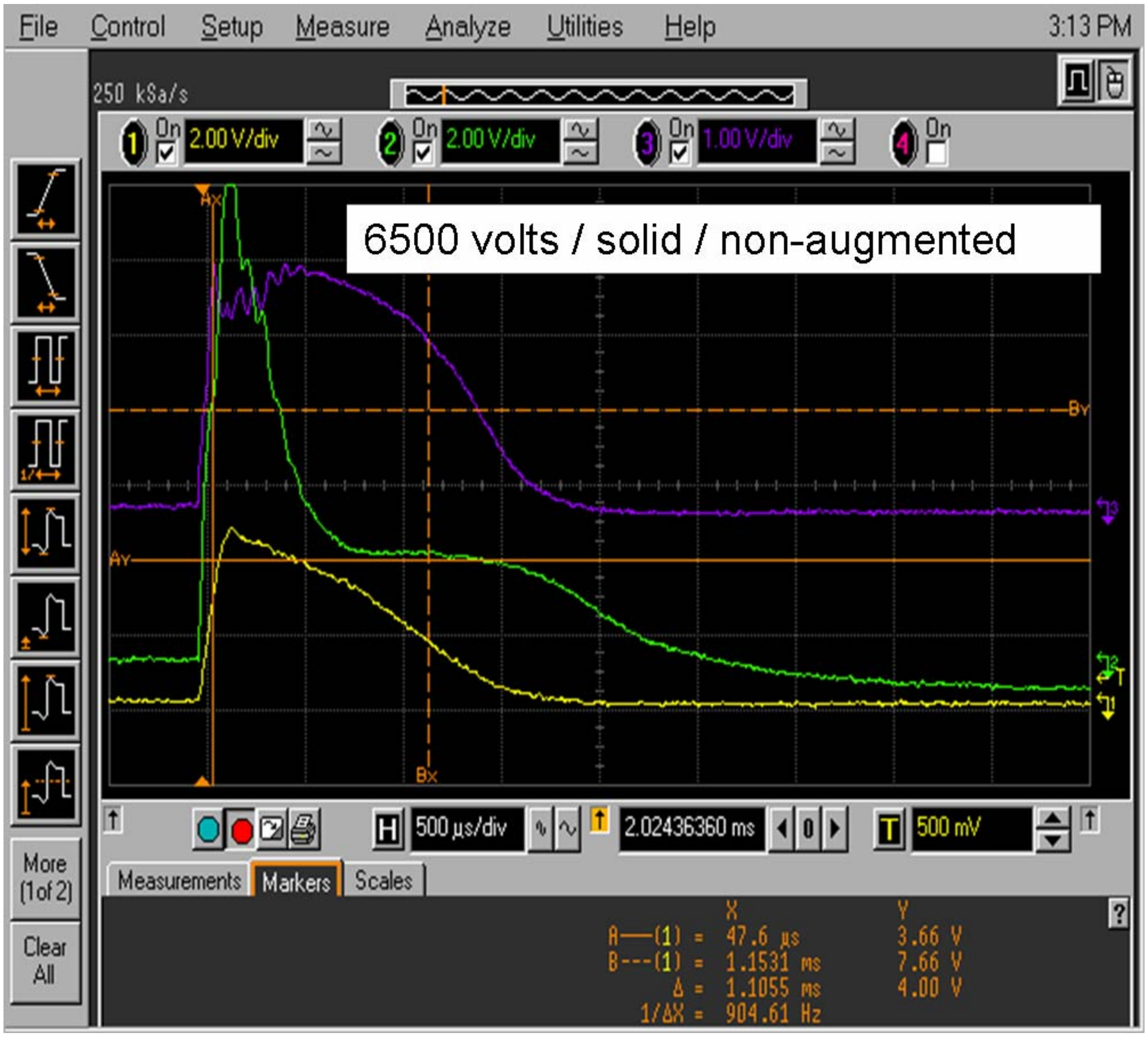


Figure 50. Solid Non-Augmented Current Profiles

Green and Purple Traces are the Pearson 1330 current monitor traces through the individual TVS-40 switches, the Yellow curve is the Pearson 1423 total current to the railgun.

6500 Volt, Slotted Rail, Non-Augmented

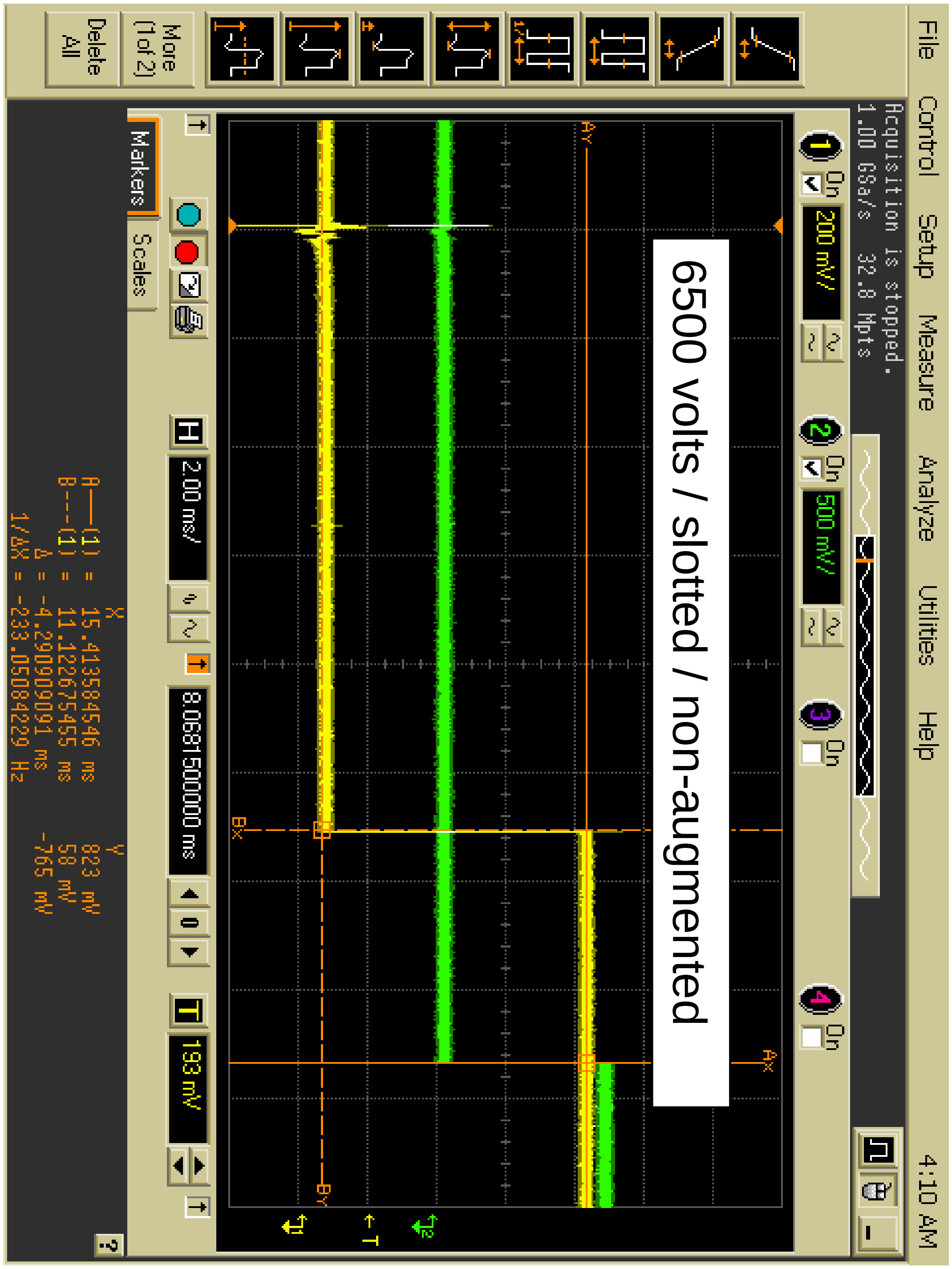


Figure 51. Slotted Non-Augmented Velocity Measurement

See caption for Figure 49.

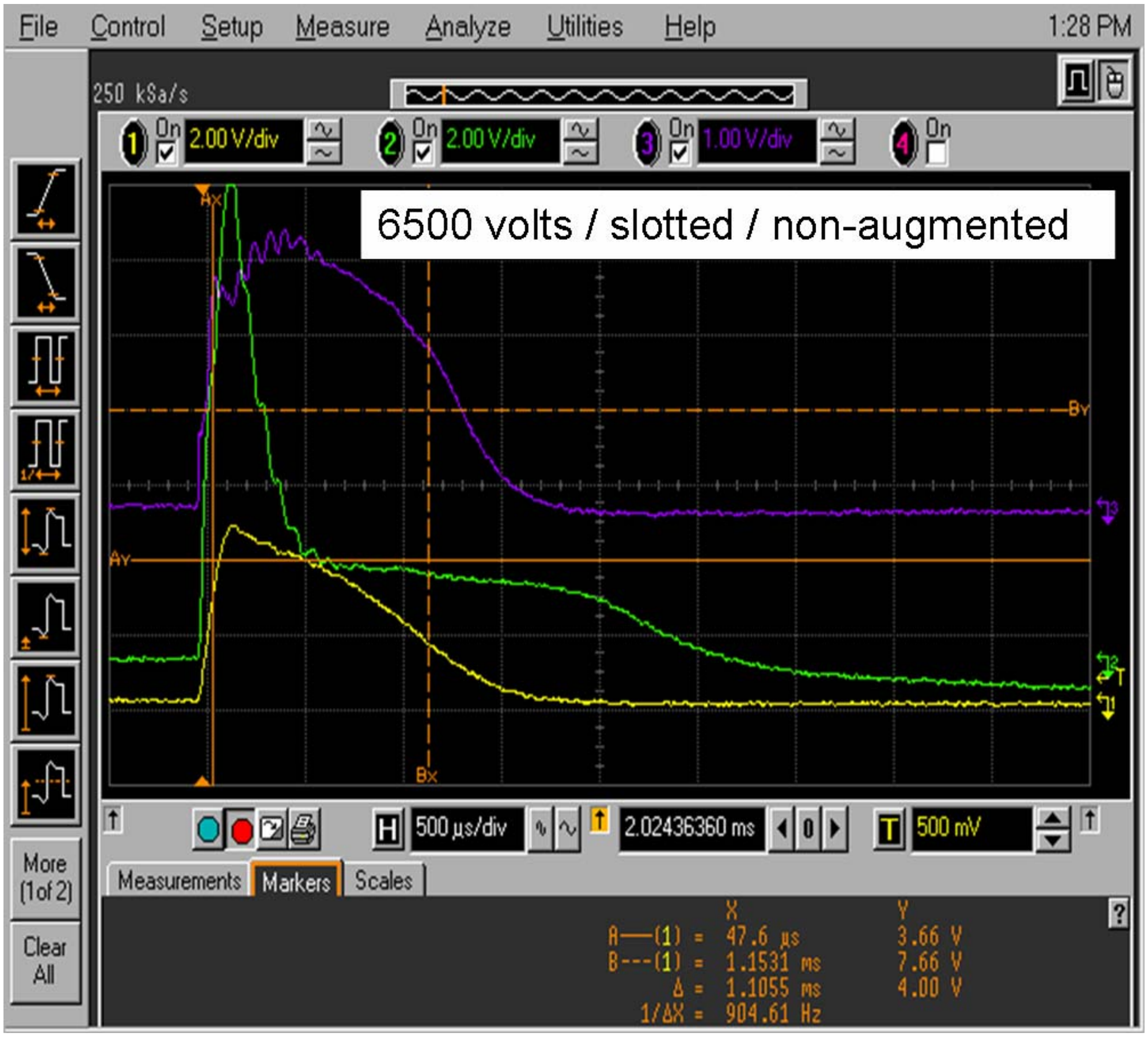


Figure 52. Slotted Non-Augmented Current Profiles

See caption for Figure 50.

6500 Volt, Solid Rail, Augmented

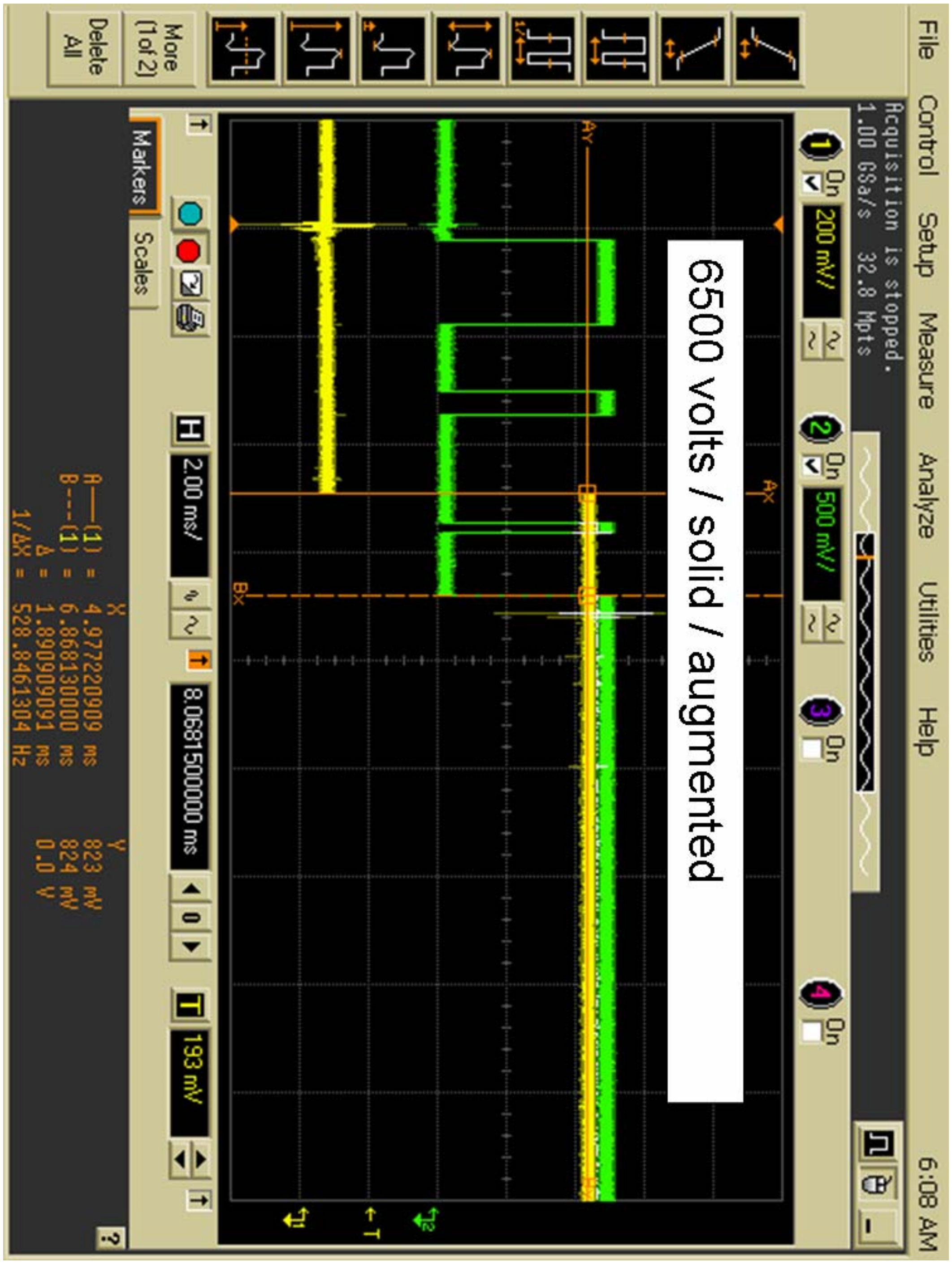


Figure 53. Solid Augmented Velocity Measurement

See caption for Figure 49. Fluctuation in green trace is due to loose electrical connection and vibration during shot at break-screen mount, corrected for subsequent shots.

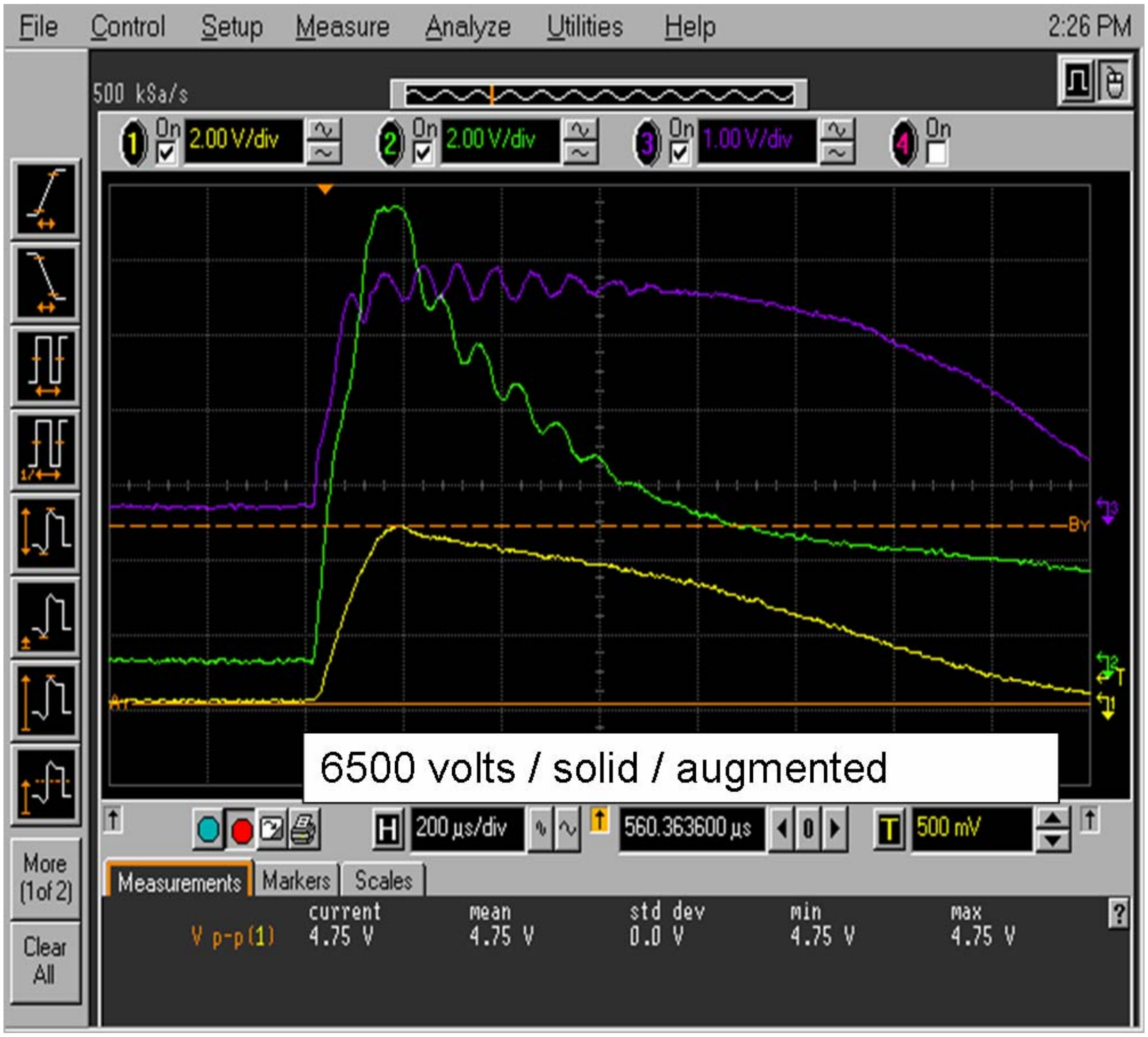


Figure 54. Solid Augmented Current Profiles

See caption for Figure 50.

6500 Volts, Slotted, Augmented

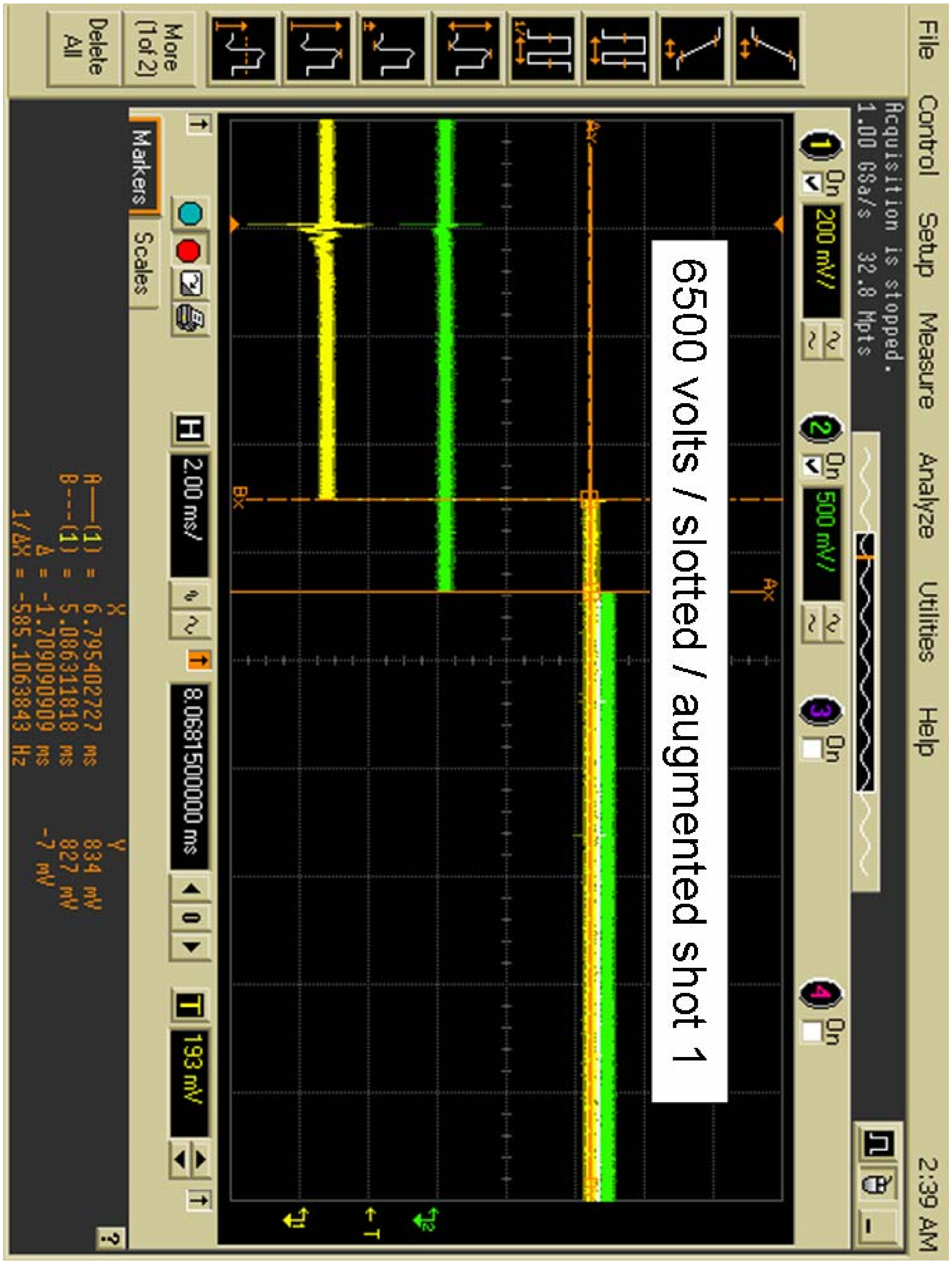


Figure 55. Slotted Augmented Velocity Measurement

See caption for Figure 49.

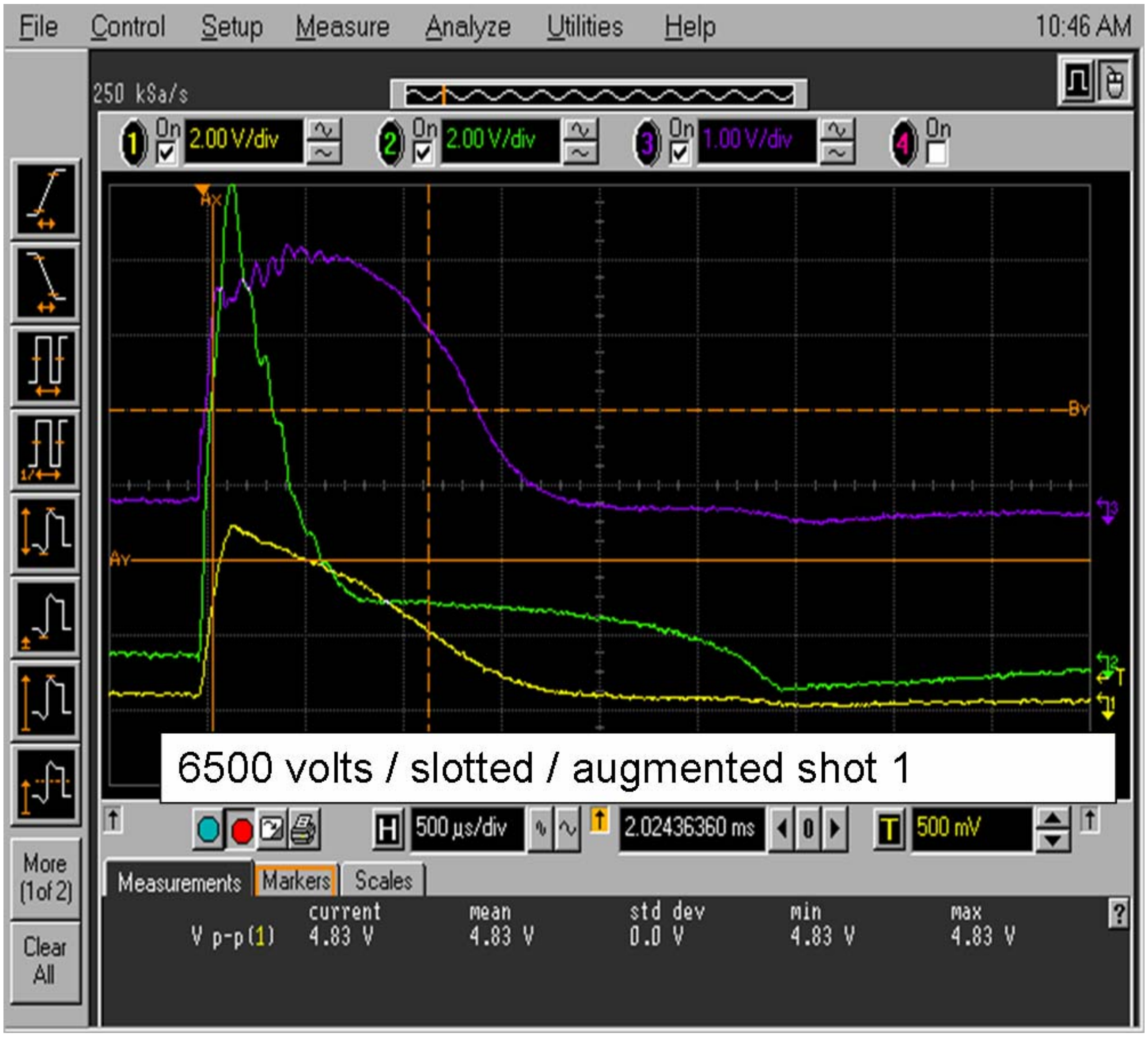


Figure 56. Slotted Augmented Current Profiles

See caption for Figure 50.

# APPENDIX F. TYPICAL POST-SHOT MATERIAL CONDITIONS

Rails and Insulators

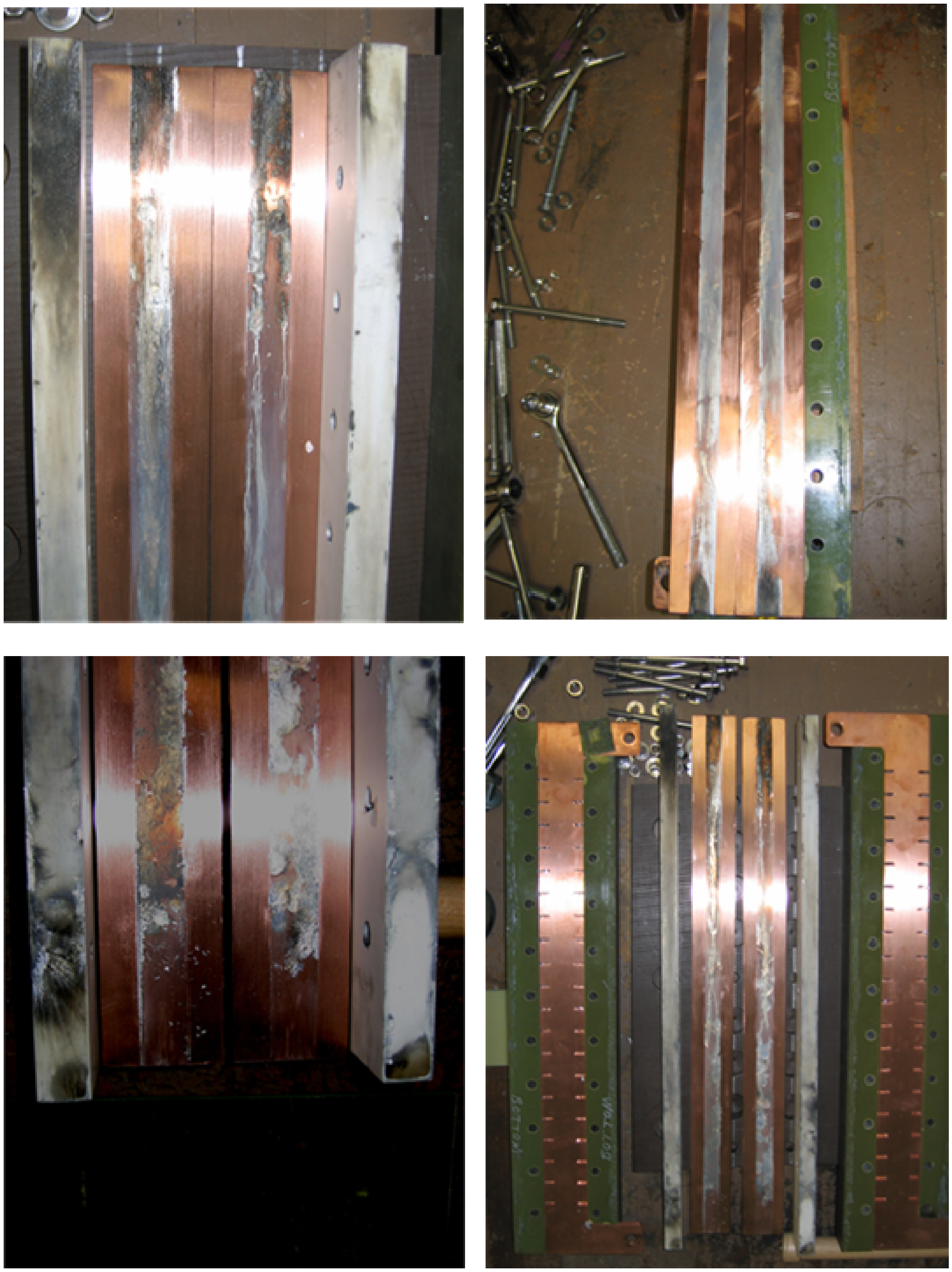

Figure 57. Typical Post-Shot Rail and Insulator Wear

Armature Wear

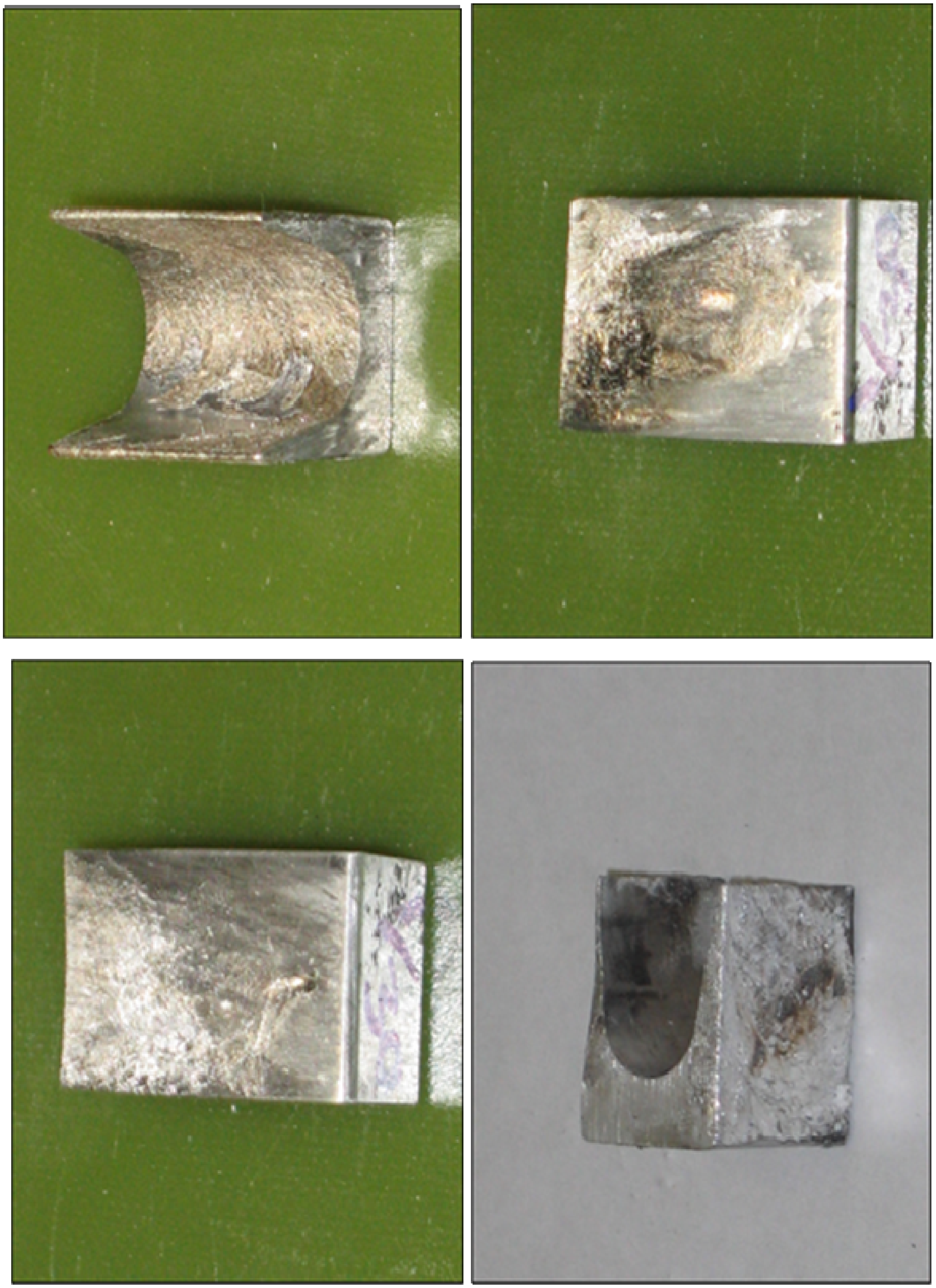

Figure 58. Typical Post-Shot Armature Wear

Muzzle


Figure 59. Muzzle Block Indicating Muzzle Flash Arcing

THIS PAGE INTENTIONALLY LEFT BLANK

# LIST OF REFERENCES


1. McNab,I.R., Stefani,F., Crawford,M., Erengil,M., Persad,C., Satapathy,S., Vanicek,H., Watt,T., and Dampier,C., *Development of a Naval Railgun*, IEEE Transactions on Magnetics, Vol.41, No.1, pp.206-213, January 2005.

2. Materials Web website, last accessed 23 February 2006, http://www.matweb.com/search/

3. Kerrisk,J.F., Current Distribution and Inductance Calculations for Rail-Gun Conductors, LANL report LA-9092-MS, Nov. 1981.

4. Maier, B., *Selected Topics in Railgun Technology Course Notes*, Naval Postgraduate School, July 2005.

5. Kotas,J.F., Guderjahn,C.A., Littman,F.D., *A Parametric Evaluation of Railgun Augmentation*, IEEE Transactions on Magnetics, Vol.22, No.6, November 1986.

6. Chen,Y.G., Dethlefsen,R., Crumley,R., *High-Coulomb Vacuum Switch*, IEEE International Digest of Technical Papers, Pulsed Power Conference 1993,Digest of Technical Papers, Vol.2, pp.938-941, June 1993.

7. Crawford, M., *Railgun System Technology*, Naval Postgraduate School Physics Department Colloquium Lecture, May 2004.

8. ACF Component & Fasteners, Inc. Specification Handbook, 2005 Edition, last accessed 05 March 2006, www.acfcom.com

9. Ugural, A.C. and Fenster, S.K., *Advanced Strength and Applied Elasticity*, Fourth Edition, Prentice Hall Publishers, Upper Saddle River, NJ, 2003, pp.527.

10. K-Mac Plastics website, last accessed 23 February 2006, www.k-mac-plastics.net/data%20sheets/Acculam-technical-data.htm

11. CoorsTek Ceramics website, last accessed 23 February 2006, www.coorstek.com/materials/ceramics/alumina/ad96.asp

12. American Micro-Industries website, last accessed 23 February 2006, www.electricalinsulationmaterial.com/electrical-insulation-products/mylar_polyester_film/ mylar-polyester-film.html#mylar-properties

13. Stefani,F., Watt,T., *Experimental and Computational Investigation of Root-Radius Melting in C-Shaped Solid Armatures*, IEEE Transactions on Magnetics, Vol.41, No.1, pp.442-447, January 2005.

14. Hackel,L., Chen,H., Laser Peening – A Processing Tool to Strengthen Metals or Alloys to Improve Fatigue Lifetime and Retard Stress-Induced Corrosion Cracking, Lawrence Livermore National Laboratory Laser Science and Technology Program UCRL-ID-155327, September 2003.

15. Renk,T., Buchheit,R., Sorensen,N., Senft,D., Thompson,M., Grabowski,K., Improvement of Surface Properties by Modification and Alloying with High-Power Ion Beams, Physics of Plasmas, Vol.5, No.5, pp.2144-2150, May 1998.

# INITIAL DISTRIBUTION LIST

1. Defense Technical Information Center
   Ft. Belvoir, VA

2. Dudley Knox Library
   Naval Postgraduate School
   Monterey, CA

3. Professor William B. Maier II, Code PH/MW
   Department of Physics
   Naval Postgraduate School
   Monterey, CA

4. Professor Terry McNelley, Code MAE/MC
   Department of Mechanical and Astronautical Engineering
   Naval Postgraduate School
   Monterey, CA

5. Engineering and Curriculum Office, Code 34
   Naval Postgraduate School
   Monterey, CA

6. LT Brian C. Black
   Pittsburgh, PA

7. Tania Zaleski
   Laser Peening Project Leader
   Lawrence Livermore National Laboratory
   Livermore, CA

8. Tim Renk
   Beam Applications and Initiatives Project Leader
   Sandia National Laboratory
   Albuquerque, NM

9. Prof. Hans Mark
   Institute for Advanced Technology
   Austin, TX

10. Prof. Ian McNabb
    Institute for Advanced Technology
    Austin, TX

11. Dr. Mark Crawford
Institute for Advanced Technology
Austin, TX

12. Francis Stefani
Institute for Advanced Technology
Austin, TX

13. Dwayne Surls
Institute for Advanced Technology
Austin, TX

14. Chadee Persad
Institute for Advanced Technology
Austin, TX

15. Fred Beach
Institute for Advanced Technology
Austin, TX

16. Robert Hebner
Center for Electromechanics
Austin, TX

17. John Pappas
Center for Electromechanics
Austin, TX

18. Dr. Roger McGinnis
Air Warfare and Naval Weapons Applications Division
Office of Naval Research
Arlington, VA

19. Roger Ellis
EM Railgun INP
Office of Naval Research
Arlington, VA

20. John Kinser
Office of Naval Research
Arlington, VA

20. Elizabeth D’Andrea
Office of Naval Research
Arlington, VA

21. Dr. Irwin Singer
    Tribology Section, Naval Research Lab
    Washington, DC

22 Robin Keesee
    US Army Research and Development Command
    Aberdeen Proving Ground, MD

23. Mark McCormick,
    Northrop Grumman Corporation Ship Systems
    Pascagoula, MS